People`s Democratic Republic of Algeria

Ministry of Higher Education and Scientific Research

University of Echahid Hamma Lakhdar - El Oued

Faculty of Science and Technology

Department of Mechanical Engineering

Dissertation

ACADEMIC MASTER

Domain: Science and Technology

Division: Mechanic Engineering

Specialty: Electromechanics

Presented by:

1. **KELLAL AZZEDDINE**
2. **HOUBA ABDELGHANI**
3. **CHOUCHANI MOHAMMED SALEH**

Entitled:

Analysis of Maximum Power Point Tracking (MPPT) Techniques for Photovoltaic Systems

Dissertation Submitted in Partial Fulfillment of the Requirements for the Master Electromechanics

Board of Examiners:

Dr. DJOUGHRAB ALAA EDDINE	**Chairman**
Dr. ZINE BACHIR	**Supervisor**
Dr. BABOUKHA ALI	**Examiner & Co-Supervisor**

Academic Year: 2024/2025

Abstract

This work is a comprehensive review of Maximum Power Point Tracking (MPPT) techniques of photovoltaic (PV) systems with constant and variable irradiances levels. Relevant algorithms such as Perturb and Observe (P&O), Incremental Conductance (INC), Artificial Neural Networks (ANN), and Fuzzy Logic Controller (FLC) are examined, and their strengths, weaknesses, and comparative strengths are documented. Simulation output for MATLAB-Simulink indicates that ANN performs optimally (96.63% with fixed solar irradiance), while FLC minimizes oscillation with rapid adaptability. The paper highlights the necessity of making an appropriate choice of MPPT methods depending on system requirement and environmental condition. Experimental verification and hybrid algorithm formation are included as future work considering enhancing the performance.

Keywords: MPPT, Photovoltaic Systems, P&O, INC, ANN, FLC, MATLAB-Simulink, Efficiency, Variable Irradiance, Hybrid Algorithms.

ملخص

يُقدم هذا البحث مراجعة شاملة لتقنيات تتبع نقطة القدرة القصوى (MPPT) في الأنظمة الكهروضوئية (PV) ذات مستويات الإشعاع الثابتة والمتغيرة. يُفحص البحث خوارزميات ذات صلة، مثل الاضطراب والمراقبة (P&O)، والموصلية التزايدية (INC)، والشبكات العصبية الاصطناعية (ANN)، ووحدة التحكم المنطقي الضبابي (FLC)، ويُوثق نقاط قوتها وضعفها ونقاط قوتها المقارنة. تشير نتائج المحاكاة باستخدام MATLAB-Simulink إلى أن الشبكة العصبية الاصطناعية تعمل على النحو الأمثل (96.63% مع إشعاع شمسي ثابت)، بينما تُقلل وحدة التحكم المنطقي الضبابي (FLC) من التذبذب مع قدرة سريعة على التكيف. تُسلط الورقة الضوء على ضرورة اختيار طرائق MPPT المناسبة وفقًا لمتطلبات النظام والظروف البيئية. كما يُدرج التحقق التجريبي وتكوين خوارزمية هجينة كعمل مستقبلي يهدف إلى تحسين الأداء.

الكلمات المفتاحية: MPPT، أنظمة الطاقة الكهروضوئية، P&O، INC، ANN، FLC، MATLAB-Simulink، الكفاءة، الإشعاع المتغير، الخوارزميات الهجينة.

DEDICATION

To my dear parents,
who have always been there for me,
supporting me with their encouragement.

To my beloved wife,
my partner in every step of this journey,
whose love and unwavering support
have been my greatest strength.

To my dear brothers,
who have always stood by my side.

To all my family,
to all my friends and colleagues,
thank you for being part of my life and inspiring me along the way.

Thanks, and Appreciation

The completion of this research would not have been possible without the tremendous support we received from many individuals who contributed directly or indirectly to this work. From this standpoint, we extend our deepest gratitude to everyone who played a role in this project.

First and foremost, we would like to express our heartfelt thanks to our main supervisor, **Dr. Zine Bachir**, who provided us with continuous guidance and support throughout the preparation of this research. Your profound expertise and insightful vision were a source of inspiration for us, and your contributions were instrumental in transforming our ideas into a comprehensive academic work. Thank you for your unwavering support and encouragement.

We also extend special and heartfelt gratitude to **Dr. Babboukha Ali**, whose pivotal role in helping us overcome the challenges we faced during this research cannot be overstated. Your extensive knowledge and valuable contributions added a new dimension to this work, and we are deeply grateful for the time and effort you devoted to ensuring the success of this project.

We also extend our thanks to all the **professors of the Electromechanical Engineering Department** who have been with us since the beginning of our academic journey. They taught us not only the technical sciences and knowledge but also the skills necessary to face the challenges of professional life. Thank you for your patience, valuable guidance, and for instilling curiosity and creativity in our minds. Every lesson you delivered was a cornerstone in building our professional future.

We also thank the **Electromechanical Engineering Department** as a whole for providing a stimulating educational environment equipped with the latest technologies and tools that helped us develop both our practical and theoretical skills. The department has been like a second home to us, where we spent years full of learning and personal and professional growth.

Additionally, we extend our gratitude to our colleagues and friends who stood by us and provided moral support and advice during the various stages of preparing this research. Your words of encouragement were always a source of strength when we faced difficulties.

Finally, we must thank ourselves – as a team of three students – for the continuous effort and hard work we put into achieving this accomplishment. It was a journey filled with challenges, but at the same time, it was full of learning and personal and professional growth.

In conclusion, we hope that this research marks the beginning of a new phase of academic and research work. Thank you to everyone who contributed to the success of this project, whether through guidance, support, or even a kind word. We will always remain grateful for your invaluable contributions.

With utmost respect and gratitude,

KELLAL AZZEDDINE

HOUBA ABDELGHANI

CHOUCHANI MOHAMMED SALEH

ACKNOWLEDGEMENTS

We collaborated as a team for this study and on writing this thesis, would here like to take this opportunity to thank from the bottom of our hearts all those who have mentored us and helped us along the way.

Most importantly, we would like to give our sincere appreciation to our supervisor, **Dr. Zine Bachir**, for the instrumental guidance, constructive criticism, and unqualified encouragement throughout this project. His professionalism, hard work, and passion were all the decisive factor in developing this work and in being able to develop it to completion well.

We are also grateful to our heartfelt thanks to **Dr. Baboubkha Ali** for his precious and crucial assistance in this study. His wise suggestions, recommendations, and technical help were of immense help in problem-solving and achieving the objectives of this thesis. We are very thankful to him and extend our deepest thanks to him for his precious assistance.

We thank science and technology lecturers at the **University of Echahid Hamma Lakhdar - El Oued**, Department of Science and Technology, because they have led us through this path in **Mechanical Engineering** with their leadership and guidance and have given us a chance to do our best. They have been our great support throughout university life with their leadership and guidance.

We also highly thank our friends and colleagues of the **Electromechanical Department** for suggestions, ideas, and inspiration at crucial phases of this work. Their dedication and shared spirit to succeed turned it into an enjoyable experience and worthwhile.

Finally, we will always be grateful to our families and friends for the unconditional support, love, and ethical direction. They had faith in us when other people did not, and they encouraged us even in the midst of turmoil, always with us throughout the undertaking.

To all the above, we are acknowledging the sincerest of our thanks for working in concert in allowing the facilitation of this research project to happen.

Table of Contents

LIST OF FIGURES

CHAPTER I: Photovoltaic Systems Overview

CHAPTER II: Maximum Power Point Tracking (MPPT) Techniques

LIST OF TABLES

LIST OF ABBREVIATIONS

Abbreviation	Full Form
AF	Activation Function
AI	Artificial Intelligence
ANFIS	Adaptive Neuro-Fuzzy Inference System
ANN	Artificial Neural Network
BMS	Battery Management System
DC-DC	Direct Current to Direct Current
DFIG	Doubly Fed Induction Generator
DOD	Depth of Discharge
DSP	Digital Signal Processor
EMC	Electromagnetic Compatibility
EMI	Electromagnetic Interference
ESS	Energy Storage System
FACTS	Flexible AC Transmission Systems
FF	Fill Factor
FLC	Fuzzy Logic Controller
FOCV	Fractional Open-Circuit Voltage
FOCV	Fractional Open-Circuit Voltage
FPGA	Field-Programmable Gate Array
FSCC	Fractional Short-Circuit Current
GA	Genetic Algorithm
GSC	Grid-Side Controller
GUI	Graphical User Interface
HC	Hill-Climbing
HMI	Human-Machine Interface
HVDC	High Voltage Direct Current
HVRT	High Voltage Ride Through
ICT	Information and Communication Technology
Imp	Current at Maximum Power Point
INC	Incremental Conductance
IoT	Internet of Things
IR	Irradiance
ISC	Inverter-Side Controller
I-V	Current-Voltage
LP	Local Peak
LVRT	Low Voltage Ride Through
MF	Membership Function
MPP	Maximum Power Point
MPPT	Maximum Power Point Tracking
P&O	Perturb and Observe
PCE	Power Conversion Efficiency
PEMFC	Proton Exchange Membrane Fuel Cell

LIST OF ABBREVIATIONS

PID	Proportional-Integral-Derivative
PMSG	Permanent Magnet Synchronous Generator
PSC	Partial Shading Condition
PSO	Particle Swarm Optimization
PV	Photovoltaic
P-V	Power-Voltage
PWM	Pulse Width Modulation
RES	Renewable Energy Source
SCADA	Supervisory Control and Data Acquisition
SEIG	Self-Excited Induction Generator
SOC	State of Charge
SOFC	Solid Oxide Fuel Cell
SPWM	Sinusoidal Pulse Width Modulation
STATCOM	Static Synchronous Compensator
SVC	Static Var Compensator
SVM	Support Vector Machine
SVPWM	Space Vector Pulse Width Modulation
TCSC	Thyristor-Controlled Series Capacitor
THD	Total Harmonic Distortion
UPFC	Unified Power Flow Controller
Vmp	Voltage at Maximum Power Point
WECS	Wind Energy Conversion System

General Introduction

Introduction

PV systems are becoming more a part of our daily lives because people are searching for cleaner ways of producing energy. The greatest advantage of PV technology is that we produce electricity from the sun directly, and therefore we use less fossil fuel and even less environmental devastation **[1]**. However, one of the main problems with PV systems is their efficiency, especially when the weather conditions, like sunlight intensity and temperature, keep on changing **[2]**. Sometimes the performance gets extremely low under low light or high temperature, which makes it challenging to rely completely on these systems without proper optimization techniques **[3]**. Hence, researchers are working hard to find solutions to maintain high efficiency regardless of the conditions. It is where Maximum Power Point Tracking (MPPT) techniques are required. MPPT techniques are an essential element of the fact that they allow PV systems to leverage their potential as much as possible since they always adjust to capture the accessible power in fluctuating conditions **[4]**.

The aim here in this thesis was to assess and compare various MPPT algorithms and determine what is optimal for what situation. Specifically, we contrasted four methods: Perturb and Observe (P&O), Incremental Conductance (INC), Artificial Neural Networks (ANN), and Fuzzy Logic Control (FLC). We simulated to determine how rapidly these methods respond, whether they are stable, and how effective they are at adapting to sunlight intensity changes **[5]**. We discovered that all of the methods had advantages and disadvantages. For example, ANN worked best overall, especially in changing conditions, while P&O was unstable at high speeds but simple to implement **[6]**.

The project has been split into three chapters.

Chapter I: Photovoltaic Systems Overview is an introduction to the PV system and the reason why MPPT is especially critical in optimizing their efficiency.

Chapter II: MPPT Techniques is a technical chapter wherein we present some MPPT techniques and categorize them as classical, intelligent, and optimization-based techniques. We compare the strengths and weaknesses of each technique and explain where each one is superior. Finally,

Chapter III: Simulation and Modeling of MPPT Techniques is where we present the result of our simulations. Here we compare the result of the four algorithms in static and dynamic light intensity. We also compare their efficiency, stability, and ability to trace sudden change.

Through this study, we wanted to provide a better illustration on how various MPPT techniques can be utilized to improve the efficiency of PV systems. Although ANN was best in the majority of the situations, FLC and INC also have their respective uses based on the situation. We believe that with our research, solar energy systems can become more efficient and reliable in the future.

CHAPTER I

Photovoltaic Systems Overview

I.1 Introduction

Photovoltaic (PV) technologies are the new technology for moving the world energy model off fossil fuels, cleaner than the fossil fuel. Solar energy, in contrast to coal, oil, and gas, exhaustible resources and main world warming culprits **[7]** , is plentiful, naturally self-restoring, and with low emissions. Solar technologies like solar heating and cooling, photovoltaics, and concentrated solar power transform the solar energy into a variety of applications, e.g., industrial processes, to electricity production. PV systems are unique in their application of semiconductor material like silicon in order to produce electricity with the power of the sun. Through the photovoltaic effect, the photons of light are consumed by the semiconductor material and utilized in exciting electrons in a bid to generate an electric current **[8]**. The constraints in terms of efficiency loss mechanisms, thermally induced dependency, and failure mechanisms in terms of hotspots and delamination provide the demand for continued innovation. Despite these, solar PV installations increased worldwide with declining costs, technological advancements, and favorable policies **[9]**. China alone, for instance, had reached 63% of the world's PV installations up to the year 2023 **[10]**, a consequence of how it is spearheading the installation of clean energy. With efficiencies spanning 15% to 28% for utility modules **[8]** and ongoing studies to always exceed these figures, solar PV systems are revolutionizing how we generate and use energy. PV systems from small roof-mounted systems for domestic use through to solar farms for utility use on a utility scale are not merely meeting energy requirements but are leading the way towards cleaner, greener times. With their drivers of performance, stakeholders, and values understood, they can be maximized and optimized to contribute more towards the battle against the climate crisis.

I.2. Background on Renewable Energy and Photovoltaic Systems

I.2.1 The Emergence of Renewable Energy Resources

Renewable energy is derived from natural sources that replenish faster than they are consumed, such as sunlight and wind, making them a sustainable alternative to fossil fuels. In contrast, coal, oil, and gas are non-renewable resources that take millions of years to form and release harmful greenhouse gases, like carbon dioxide, when burned, contributing to climate change. However, renewable energy production generates significantly lower emissions, making it essential for mitigating the climate crisis. Various renewable energy sources, including wind and solar power, are continuously replenished and will never deplete. However, renewable energy generation can be inconsistent due to environmental factors. For instance, hydroelectric power relies on rainfall to maintain water flow in dams **[11],[12]**.

Unlike fossil fuel combustion, which emits particulate matter and contributes to air pollution, renewable energy is a cleaner option. Yet, one challenge is the difficulty of generating electricity on a scale comparable to fossil fuel-based power plants **[13],[14]**. Most renewable energy originates from the sun, directly or indirectly. Solar energy is used for electricity generation, heating, lighting, and industrial applications. Wind turbines harness wind power, which is driven by solar heating. Additionally, solar energy influences the water cycle, leading to precipitation that sustains hydroelectric systems. Due to its sustainability, renewable energy is increasingly preferred in areas where conventional electricity production is impractical. Wind power, in particular, is a promising clean energy source, but variations in wind speed cause fluctuations in voltage and frequency, requiring advanced technology to maintain stability **[15],[16]**. In agriculture, irrigation systems rely on renewable energy, water availability, and market conditions. With rapidly evolving agricultural markets, modern farmers must adopt advanced technologies to enhance efficiency. Three-phase induction motors are commonly used in agricultural applications, highlighting the integration of renewable energy into farming operations.

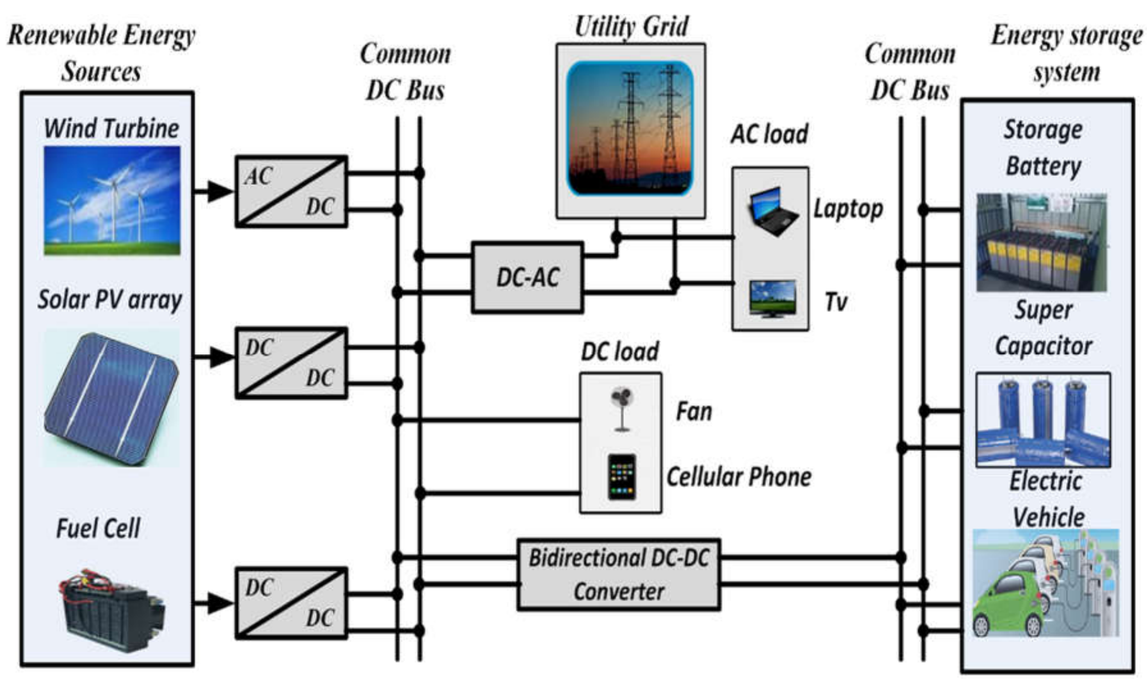

Figure (I.1): Application of power electronic converter in a removable energy system **[17]**

I.3. Solar Energy Technologies

Solar energy is the energy received from the Sun, serving as a vast and free resource capable of meeting global energy demands. The energy in sunlight is approximately 10,000 times greater than the world's total energy consumption, making solar energy a highly promising solution. Three primary technologies are used to harness solar energy: solar heating and cooling (SHC), concentrated solar power (CSP), and solar photovoltaics (PV). Solar irradiation primarily consists of infrared (IR) radiation, followed by visible light and ultraviolet (UV) radiation, all of which can be utilized for energy production. Solar panels directly convert sunlight into electricity. Solar radiation reaches Earth as photons traveling in electromagnetic waves. When light strikes a solar cell, electrons in the semiconductor material become excited, leaving behind positively charged holes. To generate electricity, the photon's energy must exceed the semiconductor's energy band gap, enabling electron movement across junctions. Greater absorption of high-energy light results in increased electron motion, producing more electricity. However, electron recombination, where electrons return to their holes, reduces efficiency. Therefore, an ideal solar cell material should support prolonged electron-hole pair lifetimes to maximize power generation. Figure (I.2) illustrates a PV system, highlighting components that contribute to efficiency losses **[18]**.

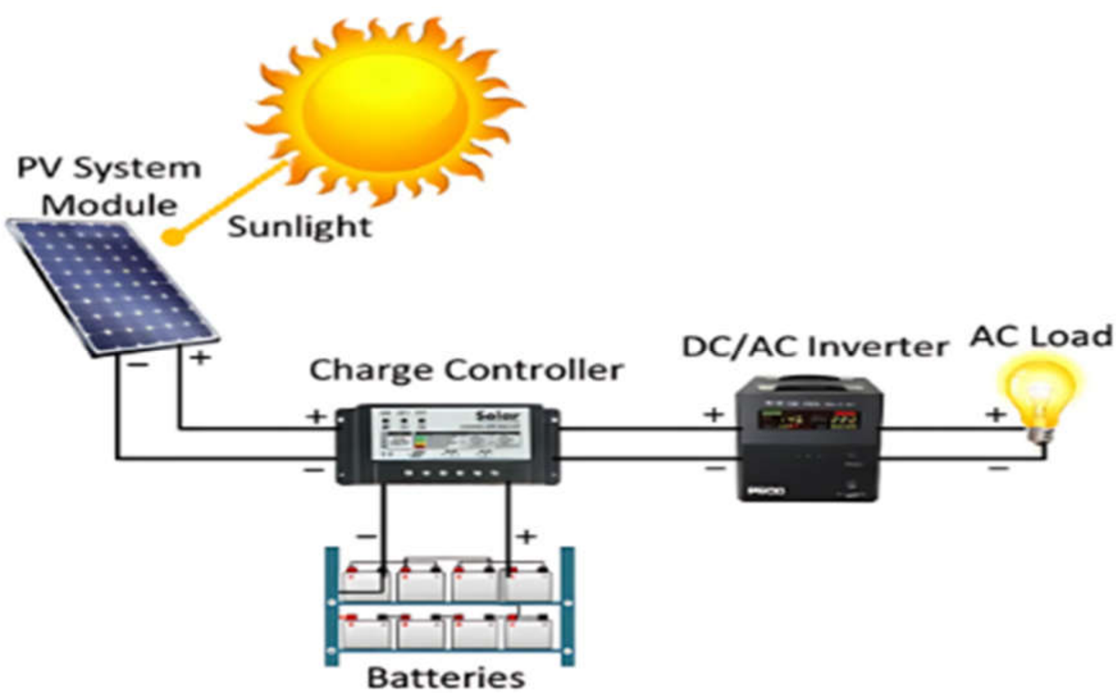

Figure (I.2): PV system schematic diagram **[18]**

I.4. Photovoltaic System

A photovoltaic (PV) system generates electricity from sunlight through key components: solar panels, an inverter for DC-to-AC conversion, and essential accessories like mounting, cabling, and electrical connections. Some systems integrate solar tracking for efficiency and battery storage as costs decline. The solar array, consisting of solar panels, forms the visible part of the system, while other components are part of the balance of system (BOS). Unlike concentrated solar power (CSP) or solar thermal technologies, PV systems directly convert sunlight into electricity, ranging from small rooftops to large utility plants **[19]**. Solar energy is a sustainable, cost-effective alternative with a longer lifespan than traditional energy sources. Governments promote solar panels in rural areas for street lighting, though battery performance is affected by overcharging and discharge cycles **[20]**. Charge controllers regulate battery charging, preventing overcharging and deep discharge, crucial for system efficiency and longevity. These controllers are essential in solar home systems, hybrid energy setups, and water pumps, ensuring stable power storage and supply **[21].** PV systems are categorized as grid-connected or off-grid. Grid-connected systems supply electricity to the grid, while off-grid systems store surplus energy in batteries for later use. Charge controllers in standalone systems prevent battery overcharging and deep discharge, which is vital due to high battery costs **[22]**. A PV system consists of a charge controller, batteries, a power converter, and solar panels (modules). The solar panel converts sunlight into DC electricity, regulated by the charge controller to charge the battery. Stored energy powers appliances via an inverter that converts DC to AC, ensuring continuous power, even in low sunlight conditions, as shown in figure (I.3).

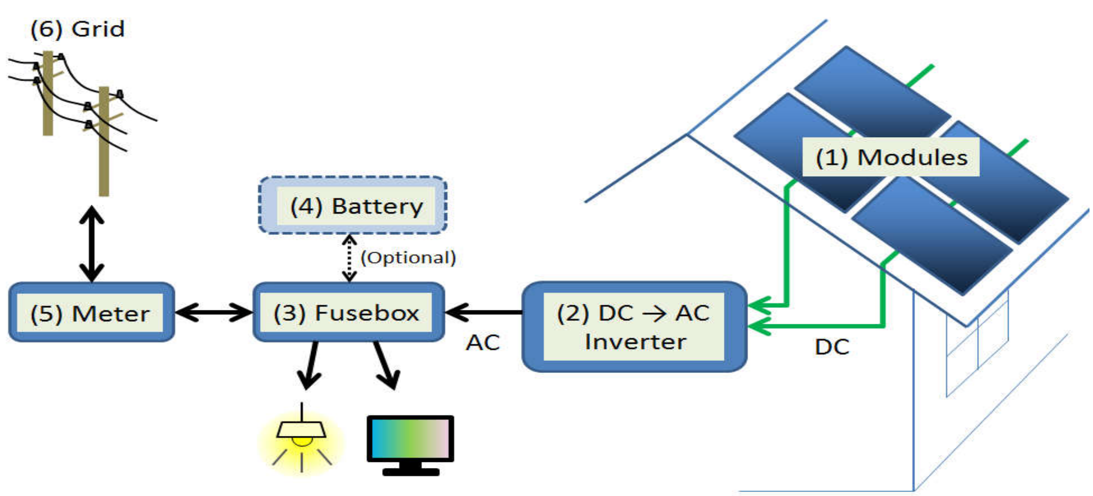

Figure (I.3): Block diagram of photovoltaic (PV) system. **[23]**

I.5. Solar PV Technology

The word photovoltaic implies the conversion of “photo” or light into “volts” or electricity. The PV technology is the only solar technology that directly converts the sunlight into electricity in direct current (DC) form using semiconductor materials fabricated usually from the elements Silicon (Si) or Germanium (Ge). PV technology applications vary from powering a scientific calculator to powering a million houses per PV station, such as the Benban solar station that has been connected to the grid in late 2019 as the largest PV station in Africa, powering about 1,000,000 houses **[24]**.

Solar PV technologies can be primarily divided into three types, such as:

1. Crystalline PV—monocrystalline and polycrystalline

2. Thin-film PV or amorphous PV

3. Emerging PV—organic PV and perovskite PV

The formation of solar PV modules will be discussed in the next chapter. An indepth discussion on each type of module is excluded, as this book intends to provide a comprehensive illustration of PV systems and their applications to familiarize the readers with minimal engineering or technical knowledge with the field terminology up to being able to do system sizing of any solar application anywhere in the world.

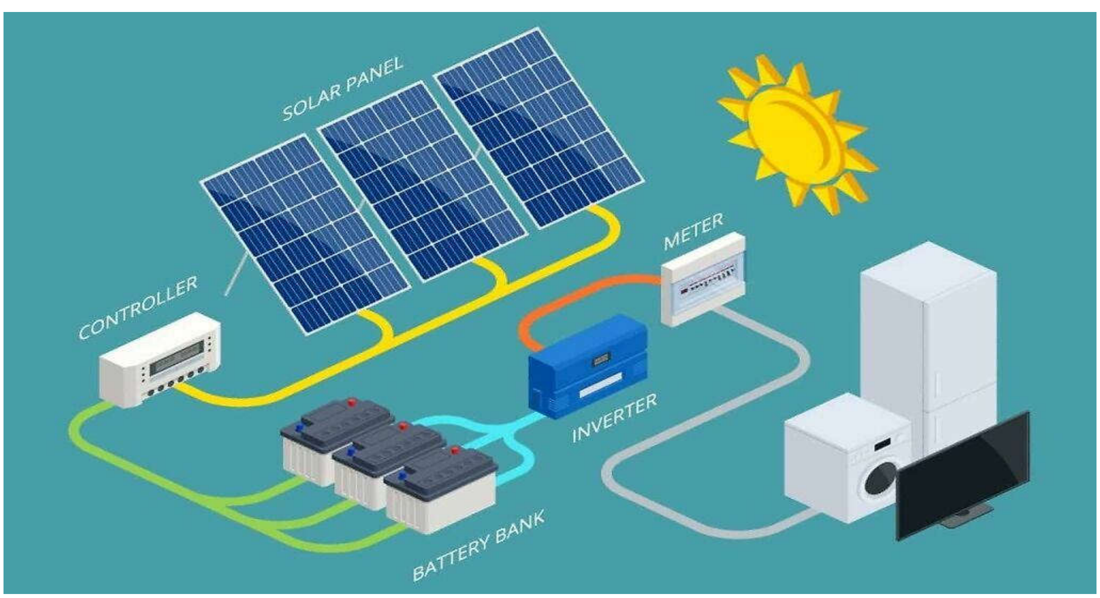

Figure (I.4): Solar PV Technology. **[25]**

I.6. Basic Principles of Photovoltaic Energy Conversion

I.6.1. Photovoltaic principles

The semiconductor material in a PV cell absorbs light (photons), and this displaces electrons to form pairs of electrons and holes, which are guided in one direction, creating a current. The semiconductor is doped to be a p-n junction with a potential difference, which will drive current flow vertically through the cell in one direction, so it can be harvested as electricity. The diffusion length is one of the important factors that affect the efficiency of the solar cell. Photons must have energy equal to or more than the energy band gap of the semiconducting material **[26]**. In summary, a photovoltaic cell is a device that converts sunlight into electricity using semiconductor materials; it has the same working principle as a semiconducting diode. The semiconductor material, such as silicon, has the property to eject electrons when sunlight is absorbed; the PV's cell then directs the electrons in one direction, which forms a current, as illustrated in Figure (I.5). **[27]**.

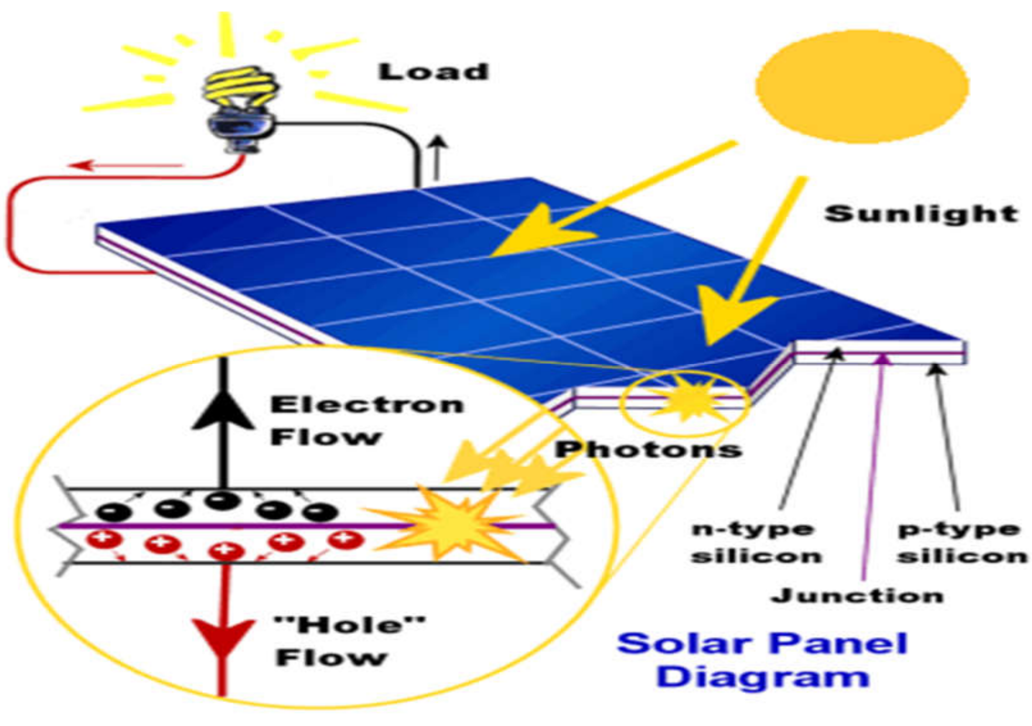

Figure (I.5): Basic principle of photovoltaic cells **[28]**

I.6.2. Growth of Solar PV

The global cumulative photovoltaic (PV) installations by region in 2023 exhibit significant growth, underscoring the pivotal role of solar energy in the global transition towards renewable energy sources **[29]**. According to the International Renewable Energy Agency (IRENA), the total global renewable energy capacity reached 3,870 GW in 2023 **[30]**, with solar energy contributing a substantial portion of this expansion.

Asia, led predominantly by China, accounted for the majority of this growth. China alone added approximately 216.9 GW of new PV capacity in 2023 **[30]**, representing about 63% of the global PV installations for that year **[31]**. This remarkable increase emphasizes China's leadership in renewable energy adoption and its commitment to reducing carbon emissions.

Other regions also demonstrated notable advancements. Europe and the United States expanded their PV capacities, driven by supportive policies and a growing emphasis on energy security **[32]**. However, despite these positive trends, disparities remain. Africa, for instance, experienced modest growth, with its total renewable energy capacity reaching 62 GW—a 4.6% increase from the previous year **[33]**. This highlights the ongoing need for equitable renewable energy development across all regions to ensure a balanced and inclusive energy transition.

The data underscores the critical importance of accelerating renewable energy deployment globally. To achieve the targets set for mitigating climate change, it is essential to address regional disparities and promote policies that facilitate renewable energy adoption universally **[32]**. This approach will ensure that the benefits of renewable energy, particularly solar PV, are realized worldwide.

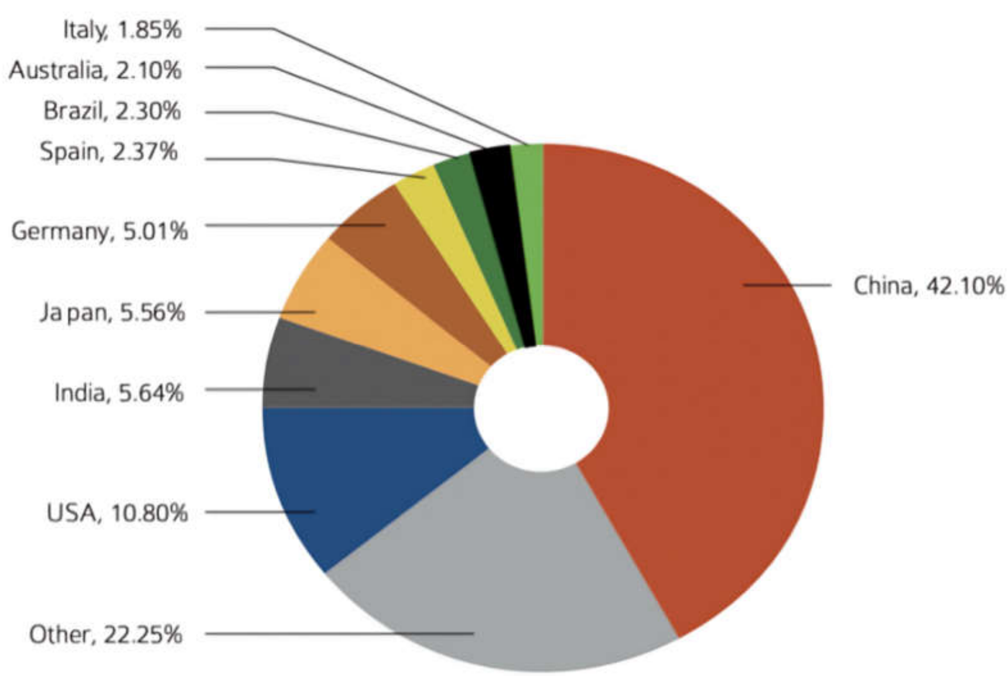

Figure (I.6): Global cumulative PV installation by region in the year 2023. **[34]**

I.6.3. Cost of Solar PV

The cost of solar PV technology has always been showing a declining trend **[35]**. PV system cost terminology varies according to the application category and the components required completing the system architecture. Thus, we will focus only on the PV module cost, which is the most critical portion of any PV system. Let us consider the cost drop of the global polycrystalline Silicon modules in the global market from 2014 to 2019. The cost of such modules started at 0.67 \$/W in the first quarter of 2014, and it went down to 0.214 \$/W in the second quarter of 2019 a 68% drop in only 5 years. The percentage of the global annual production of polycrystalline modules (60.8%) almost doubled the monocrystalline (32.2%).

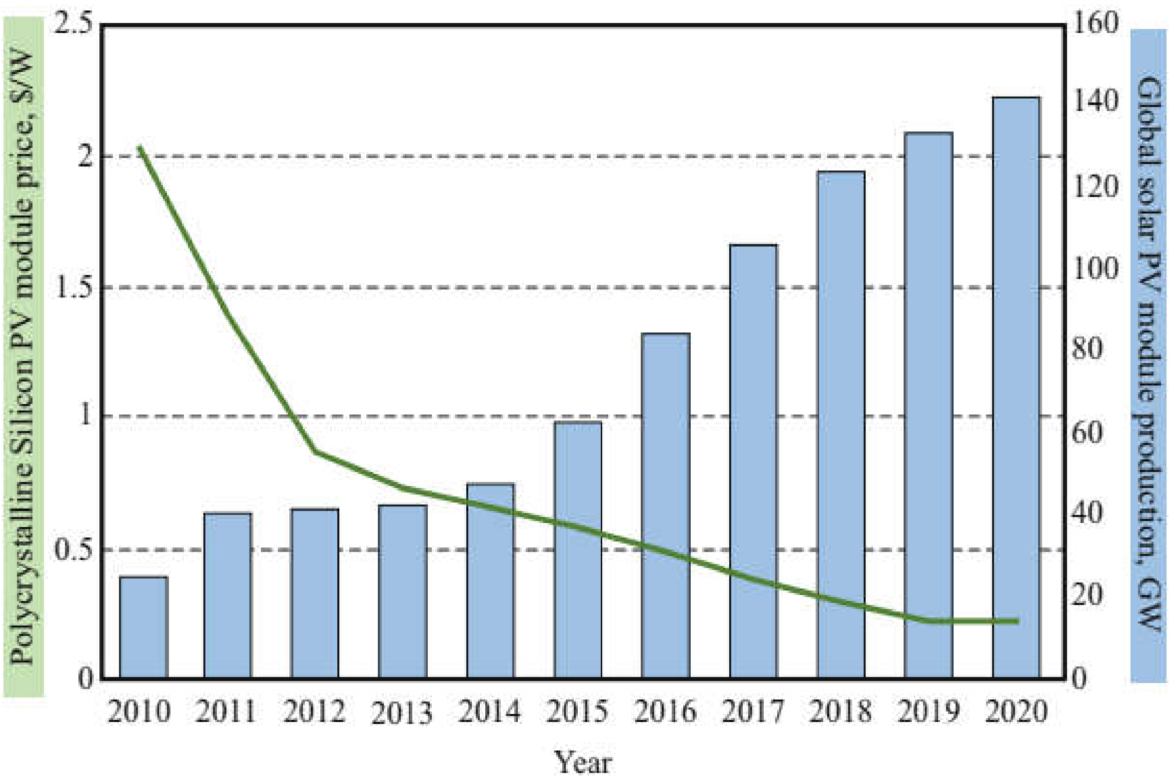

Figure (I.7): The production of polycrystalline silicon solar PV cells has increased considerably in the last decade alongside the sharp decline in the module cost **[36]**

I.6.4.The Efficiency of Solar PV

The efficiency of any energy conversion apparatus is the ratio of output power to input power. In solar PV modules, the ratio of the output electrical power provided by the module to the solar energy reaching the PV module's surface is the efficiency as represented in equation (I.1).

$$\textbf{Eff iciency}, \boldsymbol{\eta} = \frac{\textbf{Output electrical power}}{\textbf{Input solar power}} \times \mathbf{100\%} \qquad (\mathbf{I.1})$$

At present, the efficiency of single-junction solar PV cells ranges from 15 to 28%, with a maximum theoretical efficiency of 33.16% **[37]**. This implies that out of 100 Watts of energy incident on the solar module from the Sun, for example, only 15 to 28 Watts of energy are effectively converted into usable electrical energy, while the rest of the energy is lost as heat energy or lost through reflection and refraction. Each solar module contains many PV cells that are connected in series or parallel to make a PV module. The theoretical efficiency of both the cells and modules can be calculated using the formula above. It is to be noted that the efficiency of the module is less than that of the efficiency of the cell. It is because as the cells are connected to each other, the spacing increases due to additional mounting and accessories, which causes energy losses and reduces the module efficiency. The differences in the cell and module efficiencies are depicted in figure (I.8).

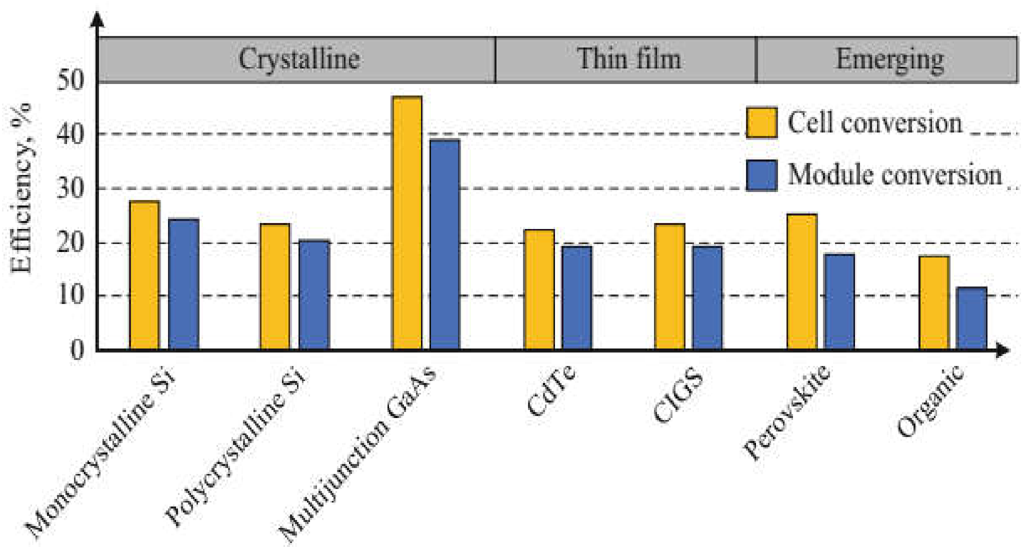

Figure (I.8): The efficiencies of the different types of PV cells and modules. It is seen that the efficiency of the cells is greater than the corresponding modules **[38]**

In 2020, the module efficiency record of the dominant PV technology (Silicon based polycrystalline) belonged to Hanwha Q Cells. This South Korean PV module manufacturer succeeded in converting 20.4% of the sunlight's power into electricity, where a majority of the incident irradiance was lost and not converted into valuable energy. The efficiency of solar PV systems is on the rise over the years, thanks to tireless research and development underway. Figure (I.9) demonstrates the rise in efficiencies of different types of PV systems, concentrated solar PV systems or concentrators, crystalline Silicon, and thin-film PV systems over the years.

Varies from the test conditions due to several factors such as orientation, tilt, shading, aging, overheating, and so on. It is evident from the figure that the efficiency of the concentrators has increased significantly, from about 14% in 1995 to 25% in 2020. The efficiency of these Modules are prognosticated to increase in the coming years. The increase in efficiency will also correspond with the decreasing prices of PV systems in the near future. However, the efficiency of practical solar PV systems.**[39]**

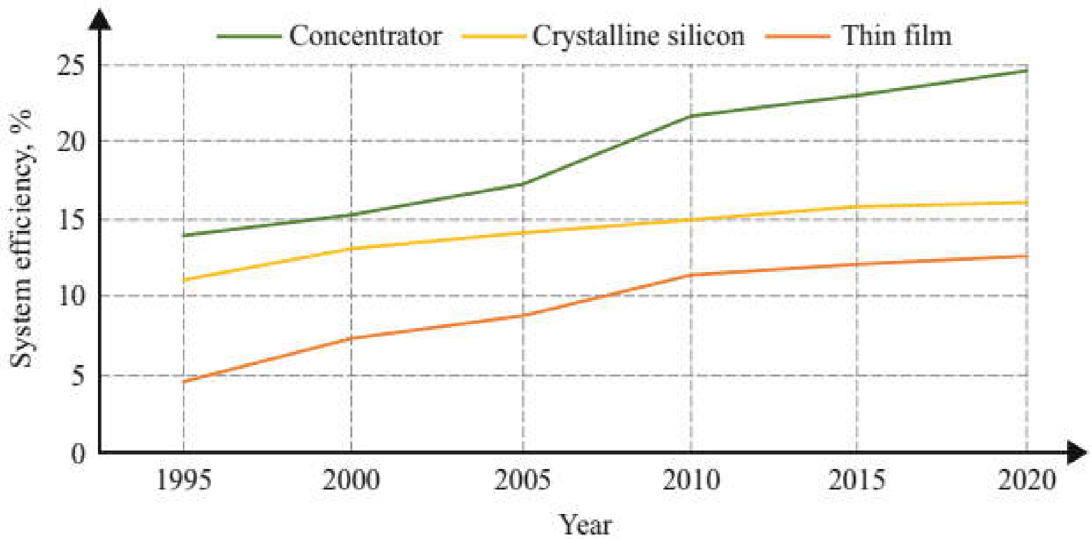

Figure (I.9): The efficiency of solar PV systems has been increasing with a positive slope **[39]**

I.7. Overview of Semiconductor Processing

For understanding the principle of the photovoltaic (PV) effect, it is essential to understand the physics of semiconductor processing first **[40]**. The semiconductor is considered the core of PV technology **[41]**. Using its inherent feature, the solar module can convert the exposed sunlight into a direct electrical current. Conductivity is defined as the characteristic of a material to allow the flow of electric current through it. It is the inverse of the electrical resistance and measured in Ω^{-1} or Siemens. Based on electrical conductivity, materials can be divided into three main types' conductors, insulators, and semiconductors **[42]**.

I.7.1. Conductors

Since the electrical current is a flow of electrons through a material, conductive materials show a minimum resistance toward the movement of electrons due to the redundant available free electrons in them. In other words, these materials facilitate the electronic movement from one atom to another once voltage is applied. Conductor materials, such as Aluminum and

Copper, are mainly used to manufacture cables or motor windings **[43]**. It is worth noting that all metals are considered good conductors of electricity and heat **[44]**.

I.7.2 Insulators

Unlike conductors, insulators have shallow conductive properties, which means that they display a high resistive behavior toward electron flow through the material due to the low number of free electrons **[45]**. Glass, rubber, ceramic, plastic, and some chemical alloys are a few examples of insulators. These materials are used as the cover of the conductive materials in cable or motor applications to protect the users or maintenance personnel from any electrical shock. Insulators are also used in high voltage applications to separate the conductive lines and the metallic structure of the power transmission pole **[46]**.

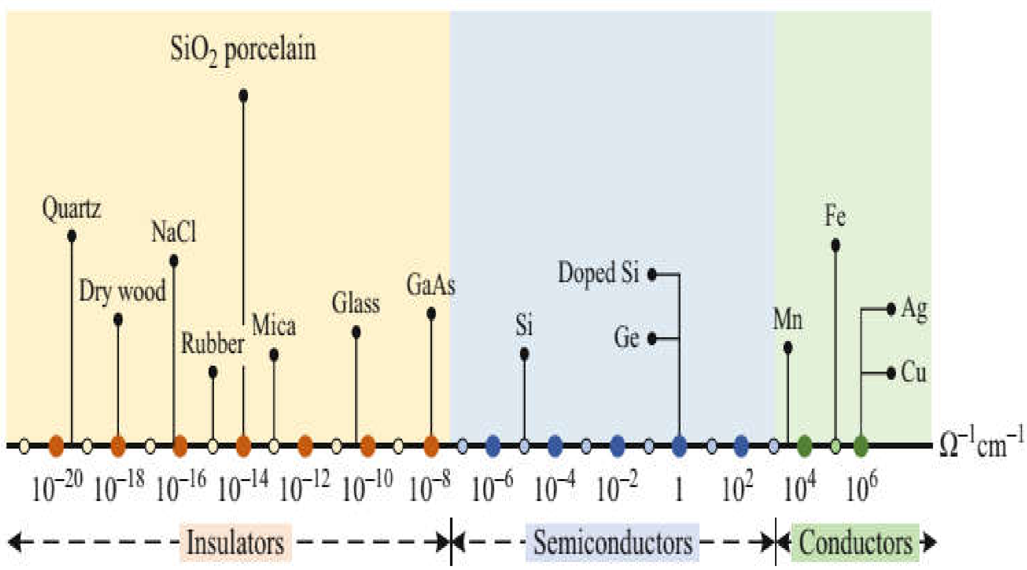

Figure (I.10): Conductivity values of different types of materials **[47]**

I.7.3. Semiconductors

Semiconductors such as Silicon (Si) and Germanium (Ge) can show both conductive and insulating behavior toward the flow of electrons based on the surrounding or internal circumstances. Temperature rise shifts the semiconductor material behavior toward conductive materials. Moreover, the intentional addition of impurity in materials to improve chemical performance through a process called doping is used to increase the material conductivity regardless of the temperature. The doping process is used in all semiconductor applications, such as in the manufacturing process of electronics (diodes, transistors, thyristors, etc.) and solar modules. Figure I.10 illustrates the conductivity of a variety of materials used in the electricity field. Resistivity value of the materials can also be derived from the figure by obtaining the reciprocal of the conductivity **[37].** Silicon is an essential material in the PV industry.

I.8. Factors Affecting PV System Performance (Irradiance, Temperature, Shading)

I.8.1. Doped Silicon

Silicon is a chemical element with 14 electrons in its atom that fills the first and second shell with two and eight electrons, respectively. The last four electrons, known as valance electrons, remain in the outer shell. These four electrons allow the Silicon atom to bond with the other four Silicon atoms. This process prevents Silicon from being conductive because all valance electrons are bonded with electrons of other atoms. In other words, there are no free electrons to make the material conductive. Therefore, the doping process is introduced to provide the material with an extra electron or hole by adding some dopant materials such as phosphorous, arsenic, and gallium. Through doping, a controlled amount of impurities (dopants) is added on purpose within a pure semiconductor (also called intrinsic semiconductor) for altering its electrical, structural, and optical properties. Si doping is done by the intentional addition of trivalent or pentavalent atoms, involving chemical reactions so that the introduced impurities form a covalent bond by sharing electrons with the Silicon atoms. **[47].**

I.8.2. Hotspot Heating

Hotspots appear when one or multiple solar cells connected in series are shaded by snow, lead, dirt, or hard shadows. The shaded solar cell(s) will not be able to generate the same current value as the neighboring illuminated cells. The shaded cell will limit the current to the value that it generates, causing a lot of energy loss or dissipation in the form of heat. Since the heat resulted by the energy dissipation takes place in a relatively limited and small area, the temperature rises near the defective zone starting from 1–80 ◦C and can increase more than 200 ◦C, causing one or several effects such as low damage, back sheet bubbles, glass cracking, or cell cracking when the temperature reaches more than 200 ◦C **[35].**

a)- Causes of Hotspots

Hotspot phenomena might show up or increase due to several causes, such as:

1. **Cell mismatch:** Series connection of solar cells having dissimilar current ratings can cause more energy dissipation as heat, which increases the temperature at some places of the cell, causing hotspots.
2. **Shading of solar cell:** Partial shading in any solar cell or any string of cells can be a major disadvantage in the solar cell, causing hig the shaded part. This increases more heat dissipation on the shaded solar cell, and thus hotspot is seen.
3. **Manufacturing defects:** The manufacturing of solar cells includes many steps, and fault in any step can cause a hotspot when the solar module is in use.
4. **Contaminating impurities:** Contaminating impurities such as dirt, sand, etc give rise to hotspots.
5. **Solar module installment defect:** While installing a solar module, it is necessary to check the roof conditions to avoid unnecessary shadings; otherwise, it causes hotspots.
6. **Imperfect screen-printing:** Screen-printing of solar cells includes many steps such as adding an n-type layer, isolating edges, and many more. Defects caused in these stages can disrupt the flow of electrons and electricity in between the two terminals, further causing hotspots. **[35].**

b)- Effects of Hotspots

Hotspots can have several detrimental effects on the solar PV system, which includes:

1. Increase of the equivalent resistance of the solar cell that disrupts the current flow.
2. Rise in temperature that may lead to a fire.
3. Rise in temperature that can melt the solar cells at small places, making holes.
4. Breakage and melting at many small places of the solar module can cause shattering.

All these defects should be detected using several methodologies before selling the module. However, some defective modules may still be available in the market and installed in a large utility-scale solar plant. So, how will the defective cell or module be detected? Nowadays, thermal cameras fixed on a drone take video shots to detect the hotspots before delivering the project to the end customers. The defective module can be changed, and more improved performance can be ensured **[48].**

I.8.3. Nominal Operating Cell Temperature

All the electrical characteristics of the solar modules are taken under specific standard test conditions, which may differ from the actual operating parameters. Solar modules are installed worldwide with different ambient temperatures, tilt angles, Sun positions, and solar irradiance. Due to the direct effect of these factors, it is essential to know the actual operating conditions such as the cell operating temperature, which is the actual temperature of the solar cell when the PV module is operating in some specific conditions, such as:

• Solar radiation: 800 W/m^2.

• Ambient temperature: 20 °C.

• Wind speed: 1 m/s.

The nominal operating cell temperature (NOCT) is defined as the temperature of open-circuited PV cells subject to the above conditions. Most manufacturers consider the value of NOCT as 41–46 °C. The ambient temperature can be obtained from the weather data. The cell temperature from the available ambient temperature can be determined using the formula in equation (I.2).

$$\mathbf{T_{solarcell}} = \mathbf{T_{ambient}} + \frac{\mathbf{NOCT-20}}{\mathbf{80}} \times \mathbf{S} \qquad (\mathbf{I.2})$$

Where S is the irradiance in m W/cm^2. An example of the determination of the PV cell temperature from the NOCT and solar irradiance is given below

Example

Determination of PV Cell Temperature from NOCT and Solar Irradiance) A solar module is installed in Cairo, Egypt, where the average daytime ambient temperature is 35 ◦C in June, July, and August. What is the average temperature of the PV cell when the irradiance is 80 m W/cm^2, and the NOCT is 46 °C?

Solution

• Ambient temperature, $T_{ambient}$ = 35 °C,

• Irradiance, S = 80 m W/cm^2.

• According to equation (I.2)

$$T_{solarcell} = 35 + \frac{46-20}{80} \times 80 = 60\ °C$$

So, the operating temperature of the solar cell is greater than the ambient temperature by 61 - 35 = 26 °C while the PV module is installed on an open backside mounting system.

However, the PV modules can be installed on different mounting systems that might block the cooling process provided by the wind, for instance, in a rooftop mounting system, where the module temperature is expected to be much higher than the open backside of the module. Therefore, a new terminology called installed nominal operating cell temperature has been introduced to consider the effect of the mounting configuration type on the solar module's actual temperature.

Table (I.1): Values of X based on the standoff/entry/exit height (whichever is minimum) **[49]**

Height	X
1 in.	11
3 in.	2
6 in.	-1
9 in.	-3
If there is channeling under the array	4

For rack mounting, the INOCT is 3° less than the NOCT. For direct mounting, the INOCT is 18° more than the NOCT. However, for standoff or integral mounting, the relation between INOCT and NOCT is determined using the formula shown in equation (I.3).

$$INOCT = NOCT + X \qquad (I.3)$$

Where X is the additional temperature in °C depending on the mounting type, which is determined from table (I.1). The standoff height can be measured from the roof to the frame of the module.

I.8.4. Degradation and Failure Modes

During manufacturing the solar cells or forming, testing, and installing solar modules, modules, in general, might be defected by reasons related to a failure due to human or machine error or an environmental reason associated with the geographical location of the solar station **[50]**. These defects can be summarized as the following:

1. Module Delamination: It is a systematic degradation for all PV modules that happens when adhesion between the front glass, the transparent encapsulate, and the back sheet occurs. It is caused due to the weak bonds between the components used in PV cells due to some environmental operating conditions such as moisture, thermal expansion, or aging **[51]**.

2. Junction box failure: These failures refer to the poor fixing materials of the junction box placed on the PV module's backside or the poor installation of the junction box **[52]**. Junction box failure causes water or moisture penetration to the electronic components inside the junction box, leading to corrosion in the metallic connections between the bypass diode and the terminals of the module. Moreover, bad bypass diodes soldering is the main reason for arc failure in the junction box, igniting a fire **[53]**.

3. Module glass breakage: It is mostly caused by a mechanical force such as snow load, ice, extreme thermal stress, wind, and hail drops **[54]**. In some conflict zones shrapnel might be most likely because of a module glass failure **[55]**.

4. EVA discoloration: EVA (Ethylene Vinyl Acetate) is one of the encapsulates used in the PV modules, which might lose its transparency due to discoloration resulted from environmental and aging conditions. UV radiation is also a main cause of browning or yellowing the EVA layer, which causes a major decrease in the module output **[56]**.

5. Cell cracks: The thickness of the solar cell is 150–200 μm, which makes it easier to be cracked with minimal mechanical force **[57]**. These cracks might be visible to the naked eyes or even needs special techniques to locate the cracked cell in a module. The damage is a possible failure during the processing and assembling of the solar module, which is not inspected instantly but later on. Cracks can start from the cell itself when the manufacturer starts connecting the ribbons (bus bars) on the cell during the soldering process or starting from the edge of the cell when a hard object bounces the cell **[58]**.

6. Burn marks: The main cause of this failure is the initial failure of the soldering bonds, ribbon breakage, or localized heating **[59]**. All these failures are physically converted to resistance, which increases toward the passing current through the cell, which will lead to extreme heat followed by unhandled thermal stress on the cell. These marks can also be a result of a failure in the bypass diodes, which leads to reverse bias on the cell, which will cause an electrical pressure on it with a burn mark that can be visually inspected **[60],[61].**

I.9. Current-Voltage (I-V) and Power-Voltage (P-V) Characteristics of PV Systems

I.9.1.The I-V Curve

The current–voltage characteristic curve, also known as the I-V curve, is an essential characteristic of solar cells, which is used to illustrate the relationship between the voltage and the current produced by the solar module under the standard test conditions. Under these conditions **[62]**, the solar module considers a voltage-controlled current source, which means that the I-V curve will have a constant current value while the voltage value might change based on the connected load **[63]**. As illustrated in figure (I.11), different resistive loads are connected to the same solar module.

The point of intersection between the I-V curves and the linear resistive load determines the operating power point **[64]**. The electrical behavior of the solar module is plotted in this curve, where the x-axis represents the voltage and the y-axis represents the current. Three important points are to be noted from this graph, which are as follows:

1. Open-circuit voltage
2. Short-circuit current
3. Maximum power point **[65]**

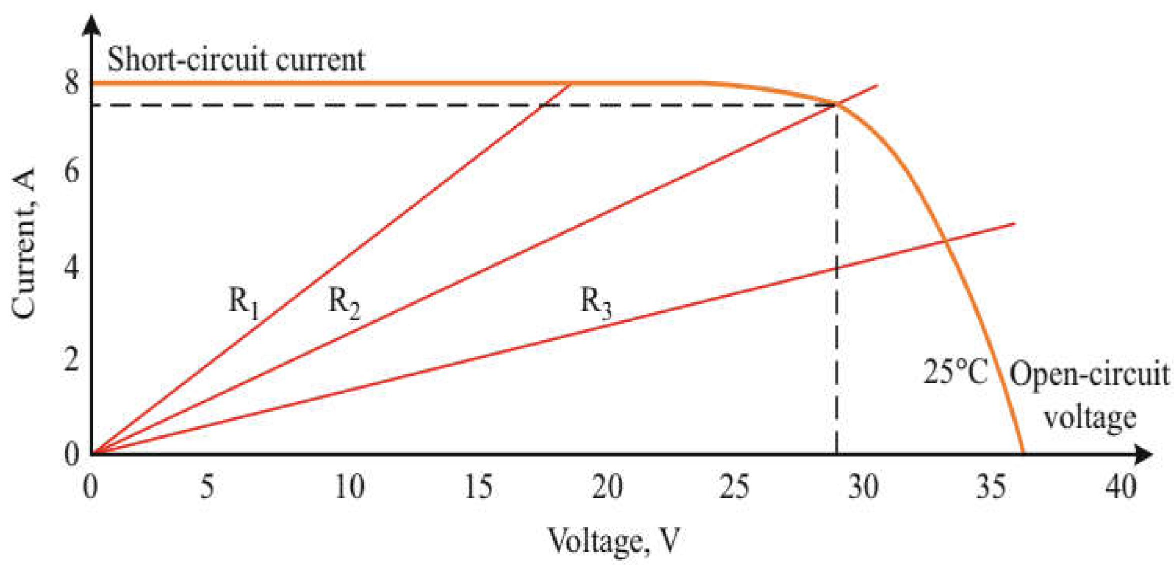

Figure (I.11): The effect of resistance on the I-V characteristic curve of the solar module with different resistive values, where $R_3 > R_2 > R_1$ **[47].**

This curve can be plotted by connecting the module to a variable resistor (potentiometer) and by raising its resistivity from 0 ohms (short-circuit, where the curve has its Y-axis intersection) to a very large value (open circuit, where the curve has its x-axis intersection) **[66]**. At this range, the resistor passes a resistance value ($R2$ in figure (I.11)) where the product of the current passing and the voltage drop reaches a maximum value. This point is called the maximum power point (MPP), and this is the point where the maximum power is obtained from the cell **[67]**. The I-V characteristic curve found in terms of diodes is not linear, in contrast to resistors, as shown in figure (I.12) **[68]**.

When the cathode (n-type) is connected to the negative terminal of the voltage applied, and anode (p-type) is connected to the positive terminal, the current passes through the diode, which is considered a forward-biased state of the diode but current does not flow as soon as the voltage is applied as there is a potential barrier between anode and cathode, which needs to be conquered **[69]**. This minimum required voltage varies for different materials, for instance, 0.7V for Silicon **[70]**. Once the applied voltage exceeds the barrier voltage of the diode, an astonishing rise of current is evident for a small increase in the applied voltage **[71]**. In the case of a reverse-biased situation, the cathode is connected to the positive terminal whereas the anode is connected to the negative terminal, which blocks the current flow through the diode **[72]**. A small amount of current, known as leakage current, flows across the circuit as no circuit is found in an ideal state as long as the voltage does not reach a particular voltage, named the breakdown voltage **[73]**. The breakdown voltage is the largest reverse voltage, which keeps the leakage current to a limited value **[74]**. An exponential current flow is evident once the diode crosses the breakdown voltage as the voltage goes out of control at this stage **[75]**. This large value of current is known as the avalanche current **[76]**.

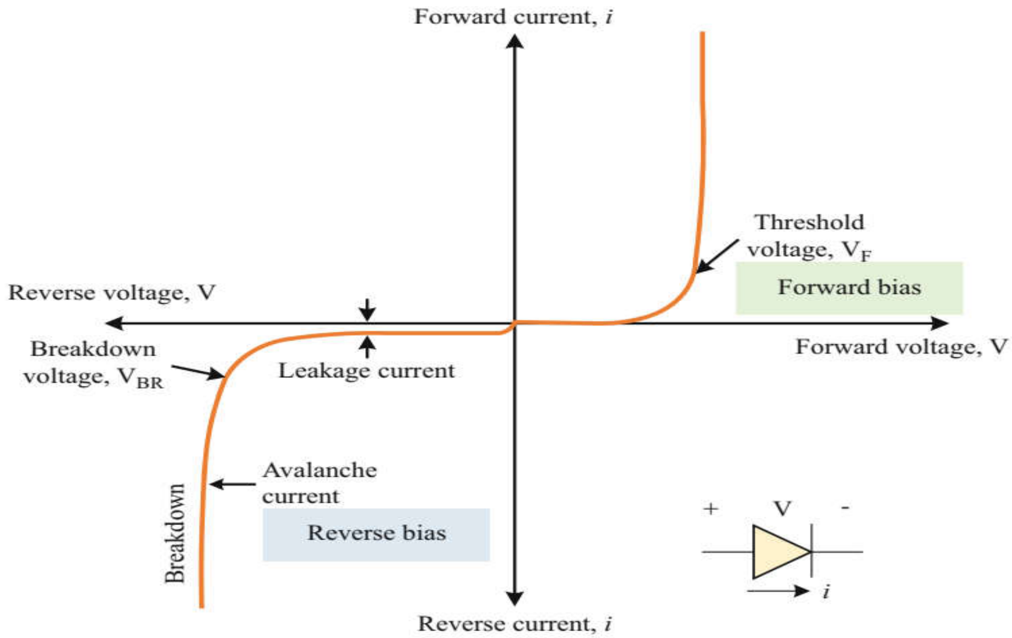

Figure (I.12): I-V characteristic curve of a diode **[47].**

I.9.2. Open-Circuit Voltage

The open-circuit voltage, V_{oc}, as marked in figure (I.11) is the measured value of the voltage between the solar module's terminals when an infinite-resistance load is applied. This voltage is the highest possible voltage that the module can produce. The V_{oc} can be measured using a digital multimeter connected in parallel with the solar module terminals, showing a positive value as the output. **[47].**

The output voltage value can be found in each module datasheet or determined from the I-V curve intersection between the x-axis and the curve. In figure (I.11), the open-circuit voltage value is found to be 36 V. **[47].**

I.9.3. Short-Circuit Current

The short-circuit current I_{sc}, as shown in figure (I.11) is the maximum current that it can produce and is measured when the two terminals are connected without any load **[77]**. This value can be obtained from the datasheet of each solar module or from the I-V curve, where the intersection between the y-axis and the curve represents the value of I_{sc} It is worth noticing that the module terminals' cables are designed to handle the high value of I_{sc}. Thus, the short-circuit test can be done by disconnecting the solar modules and testing it as a standalone system after ensuring that the multimeter range is equal or greater than the expected value of the short-circuit current **[78]**. The measured value of the I_{sc} is very high, which is not recommended to be applied by any energy sources, unlike PV. **[47], [79]**

I.9.4. Maximum Power Point

As known in electrical engineering, the power extracted from DC energy sources is obtained from the product of the current and voltage ($P = V \times I$). Therefore, there will be no useful power supplied to the load when the circuit is operating in the short-circuit or open-circuit conditions because one of the factors will be equal to zero.

In PV technology, the load regulates the operating point, where the solar module delivers both current and voltage in terms of the resistive load connected to its terminals **[80]**. Therefore, when a variable resistor (potentiometer) is applied to the solar module with an increasing value, the solar module keeps increasing the delivered power until it reaches the peak value and then starts declining **[81]**. The critical point at which the module delivers the highest possible power is called the maximum power point (MPP), and its x-axis and y-axis coordinates are known as voltage at MPP, V_{mp} and current at MPP, I_{mp}, respectively. In the example given in figure (I.13). R_2 is the resistive load value at which the module can operate at its MPP, where the values of I_{mp} and V_{mp} are 7.5 A and 28 V, respectively **[82]**.

The I-V characteristics curve with open-circuit voltage, short-circuit current, and maximum power point is illustrated in figure (I.14) **[83]**.

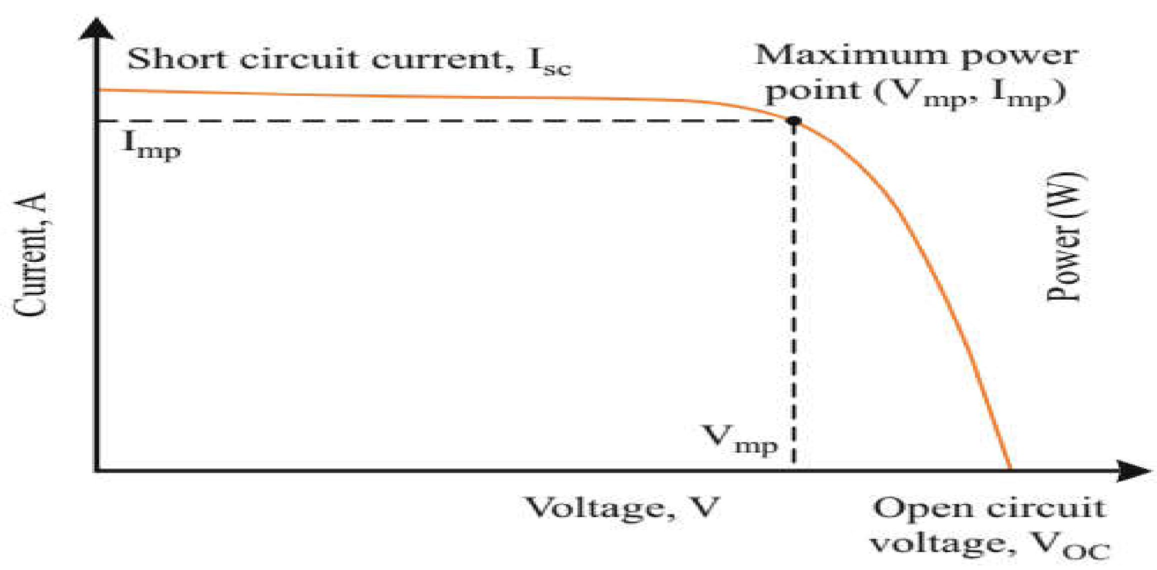

Figure (I.13): I-V characteristic curve of a solar module highlighting short-circuit current, open-circuit voltage, and maximum power point **[47].**

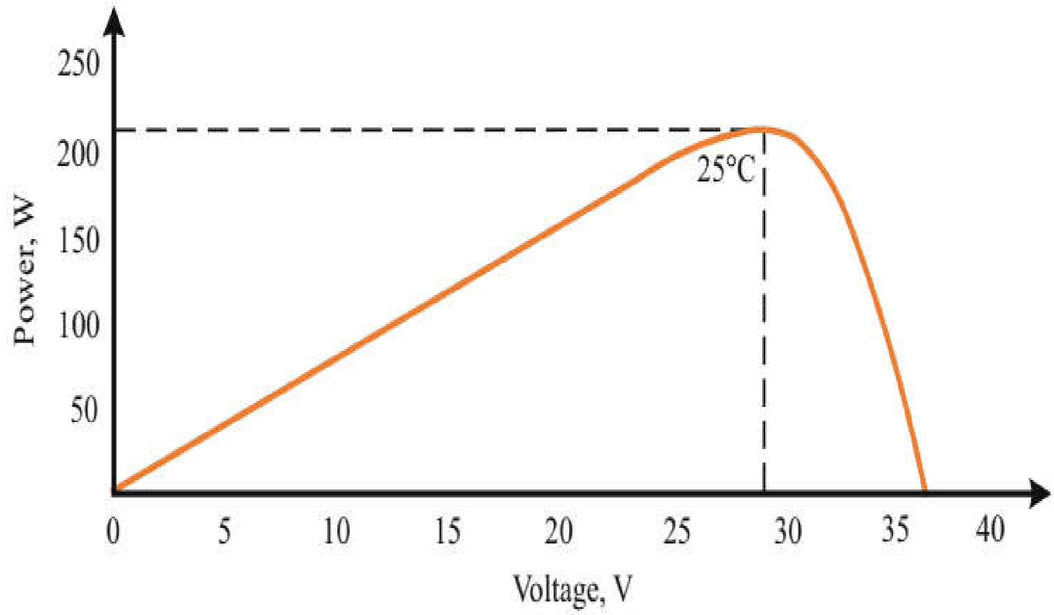

Figure (I.14): P-V curve of the solar module **[47].**

Table (I.2): Module specification **[47].**

V_{oc} (V)	I_{sc} (A)	I_{mp} (A)	V_{mp} (V)	M_{pp} (W)
36	7.9	7.5	28	210

I.9.5. The P-V Curve

The power–voltage or P-V curve (Figure.I.14) is provided by the manufacturer in the module datasheet, where the current is multiplied by the voltage to give the expected output power at every voltage dropped on the load. From both curves, we can extract several important values and list them in Table I.2 as the following:

I.9.6.Effect of Temperature

The solar module temperature is much warmer than the ambient temperature. All specifications and curves are taken under a cell temperature of 25 ◦C as one part of the standard test conditions. However, the solar module's operating conditions do not necessarily match especially in its temperature, where the modules can be installed in extreme cold or hot weather, such as in Canada or Mali, respectively. Therefore, it is important to define a few factors to define the relationship between the temperature and characteristics of the solar module, such as current, voltage, and power. The voltage, current, and power temperature coefficients discussed in the next three sections denote the relationship of these parameters with the temperature.

I.9.7. Voltage Temperature Coefficient (%/◦C)

The average value of the voltage temperature coefficient varies from -0.27 to -0.35%/°C. The negative sign reflects the negative impact on the open-circuit voltage as the temperature rises. This means that for 1 °C of temperature rise, the open-circuit voltage will decrease by a certain percentage in the mentioned range. This factor is crucial due to the nature of the power electronic devices that are always connected to PV modules, such as inverters. Each inverter has a threshold voltage value under which the inverter cannot operate. Thus, the solar array must be well-designed to compensate for voltage drops resulting from high temperatures to keep the power electronic devices in their normal operation ranges. For the purpose, the lowest possible voltage of power electronics devices or the highest possible temperature where the voltage is at its minimum value is considered. The percentage of gain or loss of the voltage can be calculated using equations (I.4) and (I.5):

$$\textbf{Operating voltage in } \% = \mathbf{V_{T-coefficient}} \times (\mathbf{T_{cell}} - \mathbf{25}) + \mathbf{100} \tag{I.4}$$

Therefore, the actual operating voltage is:

$$\mathbf{V_{specific\ temperature}} = \textbf{Operating voltage in } \% \times \mathbf{V_{STC}} \tag{I.5}$$

I.9.8. Current Temperature Coefficient (%/◦C)

The current temperature coefficient always has a positive value oscillating between 0.047 and 0.055%/°C in modern polycrystalline models. This means that for 1 °C of temperature rise, the short-circuit current will increase by a specific percentage in the mentioned range. However, the positive effect of the temperature rise on the current can be neglected compared to the negative voltage effect. The percentage of gain or loss of the current can be calculated using equation (I.6) and (I.7).

$$\textbf{Operating Current in } \% = \mathbf{I_{T-coefficient}} \times (\mathbf{T_{cell}} - \mathbf{25}) + \mathbf{100} \tag{I.6}$$

Therefore, the actual operating current is:

$$\mathbf{I_{specific\ temperature}} = \textbf{Operating Current in } \% \times \mathbf{I_{STC}} \tag{I.7}$$

I.9.9. Power Temperature Coefficient (%/◦C)

The impact of the power temperature coefficient is illustrated in figure (I.16) the output power is inversely proportional to the temperature. The coefficient value varies from -0.45 to -0.3%/°C, where the coefficient value defines the quality of the silicon based module. The negative sign implies that with 1 °C temperature rise, the output power of the solar cell decreases by a certain percentage within the mentioned range. The percentage of gain or loss of the power can be determined using equation (I.8).

$$\textbf{Operating Current in } \% = \mathbf{P_{T-coeff\ icient}} \times (\mathbf{T_{cell}} - \mathbf{25}) + \mathbf{100} \qquad (\mathbf{I.8})$$

In standard solar cell datasheets**,** it is possible to find the values of the voltage, current, and power coefficients in terms of %/K, where K is the temperature in Kelvin. However, the difference in each degree temperature is the same in Celsius scale and Kelvin scale. Therefore, the same value can be used irrespective of the values expressed in terms of %/K or %/°C.

Figures (I.15) and (I.16) illustrate the difference between I-V and P-V characteristic curves that the manufacturers give in the datasheet and the actual Curves that the module works at based on the operating cell temperature, the irradiance is fixed to 1000 W/m^2.

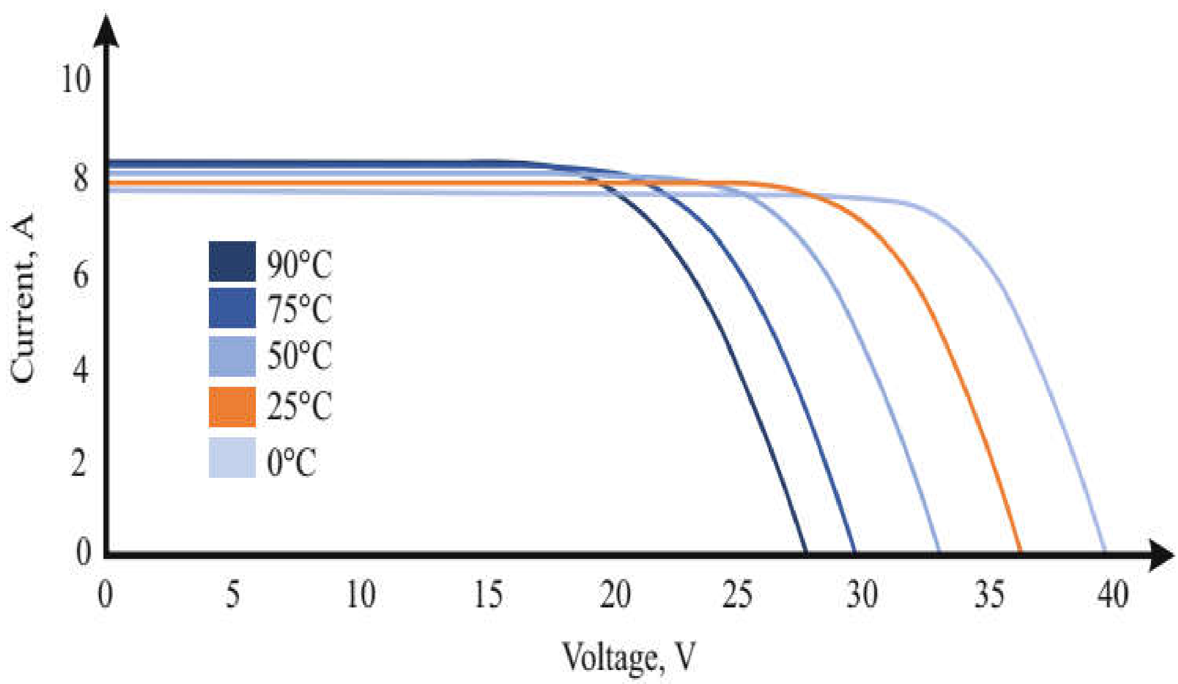

Figure (I.15): I-V curve at different temperatures **[47].**

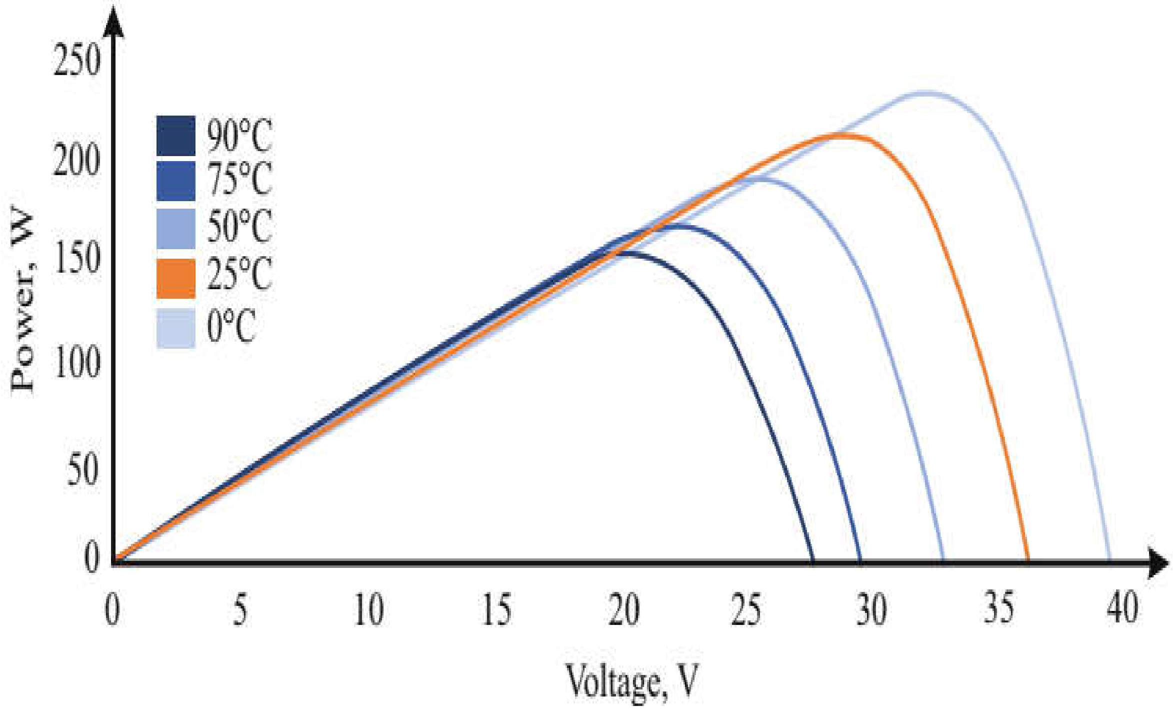

Figure (I.16): P-V curve at different temperatures **[47].**

Table (I.3) shows the response of voltage, current, and power of a solar module at different temperatures, while it can be visualized by figure (I.17).

Table (I.3): Actual gain and losses of current, voltage, and power based on V_{oc}, I_{sc}, and power coefficient at different temperatures **[47].**

Ambient temperature, °C	***Cell temperature, °C***	***V_{oc} coefficient, %/°C***	***Actual operating voltage percentage of the nominal voltage, %***	***I_{sc} coefficient, %/°C***	***Actual operating current percentage of the nominal current, %***	***Power coefficient, %/°C***	***Actual operating power percentage of the nominal power, %***
-20	6	-0.29	105.51	0.049	99.099	-0.39	107.41
-10	16		102.61		99.559		103.51
0	26		99.71		100.049		99.61
10	36		96.81		100.539		95.71
20	46		93.91		101.029		91.81
30	56		91.01		101.519		87.91

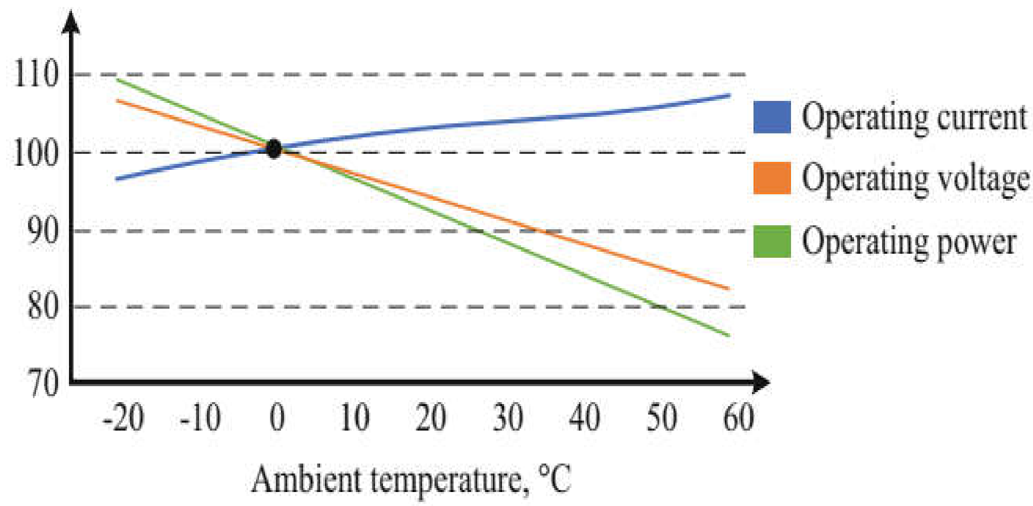

Figure (I.17): The percent gains/losses of the operating current, operating voltage, and operating power of a solar module at different temperatures **[47].**

I.9.10. Effect of Irradiance

Solar irradiance factor (x) has a simpler and more straightforward effect on solar cells or modules, where it has a negligible effect on V_{oc} and a proportional effect on I_{sc} as illustrated in equation (I.9) and figure (I.18).

$$\mathbf{I_{scx\,kw/m^2} \equiv \chi \times I_{sc_1\,kw/m^2}} \qquad \mathbf{(I.9)}$$

Where x varies from 0 to 1.25. The current in this equation refers to the short-circuit current at a specific irradiance measured in kW/m^2.

I.9.11. Fill Factor

The fill factor (FF) can be used to compare several modules together where the higher the FF, the better is the electrical performance by the PV module. FF is the ratio of the maximum power produced by the solar module to the product of V_{oc} and I_{sc} as equation (I.10) shows.

$$\mathbf{FF = \frac{P_{max}}{I_{sc} \times V_{ac}} = \frac{I_{mpp} \times V_{mpp}}{I_{sc} \times V_{ac}}} \qquad \mathbf{(I.10)}$$

The ratio between the surface area covered by the filled rectangular and the outer dashed rectangular of the I-V curve also represents the fill factor**.** Figure I.19 illustrates the fill factor of a solar module. The value of the FF ranges from 50–82%. For a Silicon PV cell, the FF is usually about 80%. The value increases with a higher shunt resistance and a lower series resistance. A higher value of FF is desired because it is a direct indicator of the quality of the PV cell.

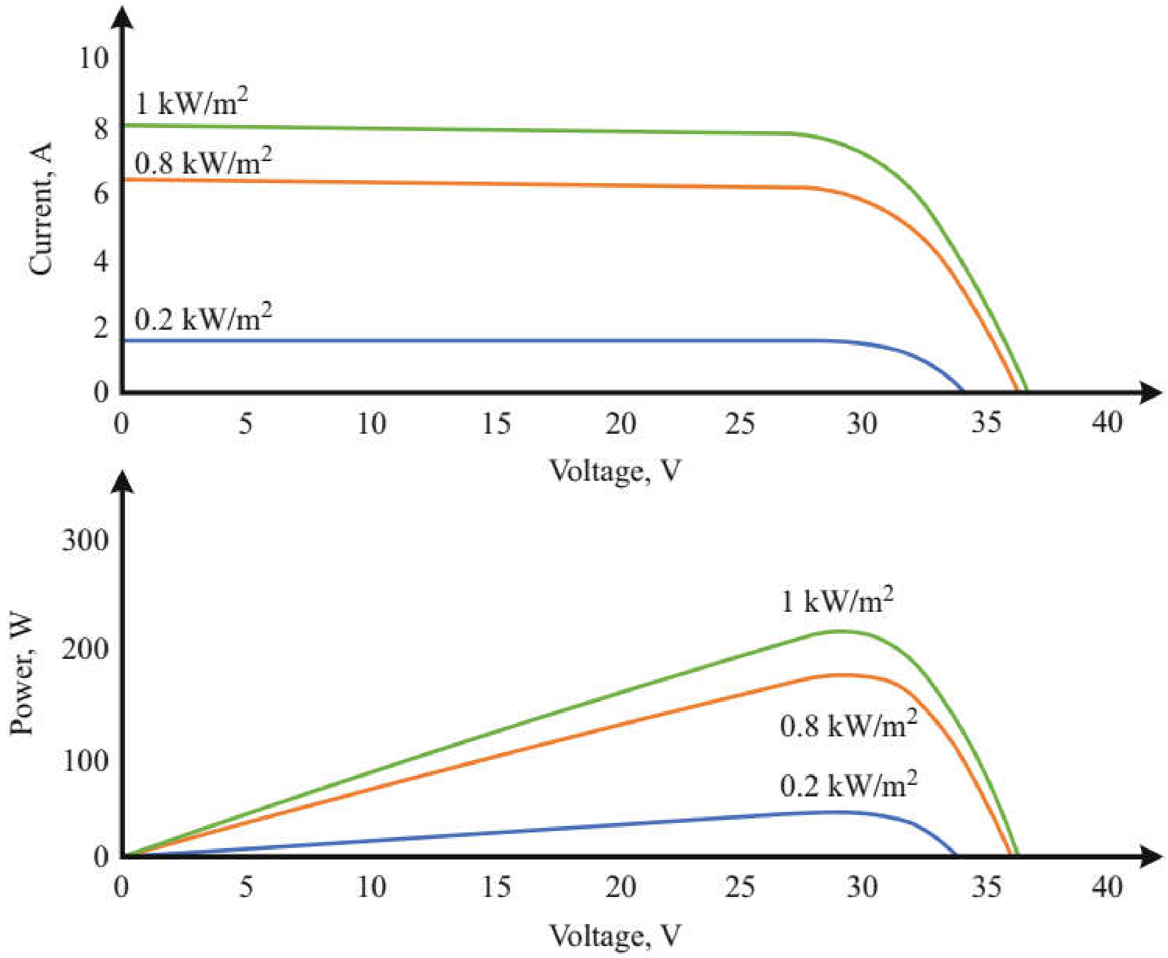

Figure (I.18): I-V and P-V curves under different irradiance values **[47].**

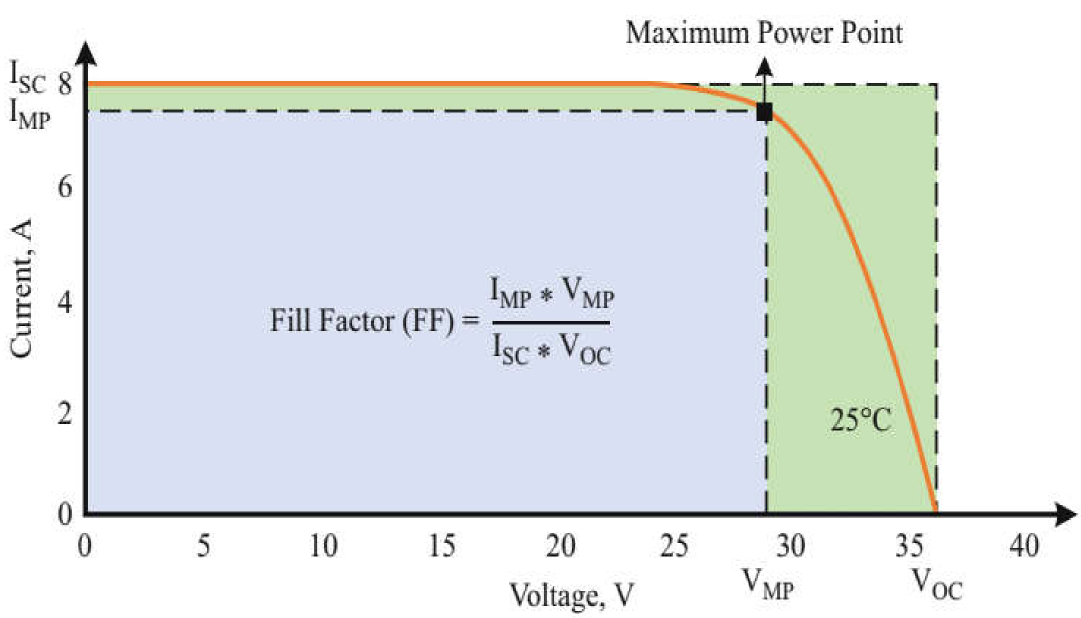

Figure (I.19): Representation of fill factor of a solar module **[47].**

I.10. Conclusion

Simply put, photovoltaic (PV) systems are the foundation of the world transition to renewable energy and a clean and adequately low-cost solution to the world growth in energy demand. By directly transferring solar radiation into electricity using semiconductor material like silicon, PV systems offer a clean alternative to fossil fuels that limits greenhouse emissions and global warming. The rate of solar technological innovation and price decline, i.e., 68% decline in the cost of polycrystalline module from 2014 to 2019 **[84]**, have increased in scale and pushed the cost of solar electricity to record low. In spite of efficiency losses, temperature sensitivity, and failure mechanisms such as hotspots and delamination, system performance and reliability improvements continue as a result of research and development. Into plans of all sizes, from low-density residential building to utility-scale solar farms, PV systems are both available and diverse and full of promise. Maybe it would be witnessed by the steeply rising peak of worldwide installation, particularly in nations like China, Europe, and the US, that solar PV can be the driver to bringing about an era of sustainability for energy. However, regional imbalance and collective take-up hold the secret to opening up the solar power prospect for every region of the world. Finally, ongoing PV technology innovation and enabling, visionary policy and solutions will be compelling drivers for propelling the world towards cleaner, more sustainable energy systems **[85]**.

CHAPETER II

Maximum Power Point Tracking (MPPT) Techniques

II.1. Introduction

With time, the conventional fossil fuels for generating electric loads are depleted, so efforts are made to harness photovoltaic (PV) solar energy to serve the continuously increasing electric loads. The energy conversion efficiency of PV modules is very low, while they are expensive in price. This calls for operating the module at the maximum power point at all operating conditions. There exist numerous maximum power point tracking techniques in today's market to maintain the operation of PV module at maximum power such as off-line techniques, on-line or hill-climbing (HC) techniques and artificial intelligence (AI) techniques. Numerous approaches for improving, adapting, and optimizing these techniques have been published. However, they differ in many aspects such as tracking speed, tracking accuracy, steady-state efficiency and dynamic efficiency, number of sensors used, complexity, and cost. These MPPT techniques fail or deviate from tracking the correct maximum power point (MPP) under sudden or ramp variations of solar irradiation and ambient temperature as well as under partial shading with oscillations around MPP. From 1954 to 2018, all the researchers focused on MPPT, which is the main target of this chapter to follow up the history of development maximum power point tracking in PV systems as well as exploring the advantages and disadvantages of the many proposed MPPT methods. **[86]**

II.2. Introduction to MPPT and Its Importance

In 1954, Fuller et al. had received a patent-pending prize in physics for their first practical photovoltaic cell. When the PV module is directly coupled to a resistive load, DC lamp as shown in figure (II.1), or to a dynamic load, DC motor as shown in figure (II.2) , the module output current (I) and voltage (V) depend on the module's operating point. The module's operating point is located at the intersection of module and load I–V curves as shown in figure (II.3) Unfortunately, the module I–V curve is non-linear with only one maximum power point (MPP) at which the intersection rarely occurs. In addition, the module I–V and P–V curves change under varying irradiation and ambient temperature conditions making the new location of the MPP as shown in figure (II.4). When the module/array is partially shaded, the P–V curve has multi-peaks as shown in figure (II.5). Starting in 1954, the maximum power point tracking (MPPT) is the aim of researchers to enhance efficiency and improve the performance of the PV systems. MPP trackers are divided into two types: mechanical single and dual-axis trackers and electrical trackers. The mechanical tracker "sun tracker" is a way to direct the PV module to follow the sun. However, this type is complex and costly in implementation and has low efficiency. Therefore, all attempts by scientists have been directed toward electrical tracking. Electrical MPPT techniques are classified into three families:

✓ **Off-line techniques:**

such as fractional open-circuit voltage (FOCV) and fractional short-circuit current (FSCC) techniques.

✓ **On-line hill-climbing (HC) techniques:**

such as perturb and observe (P&O) and incremental conductance (INC) techniques.

✓ **Artificial intelligence (AI) techniques**

including fuzzy logic control (FLC) technique, artificial neural network (ANN) technique, particle swarm optimization (PSO) technique, and genetic algorithm (GA). **[86]**

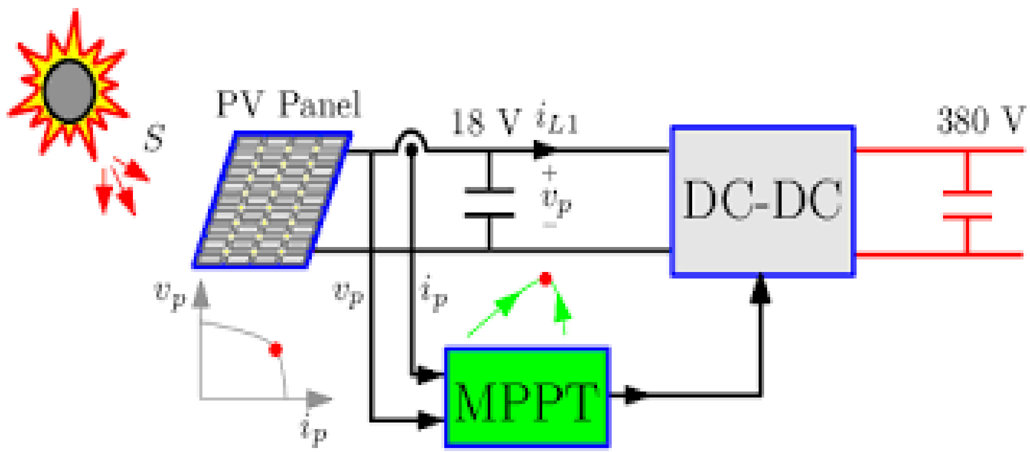

Figure (II.1): PV panel connected to a resistive load (R) **[86]**

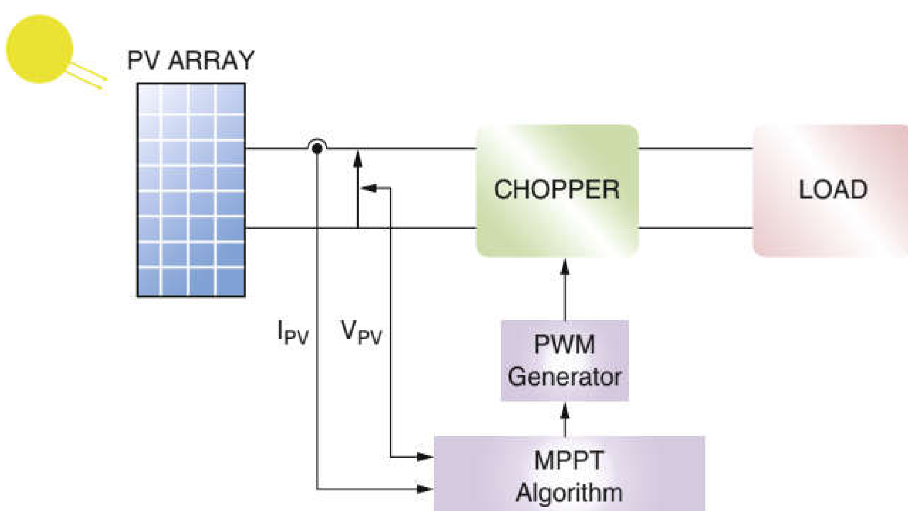

Figure (II.2): PV panel connected to a dynamic load **[86]**

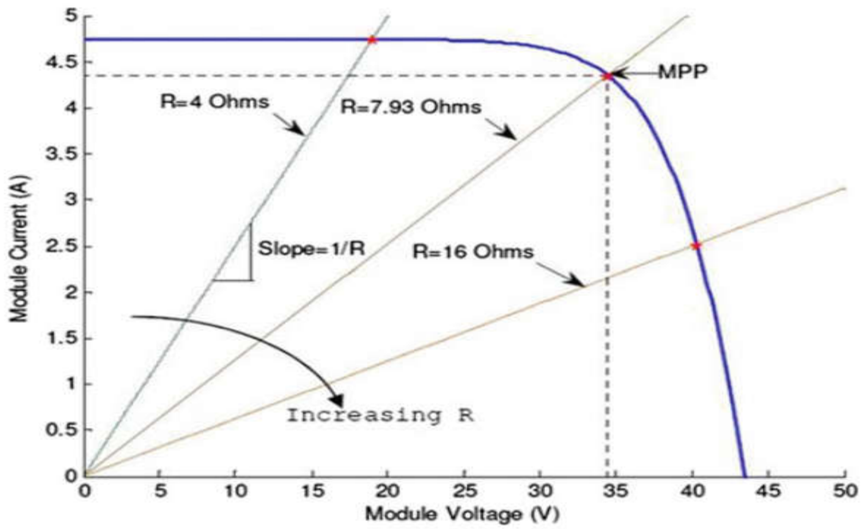

Figure (II.3): Location of operating point as influenced by load resistance (R) **[86]**

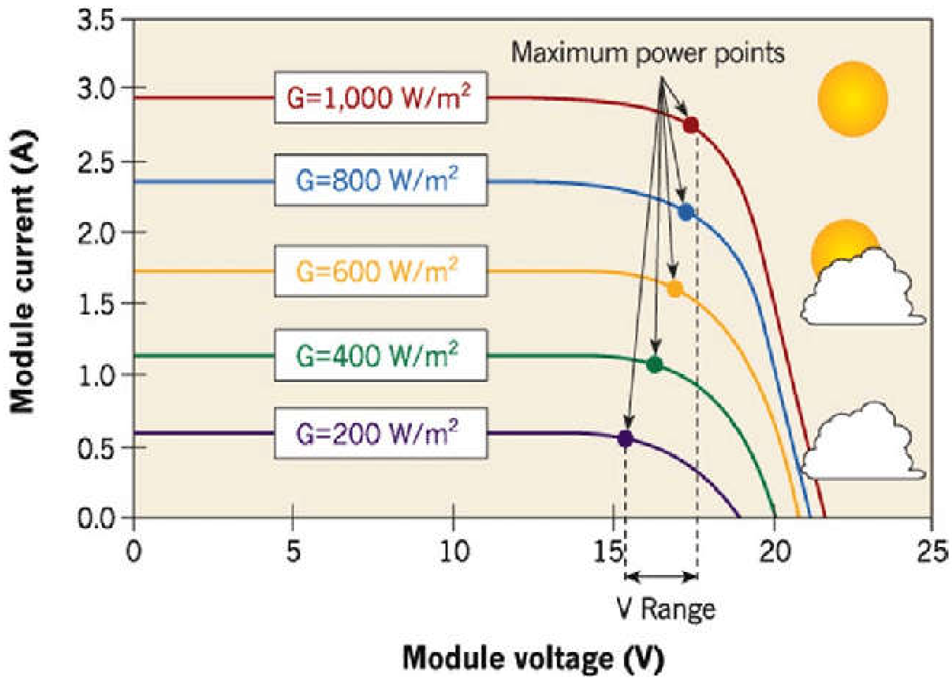

Figure (II.4): Location of MPP as influenced by irradiation level **[86]**

These MPPT techniques fail or deviate from tracking the correct maximum power point (MPP) under sudden or ramp variations of solar irradiation and ambient temperature as well as under partial shading with oscillations around MPP. **[86]**

II.3. Classical MPPT Techniques

The PV cells and modules generate different power based on different environmental conditions like wind velocity, shading and angle of solar insolation. Because of that, the generation of maximum power is not guaranteed at all electrical loads **[87].** MPPT techniques are equipped with proper controllers to extract maximum available power from PV configurations. There are various types of MPPT techniques used to run PV modules on maximum power. Nevertheless, the efficiency of the particular technique depends on its tracking ability in instantaneously changing weather conditions. So, depending on the tracking nature in PSC's, these techniques are classified. Discussion is done on all classified techniques and categorized into the following classification, as shown in figure (II.5). **[88]**

- Classical MPPT.
- Intelligence MPPT.
- Optimization MPPT.

For classical MPPT**,** the techniques include incremental conductance (INC), fractional open-circuit voltage (FOCV), fractional short circuit current (FSCC), hill climbing (HC), perturb and observe (P&O), variable step size (P&O), constant voltage (CV), adaptive reference voltage (ARV), DC- link capacitor droop control based MPPT, ripple correlation control (RCC), look up table method, linearization based MPPT, and online-MPP search algorithm. These techniques are easily implemented because of their less complexity in the algorithm. They are most efficient for uniform irradiation conditions as the PV will generate only one GMPP in these conditions. Nevertheless, these algorithms have rapid oscillations around the MPP, and these results in the loss of power. Furthermore, above all these classical strategies neglect the effect of (PSCs) results in failing of tracking the genuine MPP. **[89]**

Intelligence-based techniques includes fuzzy logic control (FLC), artificial neural network (ANN), sliding mode control (SMC), Fibonacci series based MPPT, and Gauss–Newton approach based MPPT. These techniques are intended for dynamic weather changing conditions with utmost high accuracy. Their tracking efficiencies, as well as tracking speeds, are so high. These methods also suffer from huge control circuit complexity and big data processing for the training of the system beforehand. Fuzzy logic control (FLC) is a striking technique, does not require the system knowledge for the MPPT implementation. ANN is a faster tracking technique but needs a huge amount of data (for training) to enhance the accuracy of tracking. It uses dynamic irradiation and temperature as input and stores them as data sets. SMC is the advanced technology, whose implementation is easier with tracking speeds at higher rates. Fibonacci and Gauss–Newton are two methods, emerging at a faster rate because of their intelligence in tracking MPP by updating the searching range instantaneously. **[90]**

Optimization-based techniques include PSO, grey wolf optimization (GWO), cuckoo search CS-based, ant-colony optimization (ACO), and artificial bee colony (ABC). These methods tend searching true MPP in dynamic environment conditions also. PSO method is a faster tracking algorithm with reduced steady-state oscillations. Moreover, the implementation of these techniques is easier with the help of low-cost microcontrollers. GWO can search for optimum point of working at a faster as if like wolf continuously searching for its prey. This GWO is the best evolutionary technique with independence on system knowledge. CS-based MPPT is also a bio-inspired algorithm uses the nature of brood parasitism and thereby implementing levy flight methodology to obtain optimum MPP point. ACO and ABC are two emerging methodologies that also utilize the evolutionary-based algorithm implementation. These techniques require fewer temperature and voltage sensors than classical ones. **[91]**

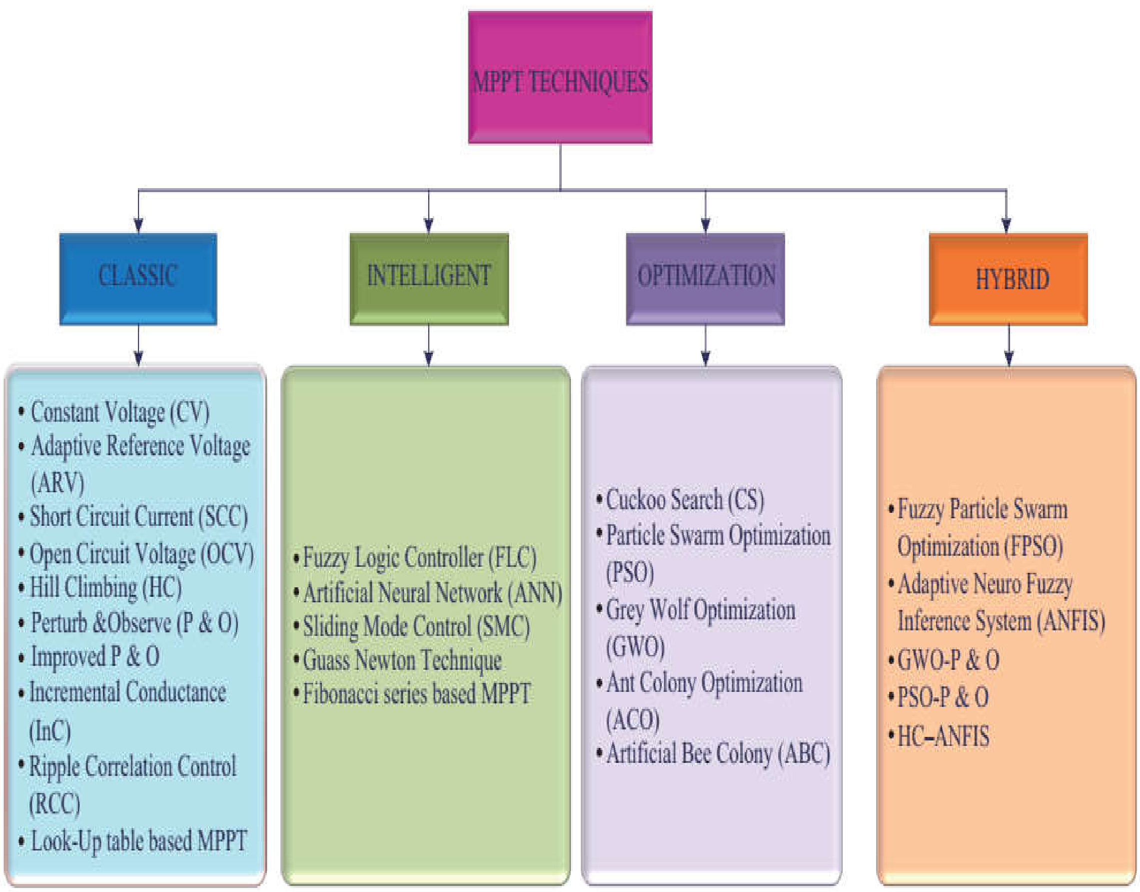

Figure (II.5): Basic classification of tracking techniques **[91]**

II.3.1. Constant voltage (CV)-based MPPT technique

The ideal working purpose of this MPPT is to make the PV power to operate near the MPP by controlling the PV voltage and comparing it to a fixed reference voltage (RV) equivalent to the VMPP. This technique of CV used for uniform irradiation conditions and neglects the effect of both insolation and temperature. This CV technique estimates MPP point a bit far away from the genuine MPP. Thus, the working point is not coordinating the MPP, and consideration of different topographical positions are necessary for the optimum RV to decrease the error value. The schematic block diagram of the CV MPPT technique is shown in figure (II.6). In this method, the required sensors are limited to one, for voltage measurement in order to have the PV module voltage V PV to get the proper duty ratio for the converter **[92]**. The method is simple, fast and easy to implement but shows limited precision. This technique requires measuring the V_{ocat} regular intervals. Moreover, this technique applies to the condition where temperature variation is less done the practical implementation of the novel MPPT algorithm using CV constant current (CVCC) DC–DC converter, which is enabling the researchers to find the optimum point precisely. **[93]**

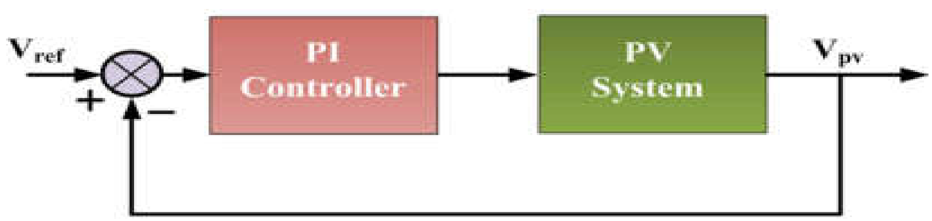

Figure (II.6): Schematic block diagram of CV MPPT technique **[93]**

- ✓ **Advantages**
- Easy to implement
- CV uses one voltage sensor; hence, the cost will be reduced
- Economical and more efficient during low radiation
- ✓ **Disadvantages**
- Priori data is needed
- Less accuracy and efficiency due to approximation (V_{MPP} = 0.76% V_{oc}), which is not right in some cases

II.3.2. Average Rectified Value MPPT technique

Average Rectified Value (ARV) based MPPT system is the extension strategy to CV technique as it has the presentation of flexibility to dynamic climatic conditions. The deliberate radiation and temperature levels adjust the RV for MPPT. The schematic block model of ARV MPPT method is given in figure (II.7). The working scope of the radiation at a given temperature is separated into several divisions, and the comparing RV is recorded off-line in a truth table. The error between the reference and assessed PV voltages is compensated using the corresponding proportional integral (PI) controller to generate a reasonable duty cycle proportional to the fitting converter that is used. **[94]**

The proposed ARV procedure does not require transient interruption of the PV module. It considers the climatic conditions by estimating the temperature (T) and irradiation (G) levels utilizing two additional sensors than the traditional CV system and one extra sensor than P&O method makes this system a bit costly. However, the increase in efficiency compensated for this factor. **[94]**

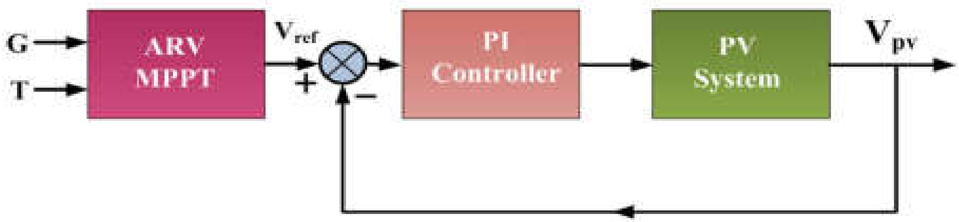

Figure (II.7): Schematic block diagram of ARV MPPT technique **[94]**

II.3.3 Fractional short circuit current (FSCC) MPPT

This technique, also called as an off-line method, appeared to be simple in its algorithm implemented in MPP tracking procedures. Usually, it happens that current at MPP (I_{mpp}) happens at the proximity of short circuit current I_{sc} under some random environmental conditions**.** The current at MPP can be calculated by using the equation (II.1).

$$\mathbf{I_{mpp} = K_i \times I_{sc}} \qquad (\mathbf{II.1})$$

Where factor K_i ranges in between 0.75 and 0.9. The implementation of this technique is shown in figure (II.8). **[95]**

This technique is appropriate for low current and high voltage applications. Above condition uncovers that this strategy is just an approximation, and consequently, it does not work at definite MPP. Besides, the whole day operation requires irregular estimations of I_{sc}, resulting in the loss of power. A novel hybrid method of FSCC with P&O method is explained**.** respectively. Advancement in this technique is implemented by connecting embedded card directly to the Simulink environment and without using the irradiation sensor. **[96]**

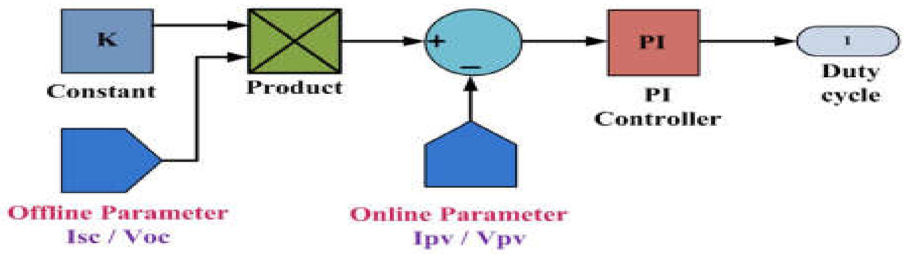

Figure (II.8): Block diagram of Off-line MPPT method **[96]**

II.3.4 Fractional open circuit voltage MPPT

In this method, as it is named as an off-line parameter or the FOCV MPPT, open circuit voltage V_{oc} is considered as an off-line parameter as given in the same Figure. II.9. the relation between (V_{mpp}) and V_{oc} is given as:

$$\mathbf{V_{mpp} = K_v \times V_{oc}} \qquad \text{(II.2)}$$

The estimation of K_V is somewhere in the range of 0.7–0.8 **[97]** .This strategy is additionally founded on estimation. It is most appropriate for low voltage, high current applications as it is mostly based on the rule of approximation. As the operation of this method depends on the estimation, it is then viable for uniform irradiation conditions. The drawback in this method will be the irregular measurement of V_{oc}, which results in unnecessary usage of power. After getting the approximated value of V_{mpp}, a closed-loop controller is used to reach the desired voltage. Since the connection is just an estimation, the PV array, in fact, never works at the MPP coined an improved FOCV technique named ‘smart timer’, which can able track MPP in PSC's also. This smart timer estimates the frequency of the sample and holds the circuit. The hardware implementation of this technique is done, and effectiveness is compared with conventional FOCV. This technique holds good for low power consumption applications, so had an area of broader scope. **[98]**

II.3.5. Perturb and observe (P&O) MPPT

The P&O is one of the most used MPPT techniques in the literature and easily implemented in practice by most of the authors**.** This technique relies upon the trial and error method in searching and following the MPP. P&O calculation compares the power obtained in two points on a P–V curve and then compares the position of voltage. Then the voltage is updated accordingly (either to left or right of P–V curve) in order to track the MPP. Block diagram representation of this P&O technique is shown in figure (II.9). **[95]**

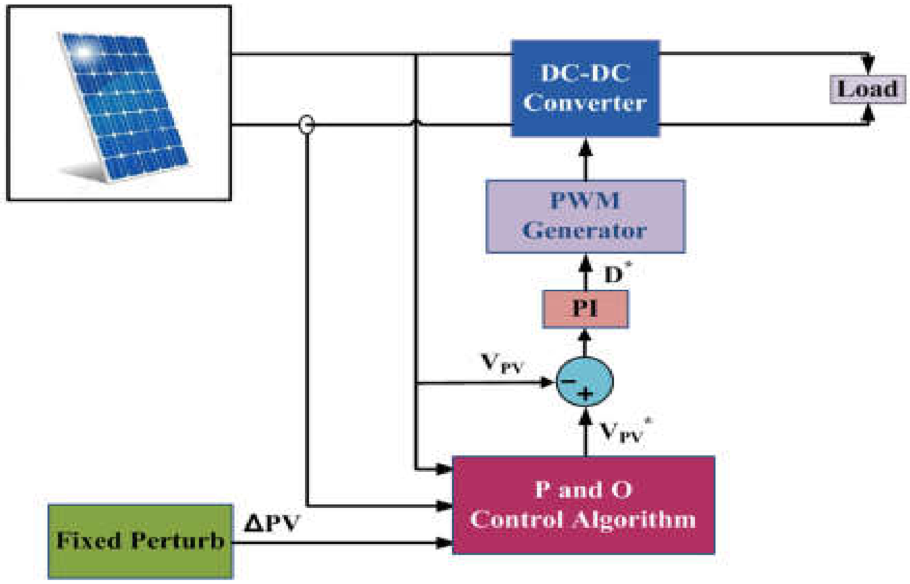

Figure (II.9): Conventional P&O with fixed perturbation step **[95]**

Fundamentally, this strategy checks for the change in PV cell power (dP), then checks for the sign of PV cell voltage (dV). According to the values obtained, D is perturbed. P–V curve data is used to analyses the actual movement of the operating point. Depending on the curve, if the (dP/dV) is positive, then the actual point seems to be in the left half of the MPP; else in negative half. Moreover, this process proceeds until (dP/dV) equivalents to zero.

Perturb and observe (P&O) technique uses the measured PV voltage, current, and the output power and then takes the decision to increase or decrease the voltage using the duty ratio of the DC–DC converter until the MPP is tracked. Figure (II.10) shows the flowchart of P&O technique. The logic of the P&O is to perturb the PV output voltage and observe the power change. If the PV power captured increased, the perturbation decision should be kept in the same direction regardless of whether the PV voltage increases or decreases until MPP is tracked, whereas if the output power decreased, the voltage increment (*V*) should be reversed. The maximum power is extracted when dP/dV = 0 **[99].**

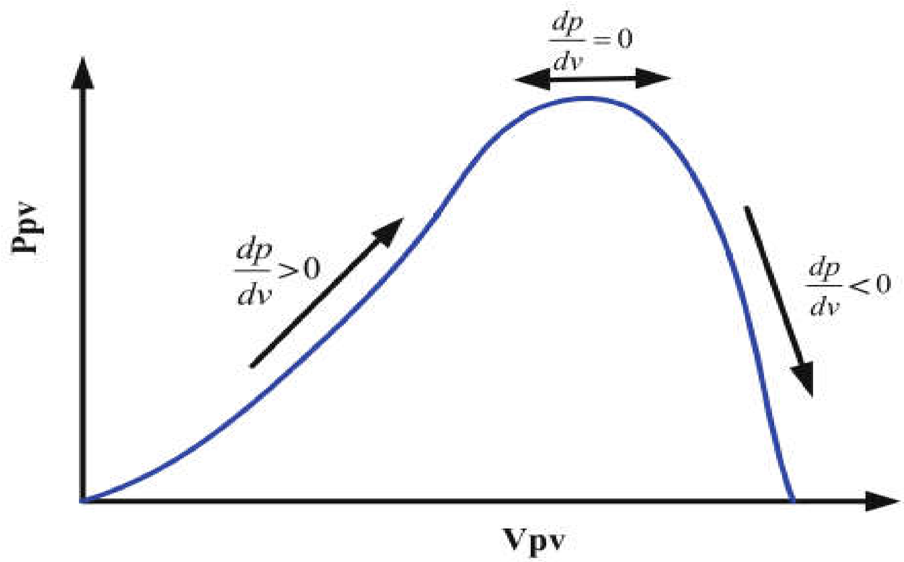

Figure (II.10): P–V characteristic of the PV array explaining the P&O concept **[99]**

The algorithm flow chart is shown in figure (II.11). At the extreme point of any P–V curve, MPP is given by equation (II.3). The position of MPP (either left or right) is determined by using same equation (II.3).

$$\left.\begin{aligned} &\frac{\mathbf{dP_{PV}}}{\mathbf{dV_{PV}}} = \mathbf{0} = \mathbf{MPP} \\ &\frac{\mathbf{dP_{PV}}}{\mathbf{dV_{PV}}} > \mathbf{0} \text{ Left side of MPP} \\ &\frac{\mathbf{dP_{PV}}}{\mathbf{dV_{PV}}} < \mathbf{0} \text{ Right side of MPP} \end{aligned}\right\} \quad (\mathbf{II.3})$$

Finally, the advantages and disadvantages of P&O MPPT technique are presented as follows: **[100]**

✓ **Advantages**

- Easy to implement
- Upright, accurate and good performance under uniform radiation
- Online and does not depend on PV array

✓ **Disadvantages**

- Oscillations around steady state occur during fast-varying environmental conditions
- Difficulty of the step size control

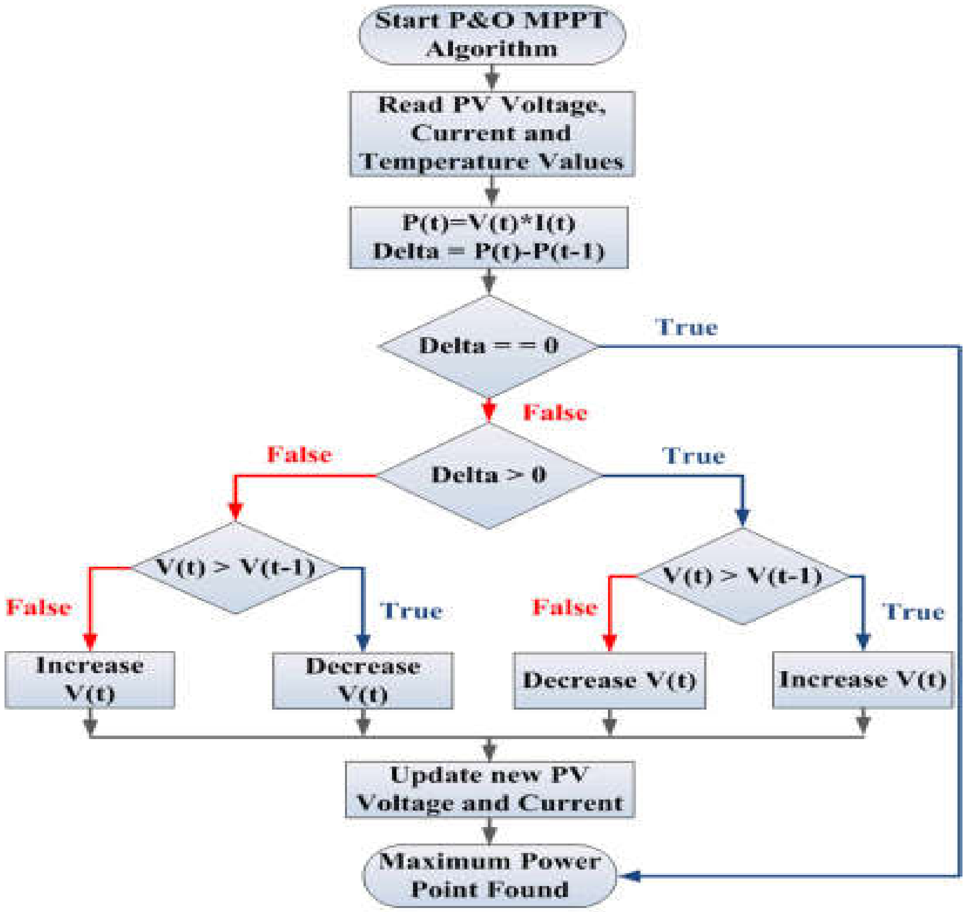

Figure (II.11): Flowchart of P&O algorithm **[100]**

II.3.6 On-line MPP search algorithm

The MPP search-identification calculation is situated inside the MPPT block, which incorporates the MPP identifier as well as an MPP tracker. In this calculation, as given below in figure (II.12), the primary task is to decide the estimation of reference greatest power and the present power is compared with it. This distinction is called the most extreme power error. To have the PV system be worked at its MPP, the most extreme power error ought to be zero or close to zero **[101].** The drawback of this particular technique is that it cannot estimate the exact MPP if the load is in less quantity. So, to overcome this load deficiency, an extra load has to be connected to feed the extra current of the PV module. The think-tank of this method will be the updating process of the previous MPP if there is a change in atmospheric conditions. Utilizing boost current converter implemented the simulation of this technique on control board. **[102]**

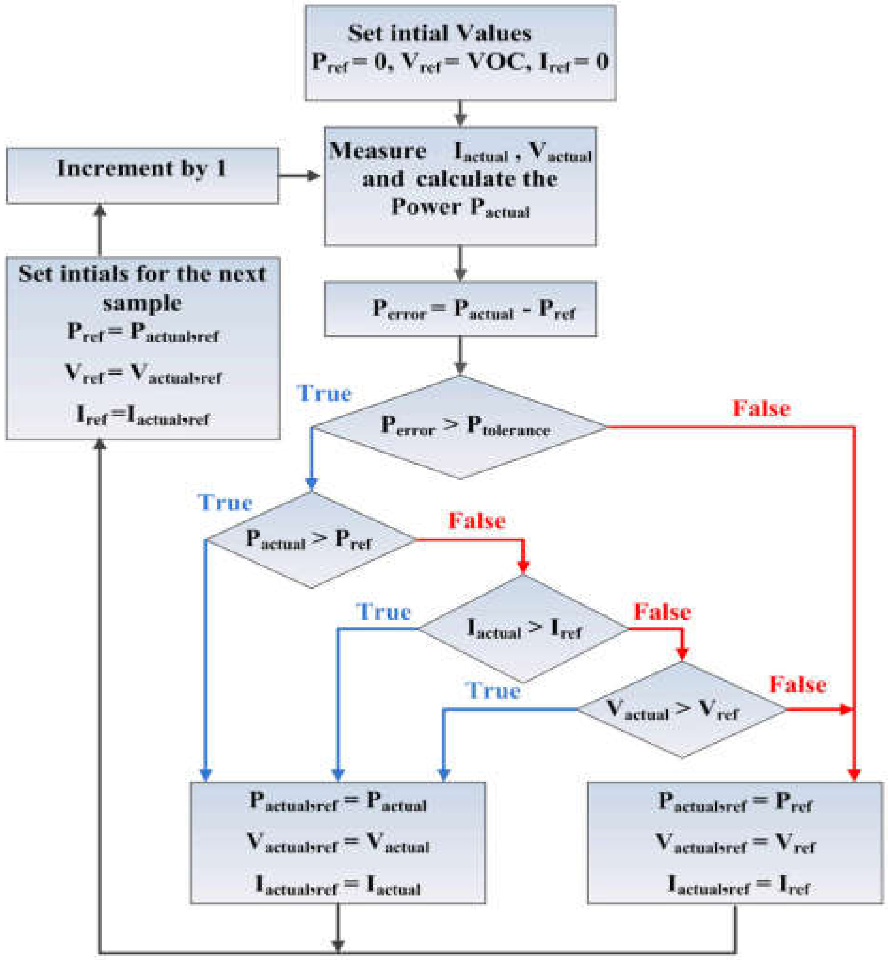

Figure (II.12): Process flow of on-line search algorithm **[102]**

II.3.7 Incremental conductance (INC) MPPT

The INC strategy depends on the way that the derivative of the output power P the panel voltage V is equivalent to zero at the MPP. The execution strategy of INC through the flowchart is shown in figure (II.13). Here in this method, all the data will be intended to use the slope of the P–V curve of the system and tracks the MPP with that data. If the slope of the P–V curve or the derivative of the PV array power (dP/dV) is zero, then only the process of tracking is accomplished. Whenever the atmospheric conditions are changing rapidly, tracking of MPP will be harder, and the rate of tracking also decreases in exponential rate due to the consistent change of the P–V curve. It is not very easy to maintain the operating point in those conditions. Many adaptive step size techniques are introducing to extract MPP without oscillations. The implementation of this method with Simulink blocks is done in MATLAB **[89],** and the same representation is given in figure (II.14). This strategy essentially utilizes the same way from P&O to reach MPP, however, utilizes the unique relationship of the current– voltage (I–V) curve. This calculation understands current and voltage estimations of PV cell and measures derivative of PV cell current (dI) and PV cell voltage (dV) **[103].** The PV current– voltage curve is utilized to decide the trajectory of the working point. The equations from (II.4) to (II.15) give the mathematical approach for calculating the position of MPP on the P–V curve.

$$\mathbf{P = V \times I} \tag{II.4}$$

$$\mathbf{\frac{dP}{dV} = \frac{d(VI)}{dV}} \tag{II.5}$$

The chain rule for the derivative of products yields

$$\mathbf{I\frac{dV}{dI} + V\frac{dI}{dV} = 0} \tag{II.6}$$

$$\mathbf{\frac{dP}{dV}I + V\frac{dI}{dV} = 0} \tag{II.7}$$

$$\mathbf{\frac{I}{V}\frac{dP}{dV} = \frac{1}{V} + \frac{dI}{dV} = 0} \tag{II.8}$$

At peak power point,

$$\mathbf{\frac{dP}{dV} = 0.\ \frac{1}{V} + \frac{dI}{dV} = 0} \tag{II.9}$$

If the operating point is to the right of the curve then we have

$$\mathbf{\frac{dP}{dV} < 0}.\text{ then if} \tag{II.10}$$

$$\mathbf{\frac{I}{V} + \frac{dI}{dV} < 0}\text{ V is decerased} \tag{II.11}$$

$$\text{if }\mathbf{\frac{I}{V} + \frac{dI}{dV} > 0}\text{ V is increased} \tag{II.12}$$

If the operating point is to the left of the curve then we have

$$\mathbf{\frac{dP}{dV} > 0}.\text{ then if} \tag{II.13}$$

$$\mathbf{\frac{I}{V} + \frac{dI}{dV} > 0}\text{ V is increased} \tag{II.14}$$

$$\text{if }\mathbf{\frac{I}{V} + \frac{dI}{dV} > 0}\text{ V is decerased} \tag{II.15}$$

Like P&O technique, it is difficult to make (dI/dV) equivalent to (-I/V), subsequently power loss was not as much as P&O has shown up. This strategy is more quickly and resistive than P&O yet it cannot discover GMPP in nearby MPPs like P&O. The basic microcontroller is well enough for the execution of this technique. Both voltage and current sensors are utilised as in the case of P&O. The improved INC prove better in many aspects of tracking speed and efficiency, and contemporary papers gave the broad implementation of this improved INC methodologies **[104].** As detailed in reference **[105],** this strategy implemented on controller board can reach MPP in 2.3 s. The bigger the increments of the system, the higher is the tracking efficiency. However, the system will oscillate around the MPP with the higher increments, which also results in inefficient yielding of MPP **[106]**.

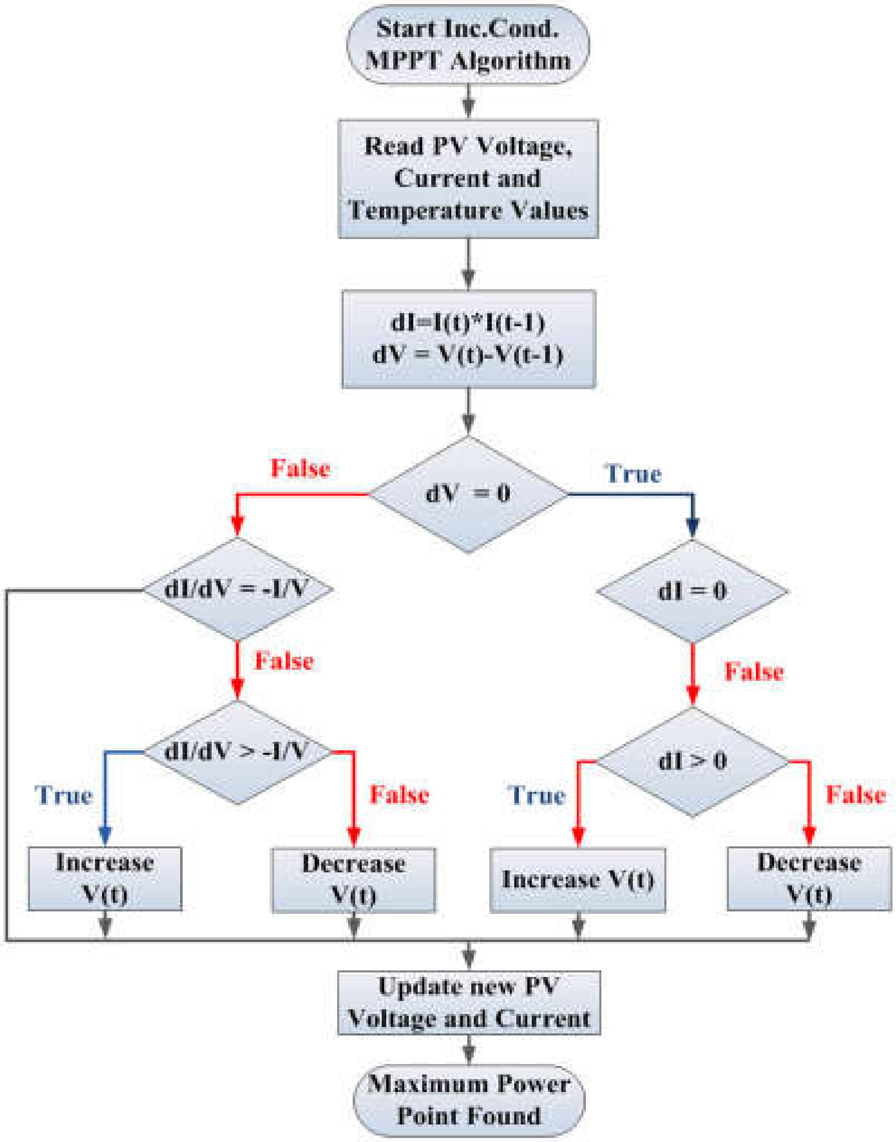

Figure (II.13): Flowchart of the INC algorithm **[102]**

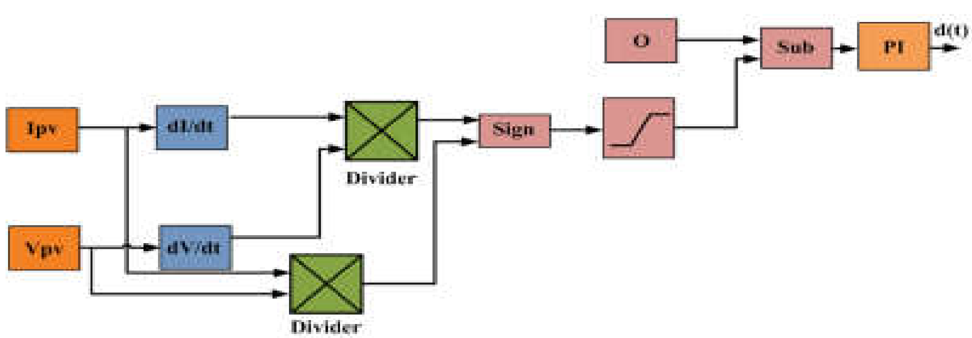

Figure (II.14): Implementation of INC method using PI controller **[89]**

II.3.8 Ripple correlation control

The basic methodology is to find the voltage derivative of power dP/dV, which is the main parameter in finding the MPP. The power converter consists of a voltage and current controller, which has the capability of sensing the voltages from the inverter in order to generate a reference signal. In this technique, the values of PV voltage and current are sensed using two sensors. Besides the low efficiency of the PV system, the addition of power converters will increase the ripple content. Implemented the grid-connected PV system by the help of this RCC technique, and the setup consists of two interface components like a controller board with slave processor and I/O interface board. This method shows good results for controlling the grid current by utilizing P-Q controller. **[107]**

II.4. Advanced MPPT Techniques

II.4.1. Fuzzy Logic Control (FLC)

Fuzzy logic is a form of many-valued logic, which deals with reasoning that is approximate rather than fixed and exact. In contrast with traditional logic, which usually sets two-value logic as true or false, fuzzy logic can have varying values. Fuzzy logic variables may have a truth or false value that ranges in different degrees.

In these cases, FLC could provide both fast process speed and the needed accuracy to some extent **[108].** The objective of FLC is to track and extract the maximum power from the PV system for a given irradiance (W/m^2) and temperature (°C). It does not require any technical knowledge of the PV system, while its simplicity gives it an advantage in tracking its MPP under fast-varying atmospheric conditions **[109].** The FLC has two inputs which are $\frac{\mathbf{d\,P_{PV}}}{\mathbf{dP_{PV}}}$ and $\Delta(\frac{\mathbf{d\,P_{PV}}}{\mathbf{dP_{PV}}})$, ($E_{rr}$) and ($\Delta E_{rr}$) which are determined from the PV output power and voltage as follows:

$$\boldsymbol{E_{rr} = \frac{P_{PV}(K) - P_{PV}(K-1)}{V_{PV}(K) - V_{PV}(K-1)}} \qquad (\mathbf{II.16})$$

$$\boldsymbol{\Delta E_{rr} = E_{rr}(K) - E_{rr}(K-1)} \qquad (\mathbf{II.17})$$

The output from FLC is the required change in the duty cycle of the DC–DC converter (de-fuzzification). The FLC block diagram is shown in figure (II.15). The advantages of using FLC are in it being a universal control algorithm, very simple, adaptive, fast tracking response, parameter insensitivity and can work properly even with an imprecise input data. Also, FLC has better and efficient response in tracking the MPP, especially in the case of rapidly changing atmospheric conditions **[110].** One of its drawbacks occurs in PSC where it may stick around LP. The figure (II.16) shows the input and output membership functions, and Table (II.1) introduces the input and output fuzzy rules **[111].** The variation step of E_{rr} and E_{rr} may vary according to the system. Once E_{rr} and ΔE_{rr} are calculated and transferred to the logic variables based on the membership functions, the FLC output, which is typically duty ratio change, ΔD of the DC–DC boost converter is estimated in rules as given in Table (II.1).

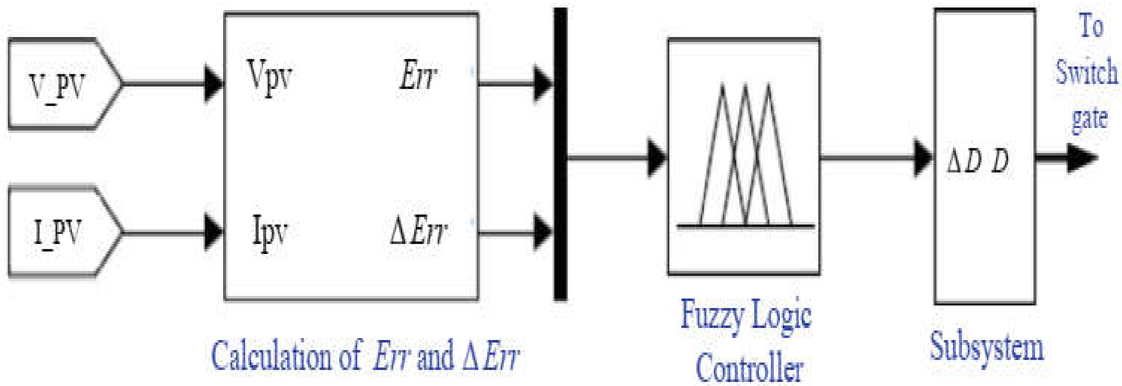

Figure (II.15): FLC block diagram in MATLAB/Simulink **[111]**

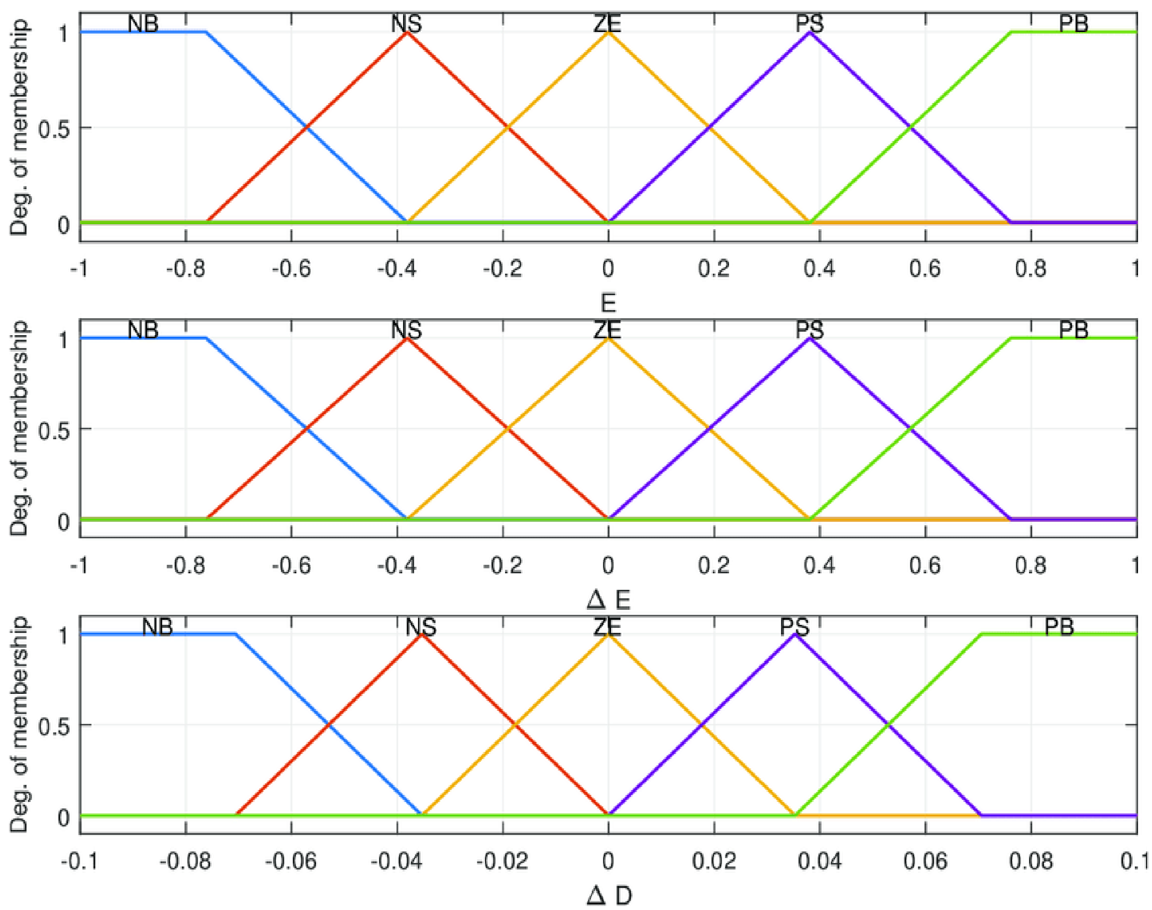

Figure (II.16): Membership functions of FLC **[111]**

Table (II.1): Fuzzy rules for the input and output variables **[111]**

E_{rr}	ΔE_{rr}						
	NB	NM	NS	ZE	PS	PM	PB
NB	NB	NB	NB	NB	NM	NS	ZE
NM	NB	NB	NB	NM	NS	ZE	PS
NS	NB	NB	NM	NS	ZE	PS	PM
ZE	NB	NM	NS	ZE	PS	PM	PB
PS	NM	NS	ZE	PS	PM	PB	PB
PM	NS	ZE	PS	PM	PB	PB	PB
PB	ZE	PS	PM	PB	PB	PB	PB

NB: Negative Big **NM:** Negative Medium **NS:** Negative Small

PB: Positive Big **PM:** Positive Medium **PS:** Positive Small

ZE: Zero

The implementation of this technique for a solar PV system is represented in figure (II.17). In fuzzification, the inputs of PV parameters are transformed into the linguistic variables, crisp quantity is converted into fuzzy quantity (fuzzy set).

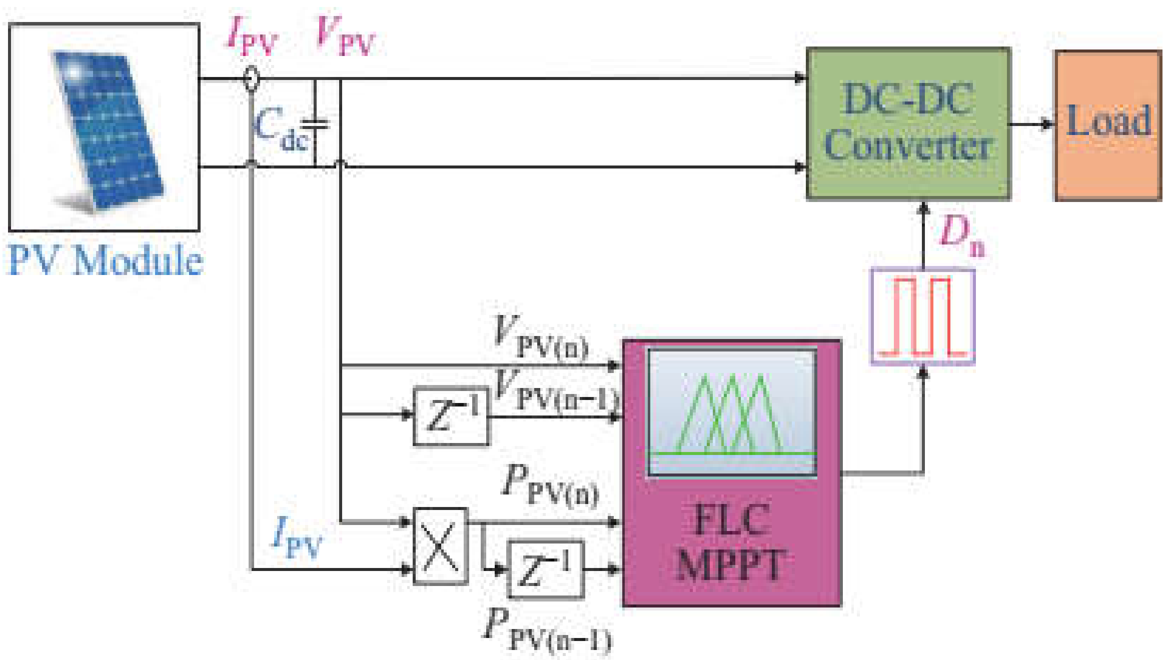

Figure (II.17): Block diagram of FLC MPPT technique **[111]**

Adaptive FLC performs well compared to the direct and indirect FLC-based MPPT during dynamic and steady state conditions regardless of the converter type **[112]**. In conclusion, FLC should be combined with a scanning and storing algorithm or other AI techniques to track the GP under PSC to achieve fast and accurate convergence, high tracking efficiency and drift avoidance **[113],** the advantages and disadvantages of FLC-based MPPT are given as follows:

✓ **Advantages**

- Highly robust, fast response, better Performance and adjustable accuracy
- Less oscillation during conditions variation
- Able to work with imprecise inputs and good efficiency
- More effective when combined with other EA techniques
- Does not require accurate mathematical model and detailed information of the system

✓ **Disadvantages**

- High complexity and expensive Offline (priori information is required)
- Efficiency of the whole system is dependent on the designer's performance and precision of the rules
- Fails to converge under dynamic states
- Rules cannot be changed, once defined

II.4.2. Artificial Neural Networks (ANN)

Artificial neural network (ANN) represents one of the artificial intelligent MPPT techniques that has the ability to solve nonlinear problems. Therefore, it can be applied to track the GP over the LPs. ANN consists of three layers: input, hidden and output layers. The input layer is defined from the PV array such as temperature, irradiance and I_{sc} or V_{oc} **[114]**. ANN adjusts and controls the duty cycle of the DC–DC converter (ANN output) to track the Global Peak **(**GP).

The ANN demonstrates high efficiency and accuracy in tracking the unique peak under uniform conditions, outperforming conventional techniques by mitigating issues related to tracking speed and steady state oscillations **[115].** However, ANN is more effective when integrated with conventional or AI-based MPPT methods to extract the Global Peak (GP) instead of Local Peaks (LP) in PV arrays. In such hybrid approaches, ANN predicts the GP region, while conventional or AI techniques handle precise tracking. Challenges associated with ANN include the high cost or unavailability of irradiance sensors, extensive training data requirements, increased network complexity, and time consumption, particularly under Partial Shading Conditions (PSC). Additionally, optimizing the ANN structure and retraining due to PV system aging is necessary for instance, combined ANN with Incremental Conductance (INC) to track the GP more efficiently than Perturb & Observe (P&O) and Fuzzy Logic Control (FLC)-based Hill Climbing (HC) **[116]**. Similarly, Jiang. integrated ANN with P&O, where ANN predicts the GP search area, and P&O performs tracking, proving superior to P&O, Fibonacci search, Particle Swarm Optimization (PSO), and Differential Evolution **[117].**

The detailed implementation of ANN is shown in figure (II.18) **[118]** demonstrates the selection of PV panels for the efficient use of this ANN technique in order to foresee the real-time problems. **[119]** coined the improved MPPT Technique using the ANN methodology. **[120]** gives the simulation of this ANN technique by considering variable PV parameters. This technique is easier to implement in a small microcontroller with low costs, and hardware implementation includes the low calculation based controller with the best AF in the model. So calculations are done at a very faster rate; thereby, the rate of convergence towards the output is high. **[121]** modelled the hybrid genetic algorithm (GA)-ANN based MPPT technique.

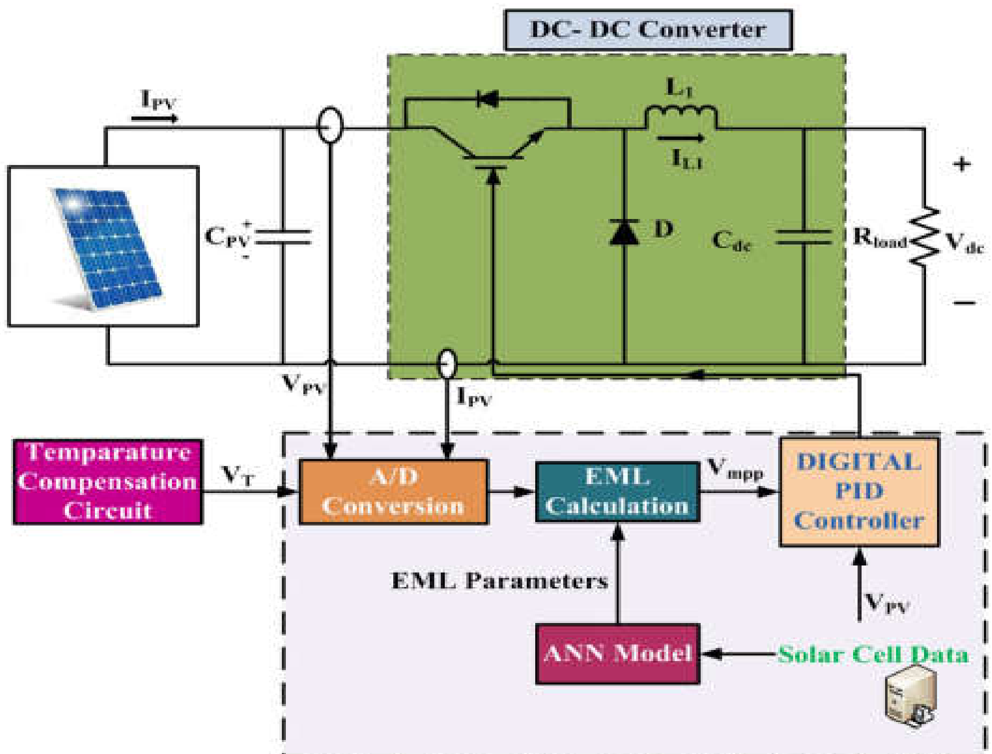

Figure (II.18): Detailed implementation of ANN method **[121]**

The advantages and disadvantages of ANN-based MPPT technique are given as follows:

- ✓ **Advantages**
- Fast tracking speed, acceptable accurateness
- Effective, less oscillations in conditions variation and good efficiency
- Can be trained offline and used in the online environment
- ✓ **Disadvantages**
- High complexity and expensive
- Requires extensive information about the PV parameters
- Additional cost of temperature and irradiance sensors

II.4.3. Particle Swarm Optimization (PSO)

Particle swarm optimization (PSO) is one of the meta-heuristic search tools that receive considerable attention in engineering applications. PSO was first introduced in 1995 by Kennedy and Ebraham this method is inspired by the natural behavior of birds flocking **[122].** This theory basically explores a specific area called the solution space, where each location has a possibility degree for the solution of problems. The PSO moves each particle throughout the solution space to determine the optimum solution according to the individual and neighboring particle experiences of the PSO during optimization. Therefore, particles involved in optimization use the memory of the particles to modify the particle fitness by following the behavior of the successful particles in the swarm. The PSO procedure starts with a random particle, continues by searching for optimal solutions within the past iterations (movement), and then evaluating the particle quality according to the fitness function **[123].** The figure (II.19) shows the flowchart of PSO-based MPPT. At the beginning, the number of duty cycles has been randomly nominated. Then, each one is applied to the PV array. The system current and voltage are measured in order to estimate PV power. Such power represents the fitness function of particle i. In the next step, the comparison between new fitness value and power corresponding to p_{best} is stored in history. In case of the new estimated power is greater than the old one, it is selected as the best fitness value. After evaluating all particles, old velocity and position for each particle can be updated. When the stopping criterion is achieved, PSO-based tracker stopped and gives optimal duty cycle, which corresponds to global power **[124].**

The basic PSO algorithm that defines the next position of the candidate solution is as follows **[125]:**

$$\mathbf{V_i^{k+1} = \omega \times V_i^k + r_1 \times C_1 \times \left(P_{bi} - X_i^k\right) + r_2 \times C_2 \times \left(G_b - X_i^k\right)} \qquad \mathbf{(II.18)}$$

$$\mathbf{X_i^{k+1} = V_i^k + X_i^k} \qquad \mathbf{(II.19)}$$

Where *i* represents the optimization vector variable, *k* is the number of iterations, V_i^k and X_i^k are the respective velocity and position of the variable within *k* iterations, *w* is the inertia weight factor, c_1 is the cognitive coefficient of the individual particles, c_2 is the social coefficient of all the particles, and r_1 and r_2 are the random selected variables in the range [0,1]. These random parameters mainly aim to maintain stochastic movement within the iterations. To maintain the search space in a certain area, the velocity values are set to the range of $[0,V_{max}]$. In PSO, the parameters *w*, c_1, and c_2 are highly mutable. The best self-experienced location (P_{bi}), which records the best position experienced by the particle up to the current iteration, is updated once equation II.18 is satisfied. **[124]**

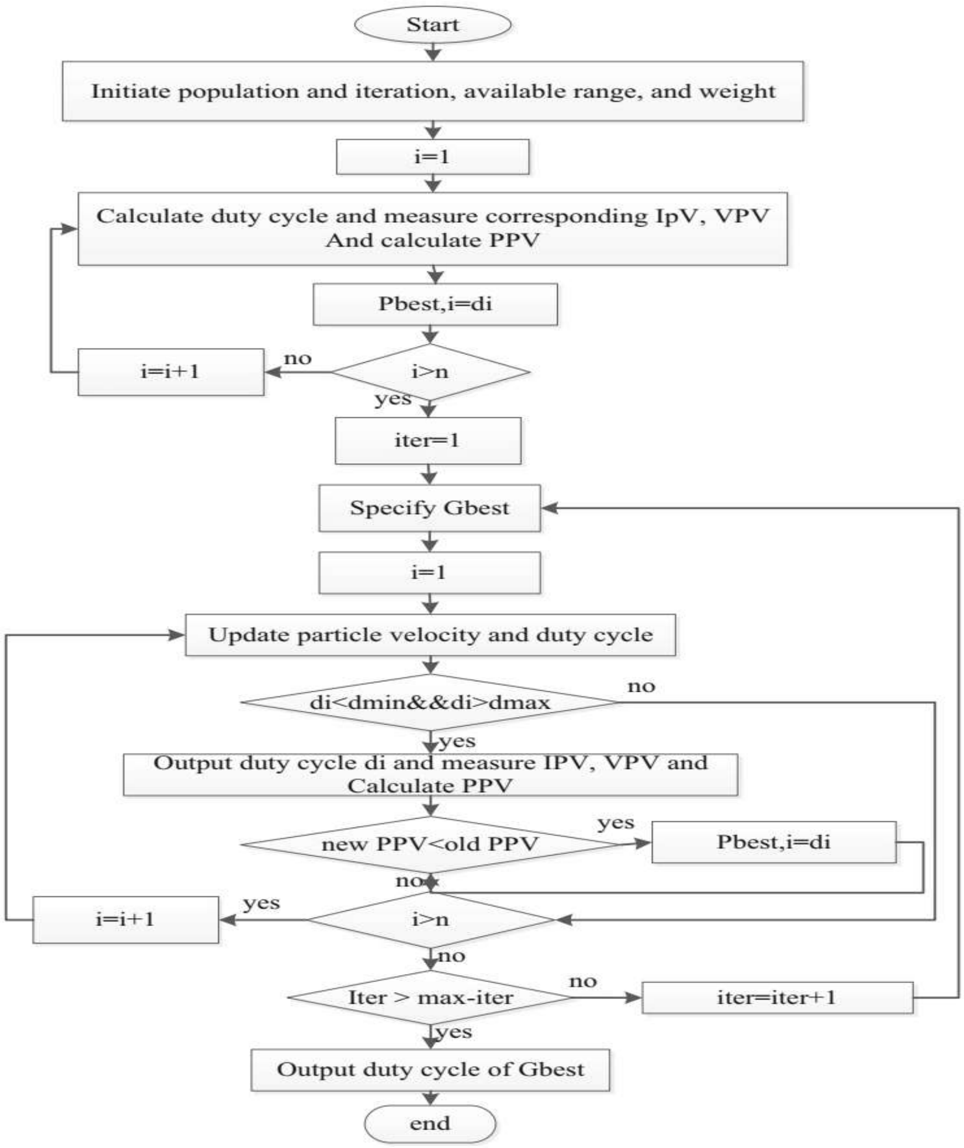

Figure (II.19): Flowchart for searching mechanism by PSO-based tracker **[124]**

In addition, the variable (G_b) records the G_b experienced location met by all contribute particles throughout the past iterations and is compared with the P_{bi} in each iteration. The update condition of G_b and P_{bi} is presented in equations. II.20 and II.21. These equations indicate that G_b is only recorded as P_{bi} if the conditions below are satisfied **[103].**

$$\mathbf{P_{bi}} = \boldsymbol{X_i^k} \qquad \textbf{if } \mathbf{F}\left(\boldsymbol{X_i^k}\right) \geq \mathbf{F}(\boldsymbol{P_i}) \tag{II.20}$$

$$\mathbf{G}_{\boldsymbol{b}} = \boldsymbol{P_{bi}} \qquad \textbf{if } \mathbf{F}(\boldsymbol{P_M}) \geq \mathbf{F}(\boldsymbol{G_b}) \tag{II.21}$$

Equation II.22 shows the location matrix of the particles as a solution to the MPPT problem in the D dimensional search space **[103].**

$$\mathbf{X_i^k} = \left[\mathbf{X_1^k}.\ \mathbf{X_2^k}\ .\mathbf{X_3^k}, \cdots \boldsymbol{X_i^k}, \cdots, \boldsymbol{X_{N-1}^k}.\boldsymbol{X_N^k}\right] \tag{II.22}$$

Where X_i^k is the location of the kth particle at the kth iteration. Practically, the generated power fluctuates because of variations in the insolation levels and partial shading degrees. Therefore, the algorithm should be initialized when Equation II.23 is satisfied. If this step is neglected, the actual values of the acquired P_{bi} and G_b values should not be considered **[103].**

$$\left|\frac{F(X_{i+1}) - F(X_i)}{F(X_i)}\right| > \Delta P \qquad (II.23)$$

Parameters affecting PSO performance are acceleration coefficients (the velocity and the position), inertia weight, population size, and maximum number of iterations. Advantages of PSO are global tracking technique, low computational complexity, and easy to combine with the basic algorithm. Disadvantages of PSO are standard PSO-based MPPTs have slow tracking speed when applying to large-scale PV arrays sensitive to the control parameters. **[103]**

II.5. Hybrid MPPT Methods

A simple and efficient hybrid MPPT technique for PV systems under PSC was developed with a combination of P&O or IC and artificial neural network **[126].** This approach was noted to be less costly with simple structure and fast response. In a different work, an FL-based P&O MPPT was studied using peak current control with a variation of the reference current for better transient with the improved SteadyState performance **[127].**

The analysis showed an improved transient response of 15% and the power loss reduction in the steady state. An ANN-Polar coordinated fuzzy controller-based MPPT control was applied for PV under PSC **[106].** The FL with polar information controller utilizes the global MPP voltage as a reference voltage to produce the required control signal for the power converter, and the MPPT is estimated through the ANN algorithm. Meanwhile, an ANN-based modified IC algorithm for MPPT under PSC was simulated and implemented in hardware using FPGA **[128].** The analysis revealed that the improved FL-P&O MPPT method is able to track the real absolute MPP for PSC. FL is adopted into the conventional MPPT to enhance the overall PV system performance and for the optimization of the solar PV array under PSC. This method has improved performance because it can facilitate the PV array to reach the MPP faster and achieve a stable output power. An MPPT algorithm based on a modified GA was also concentrated on tracking the GMPP in PV array with PSC **[129].** A P&O algorithm was integrated into the GA function to create a single algorithm. The control part and the GMPPT algorithm were implemented on a digital signal processor and tested on an experimental small-scale PV system. The assessment of GA and conventional methods for MPPT of shaded solar PV generators is carried out **[130].** They concluded that IC and P&O algorithms fail to achieve MPP of the PV if the PV panel is under PSC. To solve this problem, GA algorithm was used and it successfully enabled the system to reach the global MPP.

Alternatively, an MPPT method for PV systems PSC was formulated where a global MPP searching technique is obtained by linking IC and scanning approach method which utilizes duty cycle sweep to track the global MPP when the PV array is under PSC **[131]**. A hybrid MPPT technique based on P&O and PSO is indicated to have excellent performance **[132].** P&O was employed to assign the nearest local maximum,

II.5.1. FPSO MPPT

Hybrid MPPT techniques are advanced in their performance to increase the tracking efficiency and lower computational burden of hardware **[133].** As the problem of precisely tracking the GMPP out of many LMPPs is not well achieved by the intelligent or optimization techniques individually, then coined this hybrid method of fuzzy particle swarm optimization (FPSO). The reason behind choosing this combination is less parameter adjustment, mathematical computation reduction. These two control parameters, which are building blocks in the construction of membership functions (MFs), give the best MF distribution. In order to get the optimized solution, the fuzzy-PSO MPPT, designing of these MFs is crucial to work under PSCs. The fuzzy rules are designed in order to overcome any non-linearity in the system. The Mamdani based fuzzy MFs optimize the D of the converter used, which results in the high convergence of output at a fast rate **[134].** Also, this converter considers all weather conditions, giving the maximum power even under dynamic insolation conditions. The flowchart representation of this hybrid methodology is given in figure (II.20). as the PSO method efficiency mainly depends on the particle velocity, selection of optimum value for the initial position is necessary. Equation (II.24) gives the evaluation factor.

$$\mathbf{EF} = \int_0^{T_F} [\mathbf{P_{Peak}(T) - P_{PV}(T)}]\mathbf{1^2 dT} \qquad (\mathbf{II.24})$$

T_F is the total time period, P_{Peak} is the peak power of PV at STC. Fitness function is controlling parameter, is used to evaluate the precise functionality of the whole system. Equation (II.25) gives this function in terms of the deviation of frequency (df).

$$\textbf{Fitness Funtion}(\mathbf{FF}) = \int |\boldsymbol{df}|\boldsymbol{dT} \qquad (\mathbf{II.25})$$

PSO is hybridized with the FLC to design simplified MFs with small and optimized base rules**.** Simplifies the PSO design with the use of algorithm CMex S function. This hybrid method is used to integrate the PV to the grid, and this effectively tracks the GMPP with the THD limits well within the IEEE standards. **[135]**

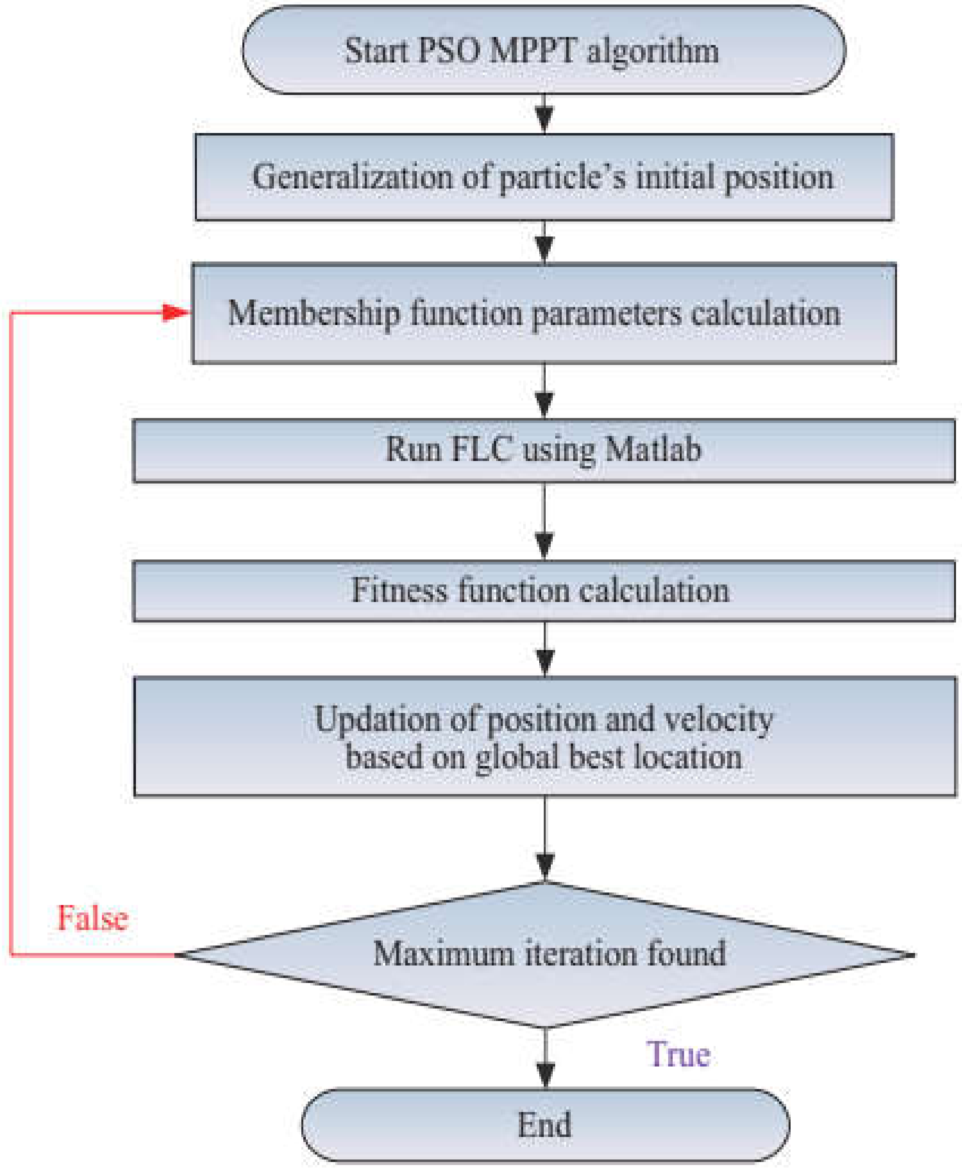

Figure (II.20): Flowchart of FPSO algorithm. **[135]**

II.5.2.NFIS MPPT

The extraction of GMPP from PV array under PSC is quickly done by this advanced method which is based on adaptive neuro-fuzzy inference system (ANFIS). The ANFIS MPPT is utilized for the approximation of the solution efficiently by using the hybrid methodology. This process consists of mapping inputs with outputs, designing and distribution of MFs, and setting fuzzy rules using FLC and ANN. The trial and error procedure will give information about the design pattern of MFs. N. Priyadarshi, et al. recently utilized this hybrid method and analyzed this technique prominence in various parameters **[136]**. Nevertheless, the ANN will come into the process by tremendously reducing the error and optimizing those parameters. Whereas, FLC acts on the non-linear inputs without the requirement of system knowledge. The main advancement of this technique is the inherent adaptive learning capabilities irrespective of the deviation of the training data. Both FLC and ANN postulates are included in this algorithm. Moreover, this technique can be applied to any system with any configuration under PSC's that is making adaptive. Also, this system has less mathematical computation making more straightforward in design with prominent efficiency. The ANFIS MPPT architecture, which includes six layers, is shown in figure (II.21). It consists of six layers with two input parameters. These input parameters have three MFs, trained rigorously by the ANFIS method. After mapping both input and output, nine fuzzy rules are derived in order to produce the maximum output power. The working methodology includes the two inputs I_1 and I_2, which are base-widths for triangular MF distribution (or) half base-width of the MF distribution. As the inputs are consisting of three neurons each, they will be resulting in 9 fuzzy rules **[137].**

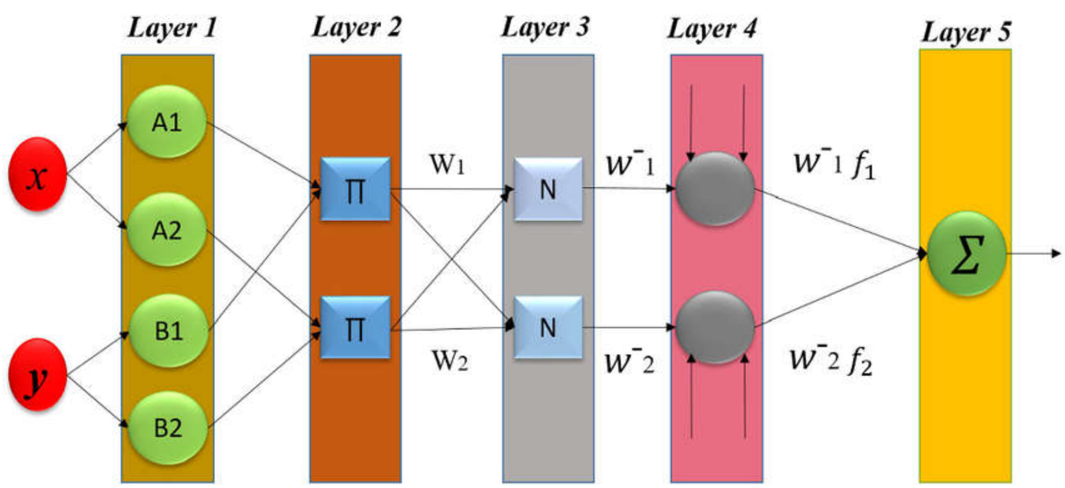

Figure (II.21): Architecture of ANN MPPT. **[137]**

Equation (II.26) represents First-order Takagi and Sugeno's model of FLC, which gives the overall output as:

$$\mathbf{y_i = a_i I_1 + b_i I_2 + c_i} \qquad \text{(II.26)}$$

Where $i = 1; 2; 3; : : : ; 9$ (Fuzzy rules), a_i ; b_i and c_i are the coefficients of output equation. The connecting weights between these layers is the normalized value V_{1avg}, which lies in the range of [0,1] and mainly depends on the base width of triangular membership function distribution. This is given by the equation (II.27).

$$\boldsymbol{V_{1\,avg} = \frac{V_{11} + V_{12} + V_{13}}{3}} \; ; \quad \boldsymbol{V_{2\,avg} = \frac{V_{24} + V_{25} + V_{26}}{3}} \qquad \text{(II.27)}$$

Where V_{11} is the weight which is connecting the 1st node in layer 1 with 1st node in layer 2, V_{12} is the weight which is connecting the 1st node layer 1 with 2nd node in layer 2, V_{24} is the weight which is connecting the 2nd node in layer 1 with 4th node in layer 2, and so on. Among all available fuzzy rules, the best-optimized value of rule is selected or fired, which is represented by w_n = firing strength. *N* is the particular node, where normalization takes place. The normalized value of firing strength $w_1$out is given in the equation (II.28).

$$W_{1\,out} = \frac{w_1}{w_1 + w_2 + w_3 + \cdots + w_9} \qquad (\text{II}.28)$$

Performance depends on the membership function distribution of input variables. a_i; *bi*, and *ci* to be optimal values of parameters, selected precisely, so ANFIS work in optimal scenario. So, prediction also is made as accurately as possible. This method has excellent dynamic responses, especially when the PV system is integrated to grid maintaining its stability. References **[136], [137], [138]** includes the novel ANFIS methodologies for making the computational procedures more simpler by keeping efficiency in the maximum extent.

II.6. Power Electronic Converters for MPPT Implementation

II.6.1. Boost Converter

Boost Converters sometimes, also known as step-up DC-DC converters are the type of chopper circuits that provides such an output voltage that is more than the supplied input voltage. In the case of boost converters, the dc to dc conversion takes place in a way that the circuit provides a high magnitude of output voltage than the magnitude of the supply input **[139]**. It is given the name 'boost' because the obtained output voltage is higher than the input voltage **[140]**.

II.6.2. Operating Principle of Boost Converter

The figure given below is the circuit representation of the boost converter:

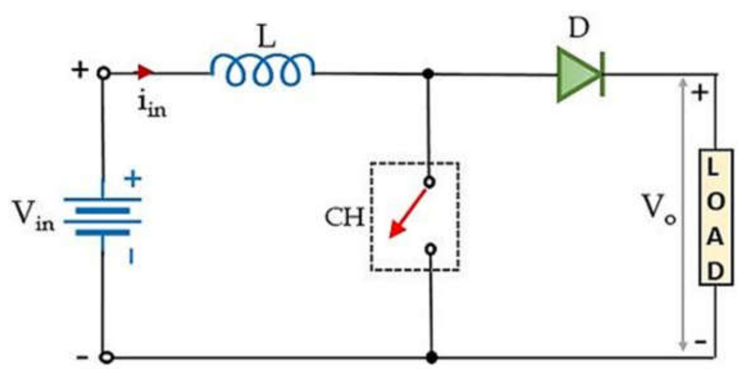

Figure (II.22): Elementary Circuit of Boost Converter **[140]**

The circuit here is an elementary form of step-up DC-DC converter which necessarily requires a large inductor L in series connection with the voltage source. The whole circuit arrangement operates in a way that it helps in maintaining a regulated dc signal at the output **[141]**.

Let us understand how the given circuit operates in order to provide an increased dc signal at the load.

Initially, when the chopper CH is in on state, then in the presence of supply dc input current begins to flow through the closed path of the circuit i.e., passing through the inductor as shown in the figure below **[142]**.

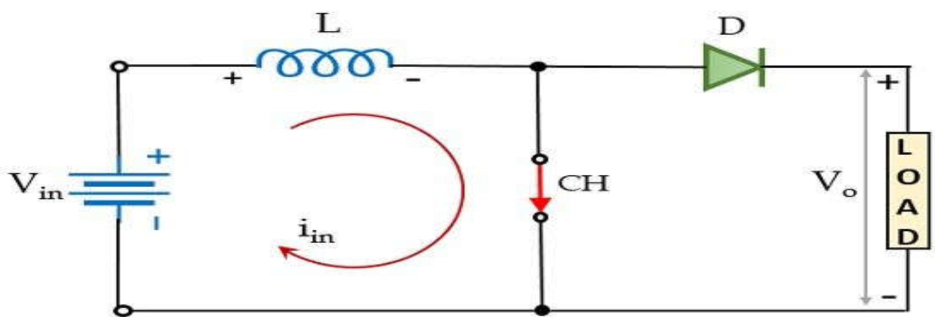

Figure (II.23): The Chopper CH is in on State **[142]**

Here, the polarity of the inductor will be according to the direction of the flow of current. In this particular case, the diode in the configuration is in reverse biased condition and so current will not be allowed to flow through that particular part of the circuit during on state of the DC-DC converter. Resultantly, the voltage across DC-DC converter will appear across the load **[142]**.

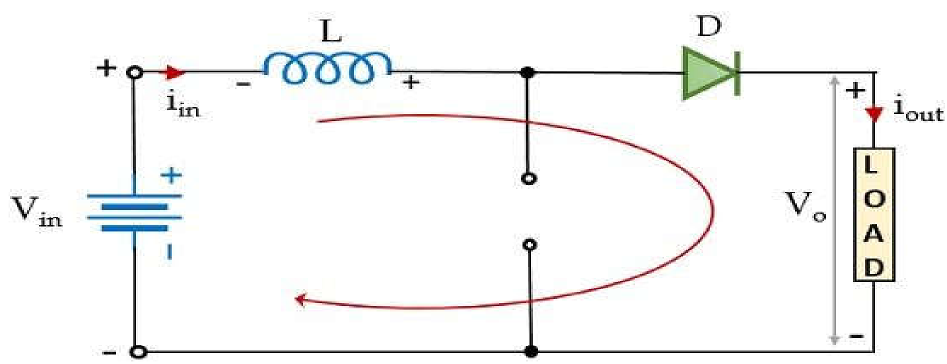

Figure (II.24): The Chopper CH is in Off State **[142]**

Furthermore, at the instant when CH is in the off state, then the part of the circuit through which the current was flowing earlier will not be active in this case. However, as the inductor stores, the energy in the form of a magnetic field and so the current through it will not die out instantly.

Also, we know according to Lenz's law a reverse current will be induced that will oppose the cause which has produced it. And so, due to the induced current, the polarity of the inductor will get reversed. This reverse polarity of the inductor forward biases the diode present in the circuit. This provides the path for the current through the diode that flows through the load during the off state of the chopper i.e., T_{off}. However, we must note here that the current through the inductor is of decreasing nature and will die out after a point in time **[143]**.

Thus, the total voltage across the load will be given as:

$$\boldsymbol{V_{\text{out}} = V_{\text{in}} + V_L} \quad \text{(II.29)}$$

This means that the output voltage exceeds the applied input voltage. Thus, performs step-up conversion as the energy stored within the inductor during the T_{on} period is released during the T_{off} period **[144]**.

During the T_{on} period, the voltage across the inductor will be given as:

$$\boldsymbol{V_L = L\frac{di}{dt}} \quad \text{(II.30)}$$

Let us have a look at the waveform representation of the step-up chopper shown below:

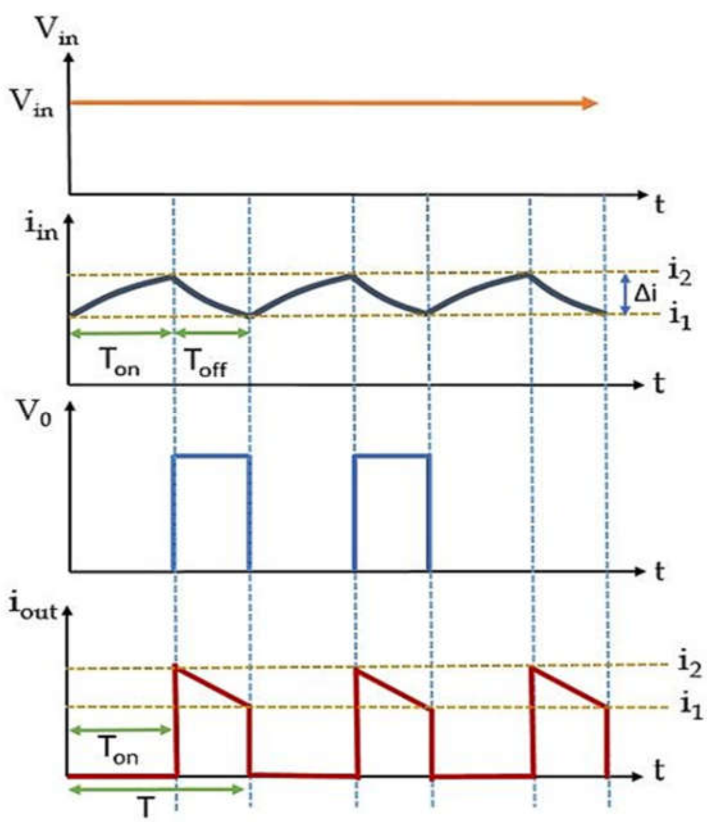

Figure (II.25): Waveform Representation **[144]**

During the T_{on} period, the current through the inductor will change from i_1 to i_2 this is clearly shown above. While during the T_{off} period, the inductor current will change from i_2 to i_1. Now, talking about voltage, so during the turn-on period, the voltage across the inductor will be equal to the supply input voltage. But when CH gets off then on applying KVL in the figure shown above, we will get:

$$\boldsymbol{V_L - V_0 + V_{\text{in}} = 0} \tag{II.31}$$

This means:

$$\boldsymbol{V_L = V_0 - V_{\text{in}}} \tag{II.32}$$

Considering that output current is varying linearly, the energy input provided by the source to the inductor, when CH is on, is given as:

$$\boldsymbol{W_{on}} = (\textbf{ voltage across the inductor })(\textbf{ average current through the inductor })\boldsymbol{T_{\text{on}}}$$
$$\boldsymbol{W_{on} = V_{\text{in}} \left(\frac{i_1 + i_2}{2}\right) T_{on}} \tag{II.33}$$

Further, the energy that the inductor releases to the load when CH is off is given as:

$$\boldsymbol{W_{\text{off}}} = (\textbf{ voltage across the inductor }) (\textbf{average current through the inductor}) \boldsymbol{T_{\text{off}}}$$
$$\boldsymbol{W_{\text{off}} = V_{\text{out}} - V_{\text{in}} \left(\frac{i_1 + i_2}{2}\right) T_{\text{off}}} \tag{II.34}$$

For a lossless system, comparing the two energies, we will have:

$$\boldsymbol{V_{\text{in}} \left(\frac{i_1 + i_2}{2}\right) T_{\text{on}} = V_{\text{out}} - V_{\text{in}} \left(\frac{i_1 + i_2}{2}\right) T_{\text{off}}} \tag{II.35}$$

On simplifying:

$$\begin{gathered}\boldsymbol{V_{in} T_{on} = V_{\text{out}} T_{\text{off}} - V_{\text{in}} T_{\text{off}}} \\ \boldsymbol{V_{\text{out}} T_{\text{off}} = V_{\text{in}} T_{\text{on}} + V_{\text{in}} T_{\text{off}}} \\ \boldsymbol{V_{\text{out}} T_{\text{off}} = V_{\text{in}} (T_{\text{on}} + T_{\text{off}})}\end{gathered} \tag{II.36}$$

Since we know, **T = T_{on} + T_{off}**, therefore:

$$\begin{gathered}\boldsymbol{V_{\text{out}} T_{\text{off}} = V_{\text{in}} T} \\ \boldsymbol{V_{\text{out}} = V_{\text{in}} \frac{T}{T_{\text{off}}}} \\ \boldsymbol{V_{\text{out}} = V_{\text{in}} \frac{T}{T - T_{\text{on}}}} \\ \boldsymbol{V_{\text{out}} = V_{\text{in}} \frac{1}{\left(\frac{T}{T} - \frac{T_{\text{on}}}{T}\right)}}\end{gathered} \tag{II.37}$$

Since, we know, duty cycle i.e., **α = T_{on}/ T**

$$V_{0ut} = V_{\text{in}} \frac{1}{(1-\alpha)} \tag{II.38}$$

Thus, we can conclude here that the average load voltage can be stepped up with the change in the duty cycle **[145]**.

II.6.3. Buck-Boost Converter

The buck–boost converter is a type of DC-to-DC converter that has an output voltage magnitude that is either greater than or less than the input voltage magnitude. It is used to “step up” the DC voltage, similar to a transformer for AC circuits **[139]**. It is equivalent to a fly-back converter using a single inductor instead of a transformer. Two different types are called buck–boost converter DC-DC converters, commonly referred to as choppers, include the versatile Buck-Boost converter **[140]**. This converter can function as either a step-down or step-up converter, depending on its duty cycle, denoted as DA typical Buck-Boost converter circuit is shown below: **[141]**

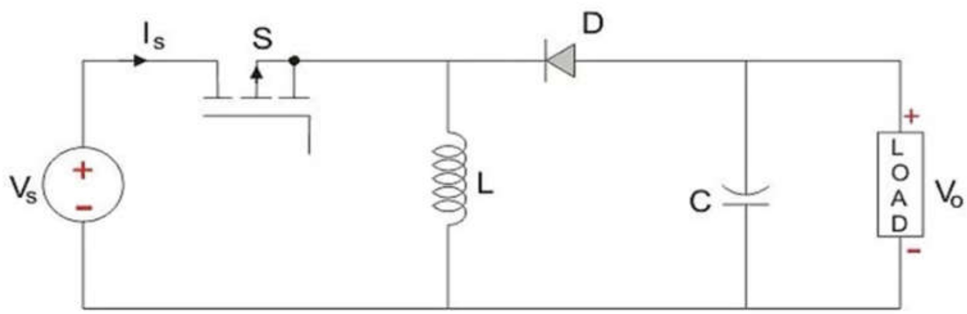

Figure (II.26): The Circuit Representation of Buck-Boost Converter **[141]**

The input voltage source is connected to a solid-state device. The second switch used is a diode. The diode is connected, in reverse to the direction of power flow from source,
to a capacitor and the load and the two are connected in parallel as shown in the figure above.

The controlled switch in the converter uses Pulse Width Modulation (PWM) to toggle on and off. PWM may operate based on time or frequency, with time-based being the more common approach **[142]**.

Frequency-based modulation, though versatile, has the disadvantage of requiring a wide range of frequencies to precisely control the switch and thus achieve the desired output voltage **[143]**.

Time based Modulation is mostly used for DC-DC converters. It is simple to construct and use.

The frequency remains constant in this type of PWM modulation **[144]**. The Buck Boost converter has two modes of operation. The first mode is when the switch is on and conducting.

Mode I: Switch is ON, Diode is OFF

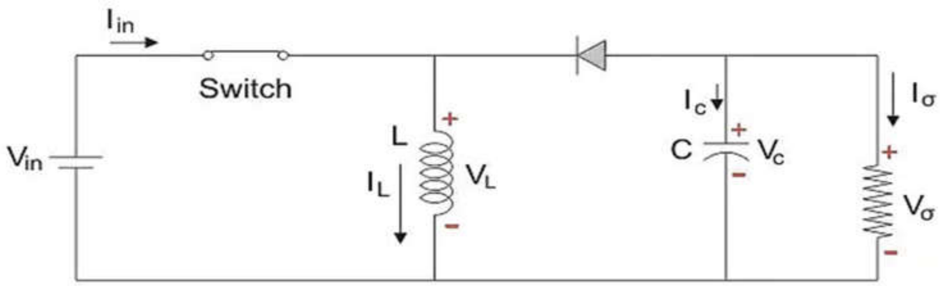

Figure (II.27): The Equivalent Circuit of Mode I **[144]**

The Switch is ON and therefore represents a short circuit ideally offering zero resistance to the flow of current so when the switch is ON all the current will flow through the switch and the inductor and back to the DC input source **[145]**.

The inductor stores charge during the time the switch is ON and when the solid state switch is OFF the polarity of the Inductor reverses so that current flows through the load and through the diode and back to the inductor. So, the direction of current through the inductor remains the same **[146]**.

Let us say the switch is on for a time T_{ON} and is off for a time T_{OFF}.
We define the time period, T, as:

$$T = T_{ON} + T_{OFF} \tag{II.39}$$

and the switching frequency:

$$f_{\text{switching}} = \frac{1}{T} \tag{II.40}$$

Let us now define another term, the duty cycle:

$$D = \frac{T_{ON}}{T} \tag{II.41}$$

Let us analyse the Buck Boost converter in steady state operation for this mode using KVL **[146]**.

$$\begin{gathered} V_{in} = V_L \\ V_L = L\frac{di_L}{dt} = V_{in} \\ \frac{di_L}{dt} = \frac{\Delta i_L}{\Delta t} = \frac{\Delta i_L}{DT} = \frac{V_{\text{in}}}{L} \end{gathered} \tag{II.42}$$

Since the switch is closed for a time T_{ON} = DT we can say that Δt = DT.

$$(\Delta i_L)_{\text{closed}} = \left(\frac{V_{in}}{L}\right) DT \tag{II.43}$$

While performing the analysis of the Buck-Boost converter we have to keep in mind that

- The inductor current is continuous and this is made possible by selecting an appropriate value of L **[148]**.
- The inductor current in steady state rises from a value with a positive slope to a maximum value during the ON state and then drops back down to the initial value with a negative slope. Therefore, the net change of the inductor current over any one complete cycle is zero.

Mode II: Switch is OFF, Diode is ON

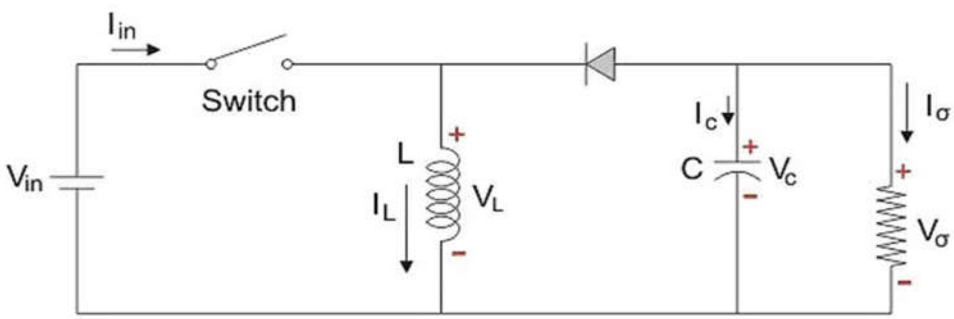

Figure (II.28): The Equivalent Circuit of Mode II **[149]**

In this mode the polarity of the inductor is reversed and the energy stored in the inductor is released and is ultimately dissipated in the load resistance and this helps to maintain the flow of current in the same direction through the load and also step-up the output voltage as the inductor is now also acting as a source in conjunction with the input source. But for analysis we keep the original conventions to analyse the circuit using KVL **[149]**.

II.6.4. Buck Boost Converter Formula

Let us now analyse the Buck Boost converter in steady state operation for Mode II using KVL.

$$V_L = V_o$$

$$V_L = L\frac{di_L}{dt} = V_o \tag{II.44}$$

$$\frac{di_L}{dt} = \frac{\Delta i_L}{\Delta t} = \frac{\Delta i_L}{(1-D)T} = \frac{V_o}{L}$$

Since the switch is open for a time

$$T_{OFF} = T - T_{ON} = T - DT = (1 - D)T \tag{II.45}$$

we can say that

$$\Delta t = (1 - D)T$$

$$(\Delta i_L)_{\text{open}} = \left(\frac{V_o}{L}\right)(1 - D)T \tag{II.46}$$

It is already established that the net change of the inductor current over any one complete cycle is zero.

$$(\Delta i_L)_{\text{closed}} + (\Delta i_L)_{\text{open}} = 0$$

$$\left(\frac{V_o}{L}\right)(1 - D)T + \left(\frac{V_{\text{in}}}{L}\right)DT = 0 \tag{II.47}$$

$$\frac{V_o}{V_{\text{in}}} = \frac{-D}{1 - D}$$

We know that D varies between 0 and 1. If D > 0.5, the output voltage is larger than the input; and if D < 0.5, the output is smaller than the input. But if D = 0.5 the output voltage is equal to the input voltage **[150]**.

II.6.5. Comparison of Converter Types

Table (II.1) summarizes the voltage gains and switch stresses for the different converter types. For these converters, the evolution of the voltage gains as a function of the duty cycle is shown. While several types can be considered as boost converters, particularly if the duty cycle is greater than 0.5, only the boost type provides a boosting capability over the entire duty cycle range **[151]**. For a duty cycle of 0.5 for example, the boost converter exhibits an output voltage twice the input voltage. Whereas for the other boost-derived type, the output voltage is equal to the input voltage for this duty cycle value. It is only when the duty cycle approaches 1 that the other boost-derived types tend to resemble the behavior of the conventional boost type **[152]**.

Table (II.2): Comparison of Converter Types **[152]**.

Converter /Parameters	Voltage Gain $\frac{Vout}{Vin}$	Voltage Controls $V_{k,max} = \lvert Vd, max \rvert$	Current Controls $i_{k,max} = V_{d,max} = i_{d,max}$
Boost	$\frac{1}{1-\ \alpha}$	$\frac{Vin}{1-\alpha} + \frac{\Delta Vout}{2}$	$\frac{Iout}{1-\alpha} + \frac{\Delta IL}{2}$
Buck	$\frac{\alpha}{1-\ \alpha}$	$\frac{Vin}{1-\alpha} + \frac{\Delta Vout}{2}$	$\frac{VC}{1-\alpha} + \frac{\Delta Vout}{2}$
Buck-Boost	α	Vin	$i_L + \frac{\Delta IL}{2}$

II.7. Conclusion

In conclusion, this chapter provides a comprehensive review of Maximum Power Point Tracking (MPPT) techniques for photovoltaic systems, covering both classical and advanced methods. The conventional fossil fuels are being depleted, leading to increased efforts in harnessing solar energy through photovoltaic (PV) systems. However, the efficiency of PV modules is relatively low while their cost remains high, necessitating effective MPPT techniques to maximize power output. Various MPPT approaches have been developed and categorized into off-line, on-line (hill-climbing), and artificial intelligence techniques, each with its own advantages and disadvantages regarding tracking speed, accuracy, complexity, and cost. Classical methods like Perturb and Observe (P&O) and Incremental Conductance (INC) are simple and widely used but suffer from oscillations and reduced efficiency under dynamic conditions. Advanced techniques such as Fuzzy Logic Control (FLC), Artificial Neural Networks (ANN), and Particle Swarm Optimization (PSO) demonstrate superior performance in complex scenarios like partial shading but come with higher complexity and cost. Hybrid methods that combine different approaches show promise in overcoming individual limitations and enhancing overall system performance. The choice of MPPT technique depends on specific application requirements, environmental conditions, and cost considerations, indicating the need for continuous research and development to optimize PV system efficiency and reliability.

Chapter III

Simulation and Modelling of MPPT Techniques

III.1. Introduction

In this chapter, we study and evaluate the performance comparisons of four famous Maximum Power Point Tracking (MPPT) algorithms: Perturb and Observe (P&O), Incremental Conductance (INC), Artificial Neural Network (ANN), and Fuzzy Logic Controller (FLC). They control the output power of the photovoltaic systems by maintaining the operational point to a suitable condition to retrieve maximum energy from the solar panels continuously. Thus, these algorithms effectively track the point where maximum power can be utilized and hence maximize the efficiency and effectiveness of PV systems, hence reflecting positively on the overall performance and energy yield. Measurement and observation patterns employed by the P&O algorithm are derived by periodic perturbations and observations. The INC technique uses the incremental conductance method for finer methods of adjustment. The ANN method employs artificial intelligence rather than depending on measurements to locate the maximum point with high precision. FLC works with fuzzy logic rules to deal with uncertainties and apparent nonlinearities in solar power behaviour, which makes it highly applicable in rapidly changing environmental conditions. Such a comprehensive analysis looks into the merits and demerits of individual algorithms and helps users know which one is suitable for their desired operating conditions.

III.2. Parameters of the PV system in simulation

The following characteristics of panel and the parameters of boost converter that are used in our PV system in simulation, are shown in the figure and table below:

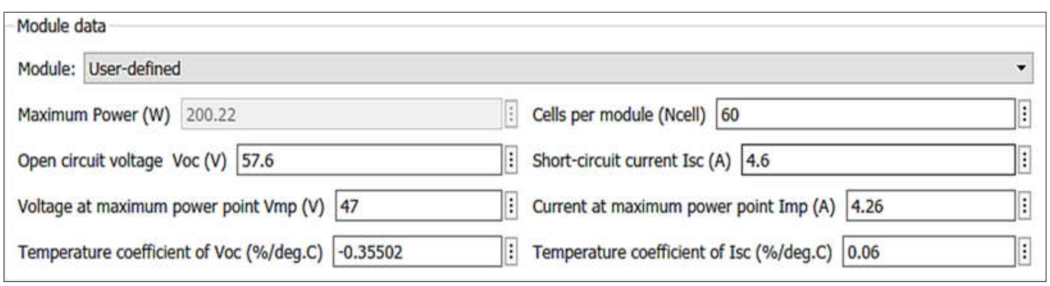

Figure (III.1): Characteristics of panel

Table (III.1): Parameters of boost converter

Boost Converter	Value
Capacitor 1	200 µF
Inductor	3.5 mH
Capacitor 2	100 µF
Resistive Load	300 Ω

III.3. Simulation results

III.3.1. The perturb and observe (P&O) algorithm

In this simulation, we used the Perturb and Observe (P&O) algorithm to obtain results for power, voltage, and current. Figure (III.2) represents the general system simulation, showcasing the overall setup and performance of the P&O -based MPPT system. The figure illustrates the integration of PV panels with the P&O -based MPPT controller, which adjusts the duty cycle to optimize power extraction.

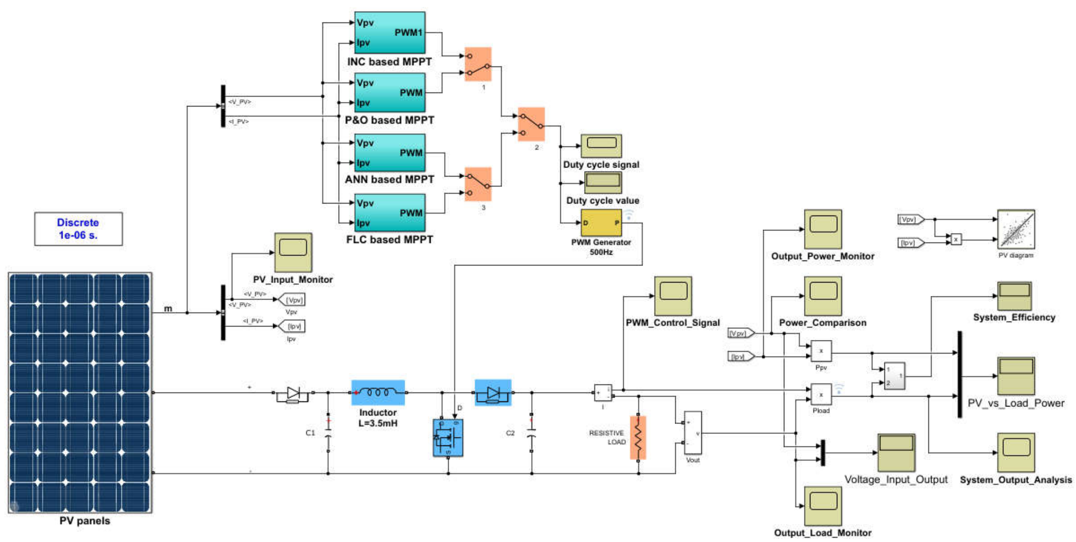

Figure (III.2): Schematic simulation system with P&O

a)- Constant irradiance (1000 W/m²) and constant temperature (25°C)

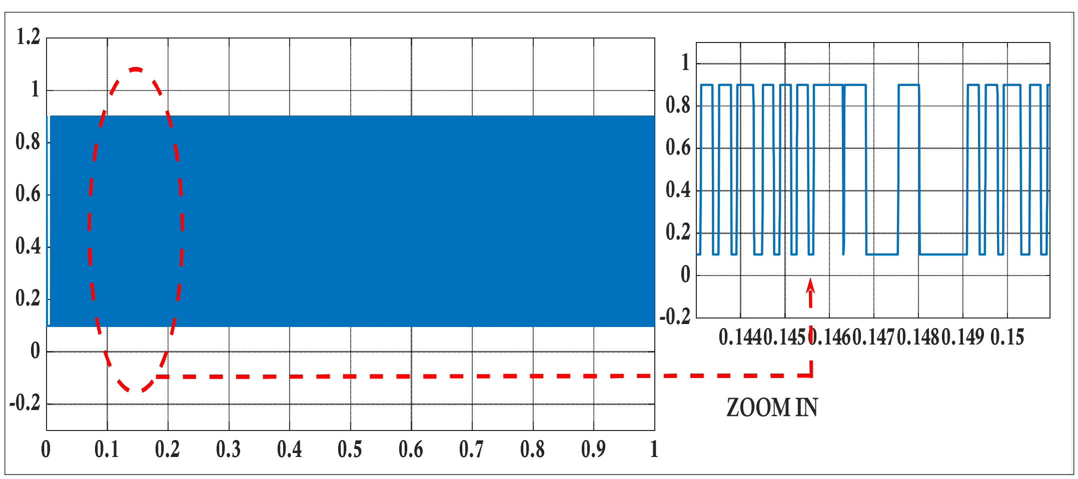

Figure (III.3): Duty cycle simulation result versus time for P&O in constant irradiance

The Figure (III.3) demonstrates MPPT system fault-tolerant behavior, with the macroplot presenting an overall picture of stability, while formerly noted views detect minute fluctuations in a critical segment of its operation of constant irradiances of 1000 W/m² and temperature of 25 °C.

In the proposed MPPT systems, adaptive simulation for modeling proper lifetimes is put to real-time application. Based on how electrically connected elements relate to solar panels, devices and currently manufactured technologies, safety has included defining electrical lines in schematics as Parliament authority circuits.

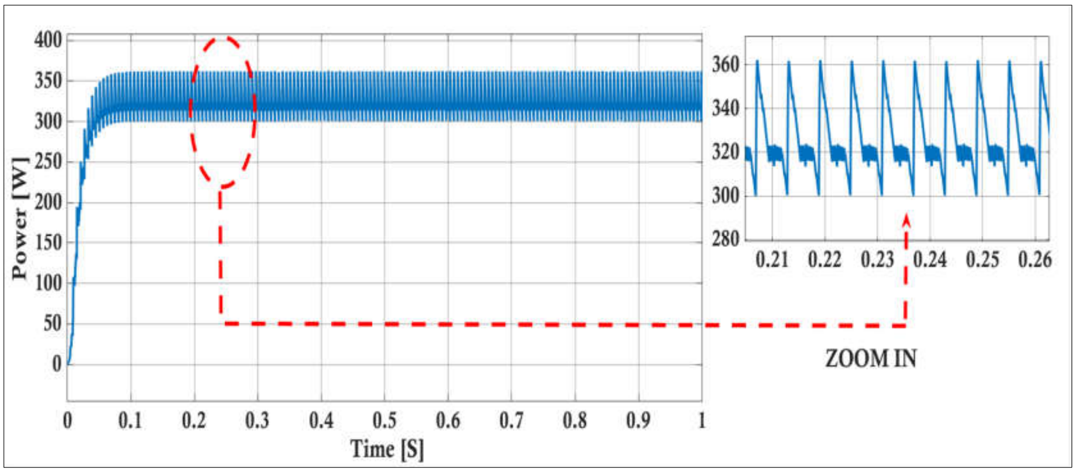

Figure (III.4): Power simulation result versus time for P&O in constant irradiance

The Figure (III.4) illustrates the power response of an MPPT system using the P&O algorithm. The main plot shows a rapid increase in power followed by stabilization around 350W. The zoomed-in view highlights the oscillatory nature of the power output, characteristic of the P&O algorithm as it continuously perturbs to track the maximum power point. These oscillations are a trade-off for maintaining optimal power extraction and are crucial for understanding the efficiency and performance of the MPPT system.

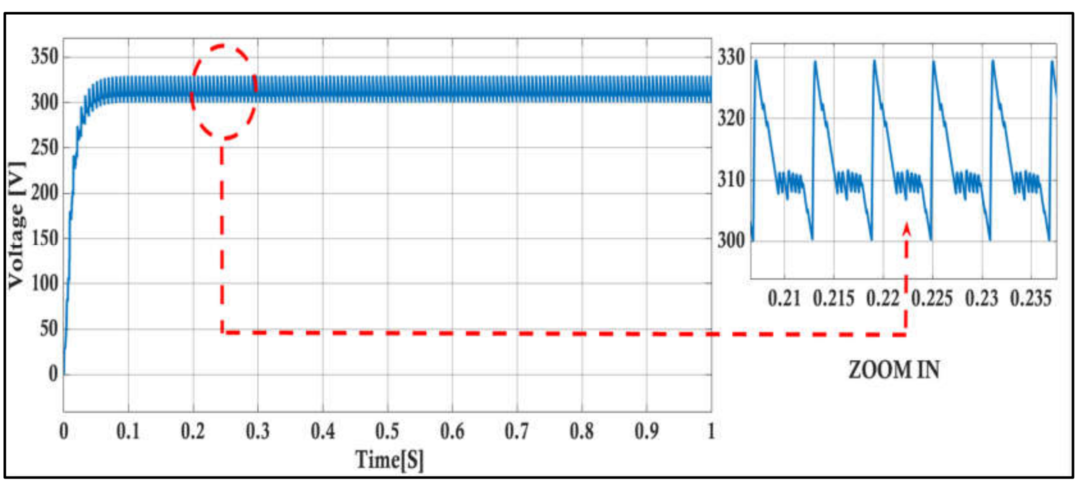

Figure (III.5): Voltage simulation result versus time for P&O in constant irradiance

The Figure (III.5) illustrates the voltage response of an MPPT system using the P&O algorithm. The main plot shows a rapid increase in voltage, stabilizing around 330V. The zoomed-in view highlights the oscillatory nature of the voltage output.

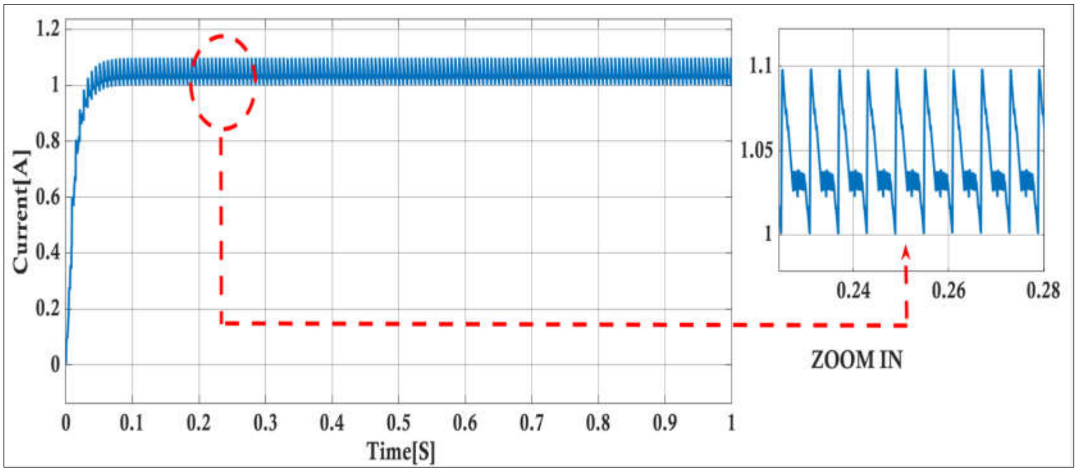

Figure (III.6): Current simulation result versus time for P&O in constant irradiance

The Figure (III.6) illustrates the current response of an MPPT system using the P&O algorithm. the main plot shows the rapid transient response leading to stabilization at approximately 1.1A, indicative of the system reaching its maximum power point. The zoomed-in view provides a closer look at the inherent oscillations around this steady-state value.

b)- Variable irradiances (1000, 800, 600, 400 W/m²) and constant temperature (25°C)

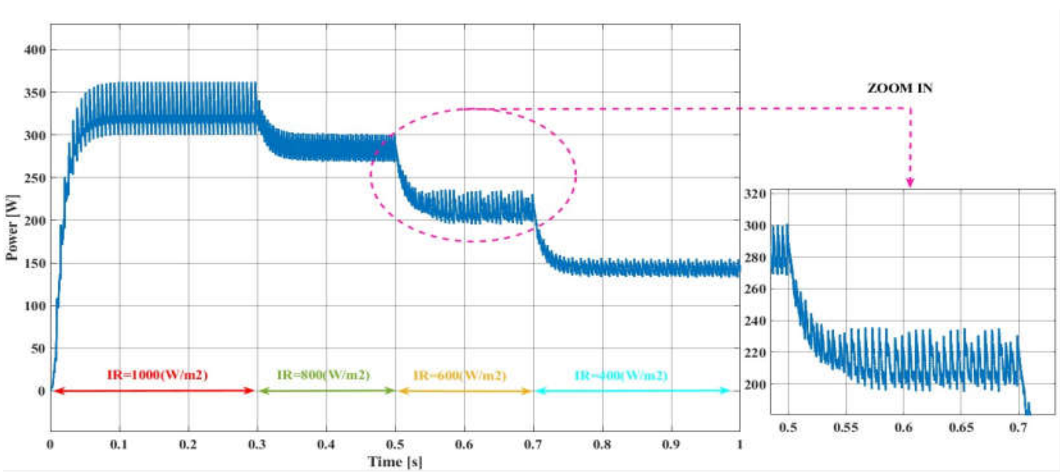

Figure (III.7): Power Simulation Result versus time for P&O in variable irradiances

The Figure (III.7) provides a comprehensive view of the MPPT system's power output behavior under varying irradiance levels. The main plot demonstrates the system's ability to track the maximum power point across different irradiances, with power stabilizing at approximately 350W, 300W, 250W, and 200W for Irradiances levels of 1000W/m², 800W/m², 600W/m², and 400W/m², respectively. The red dashed ellipse and zoomed-in view emphasize the system's transient response to a sudden drop in irradiance, showcasing the characteristic oscillations as the P&O algorithm adjusts to the new maximum power point. This detailed analysis underscores the efficiency and adaptability of the MPPT system in real-time solar energy applications.

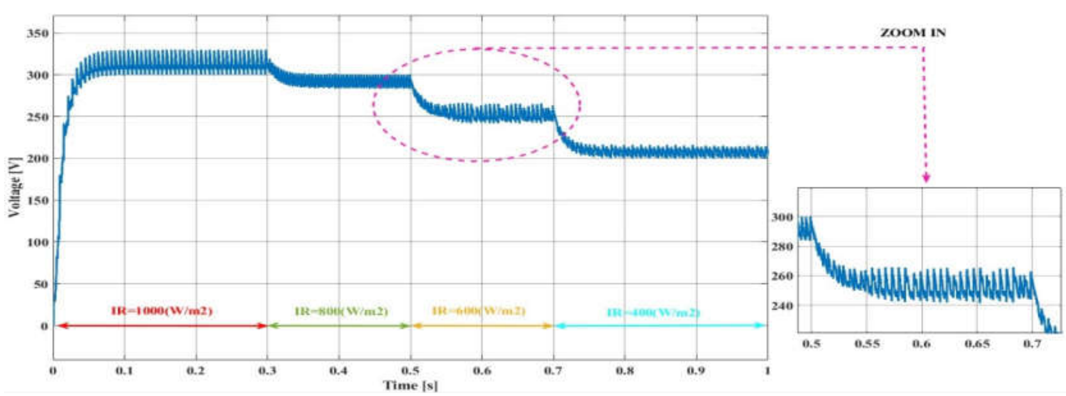

Figure (III.8): Voltage Simulation Result versus time for P&O in variable irradiances

The Figure (III.8) demonstrates how the voltage of an MPPT system using the P&O algorithm adjusts to varying irradiance levels. The main plot shows the system's quick voltage stabilization at around 320V, followed by stepwise decreases as the irradiance drops. The zoomed-in view provides a detailed look at the transient fluctuations, illustrating the algorithm's continuous adjustments to maintain optimal performance.

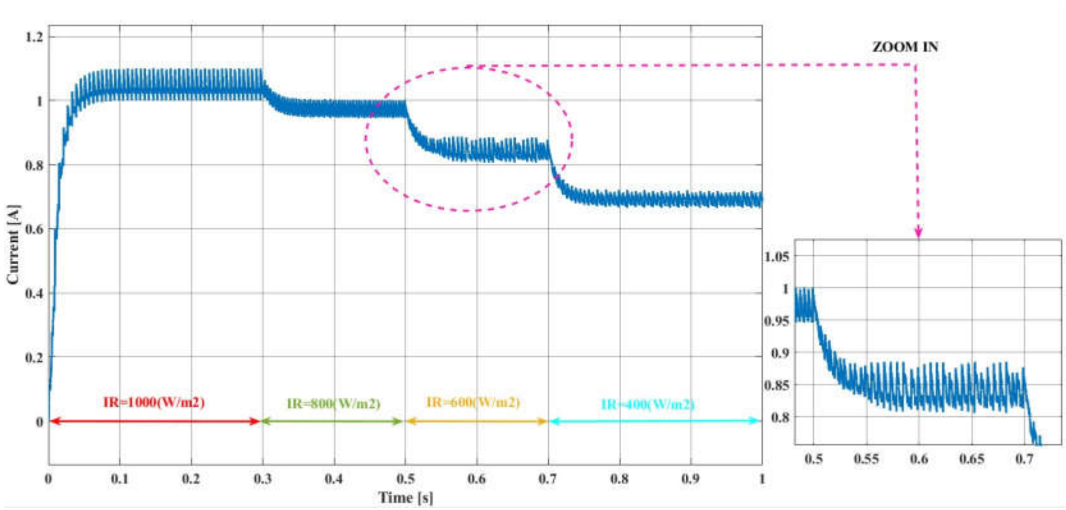

Figure (III.9): Current Simulation Result versus time for P&O in variable irradiances

The Figure (III.9) demonstrates how the MPPT system's current output, managed by the P&O algorithm, adjusts under varying irradiance levels. The main plot shows the current stabilizing around 1A and decreasing in steps as irradiance decreases. The zoomed-in view captures the transient response during an irradiance change.

III.3.2. Incremental Conductance (INC) algorithm

In this simulation, we used the Incremental Conductance (INC) algorithm to obtain results for power, voltage, and current. Figure (III.10) represents the general system simulation, showcasing the overall setup and performance of the INC-based MPPT system. The figure illustrates the integration of PV panels with the INC-based MPPT controller, which adjusts the duty cycle to optimize power extraction.

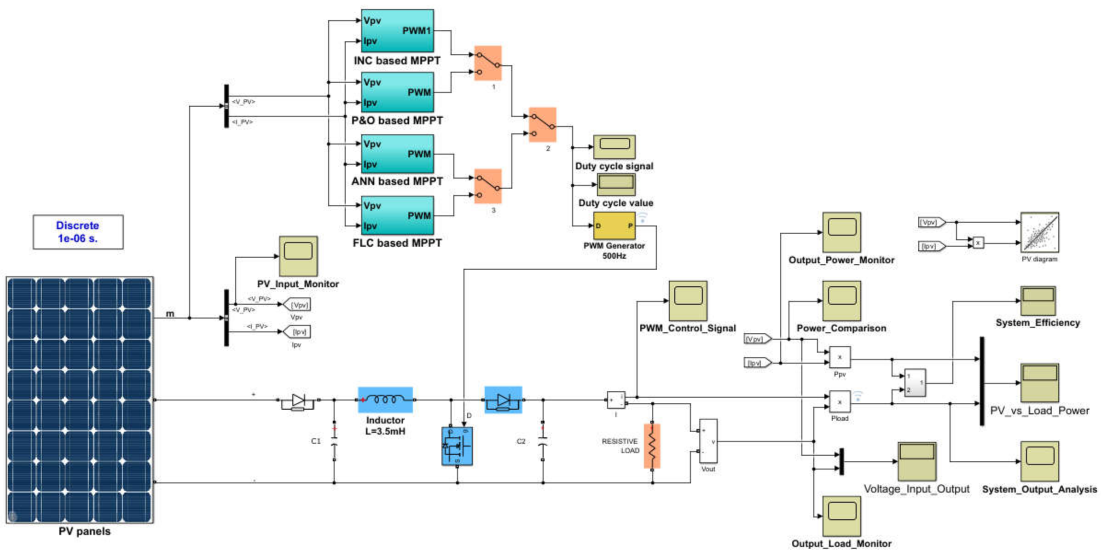

Figure (III.10): Schematic simulation system with INC

a)- Constant irradiance (1000 W/m²) and constant temperature (25°C)

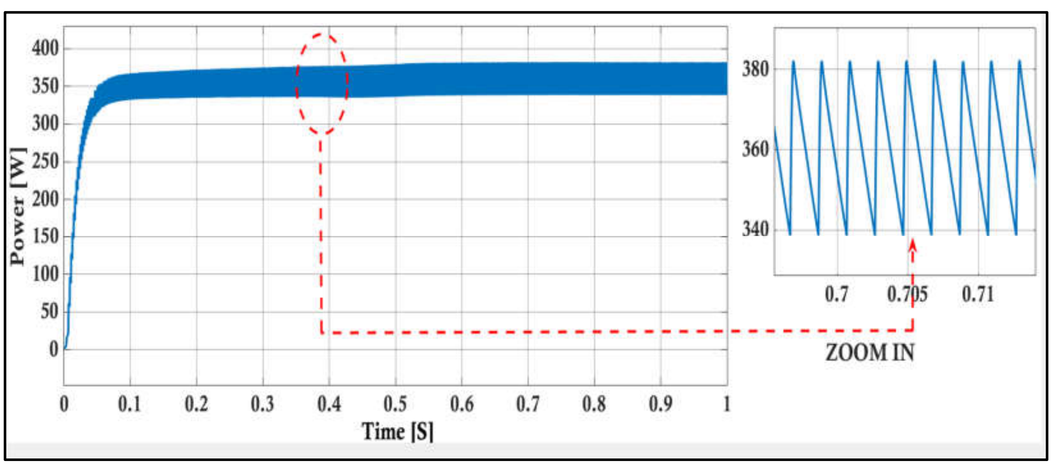

Figure (III.11): Power simulation result versus time for INC in constant irradiance

The Figure (III.11) demonstrates the power stabilization behavior of an MPPT system managed by the Incremental Conductance algorithm. The main plot shows a rapid rise and stabilization of power at approximately 380W, reflecting the system's efficiency. The zoomed-in view highlights periodic fluctuations, illustrating the algorithm's continuous adjustments to maintain optimal power output. This analysis underscores the Incremental Conductance algorithm's capability to dynamically track the maximum power point with precision.

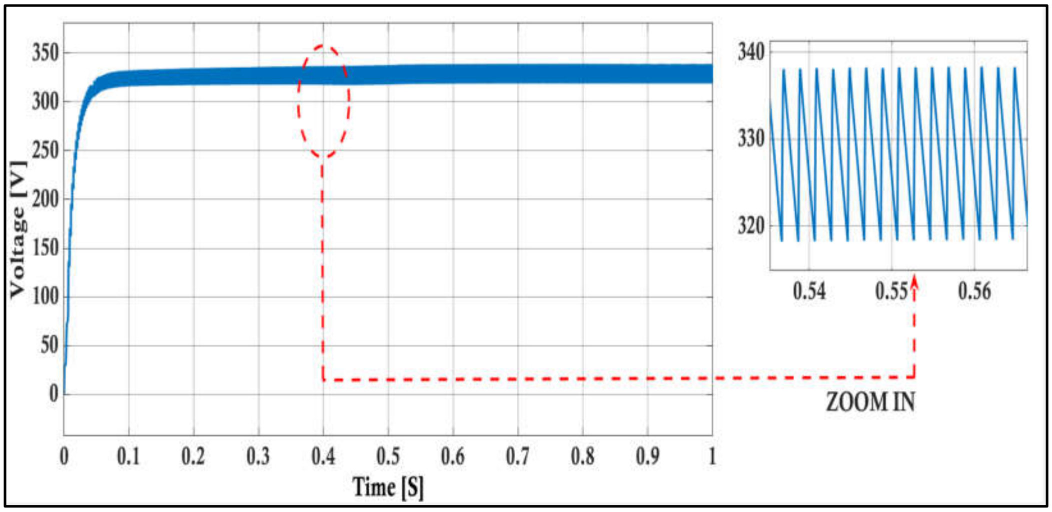

Figure (III.12): Voltage simulation result versus time for INC in constant irradiance

The Figure (III.12) demonstrates the voltage response of an Incremental Conductance-based MPPT system. The main plot shows the voltage stabilizing around 330V, while the zoomed-in view captures small fluctuations.

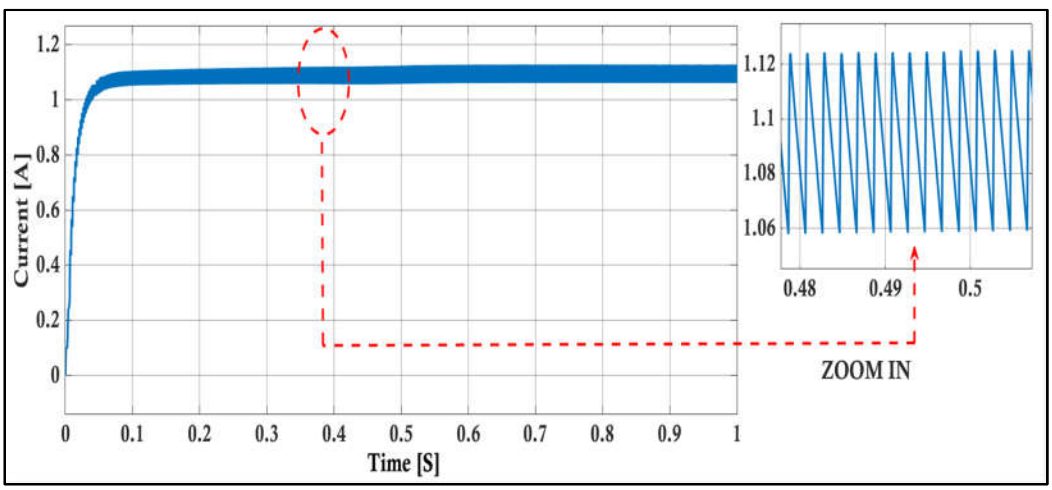

Figure (III.13): Current simulation result versus time for INC in constant irradiance

The Figure (III.13) demonstrates the current stabilization behavior of an MPPT system managed by the Incremental Conductance algorithm. The main plot shows the current quickly rising and stabilizing around 1.1A, indicating the system's efficiency in reaching the maximum power point. The zoomed-in view highlights small fluctuations in the current.

b)- Variable irradiances (1000, 800, 600, 400 W/m²) and constant temperature (25°C)

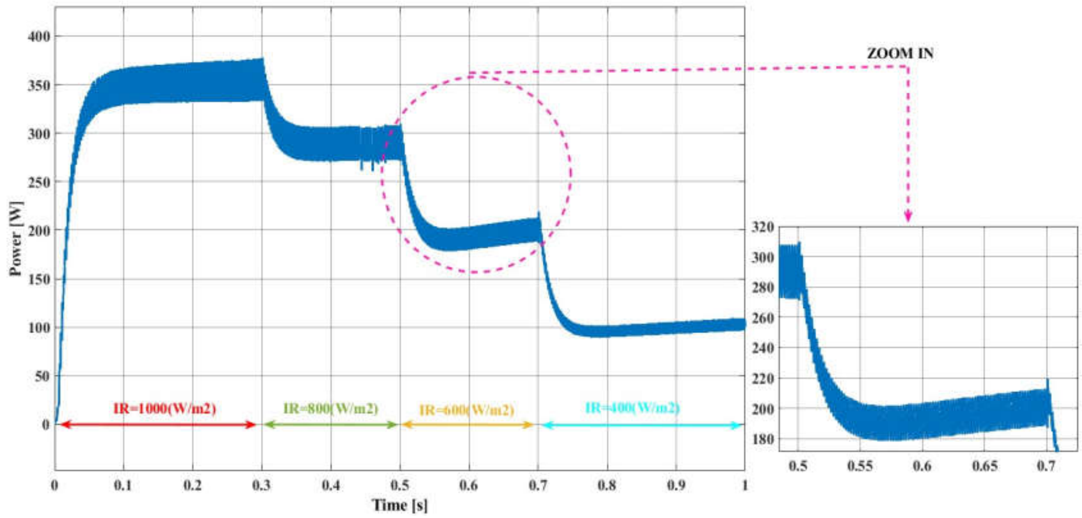

Figure (III.14): Power simulation result versus time for INC in variable irradiances

The Figure (III.14) demonstrates the power response of an MPPT system using the Incremental Conductance algorithm under varying irradiance conditions. The main plot shows the power stabilizing around 350W initially, with stepwise decreases as the irradiance drops. The zoomed-in view captures the transient fluctuations during an irradiance change.

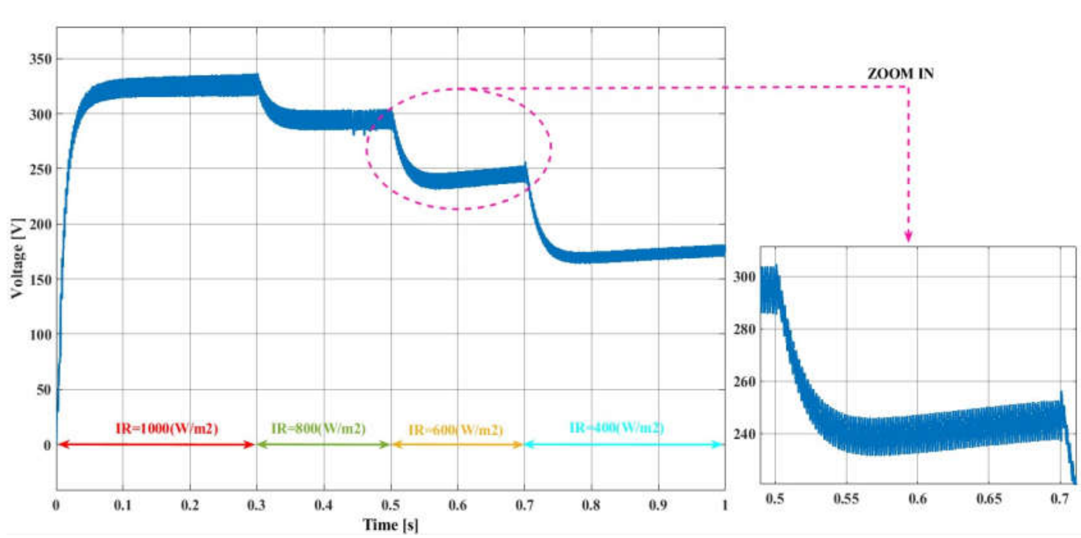

Figure (III.15): Voltage simulation result versus time for INC in variable irradiances

The Figure (III.15) demonstrates the voltage response of an Incremental Conductance-based MPPT system to varying irradiance levels. The main plot shows a rapid rise and stabilization around 330V, with stepwise decreases as irradiance drops. The zoomed-in view highlights transient fluctuations.

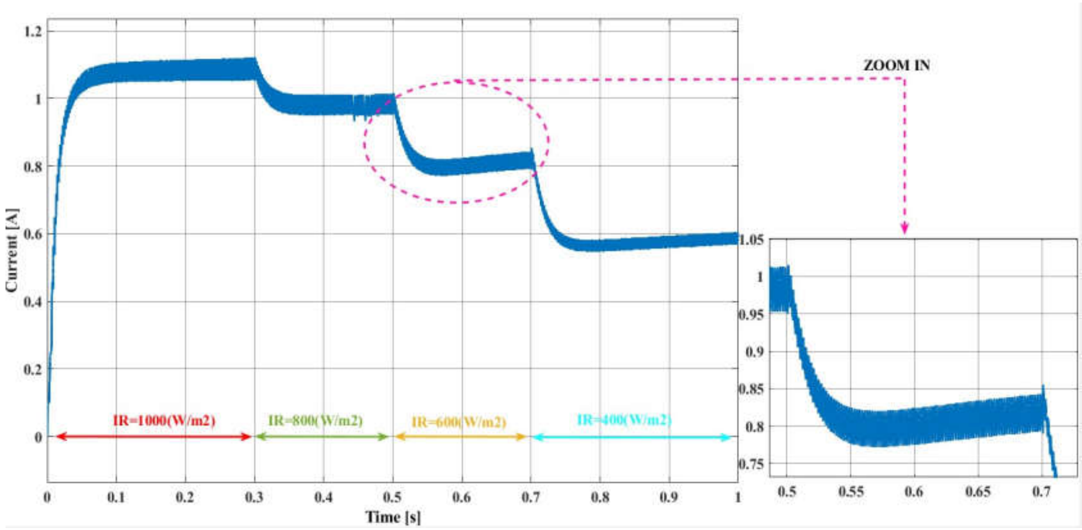

Figure (III.16): Current simulation result versus time for INC in variable irradiances

The Figure (III.16) demonstrates the current response of an MPPT system using the Incremental Conductance algorithm under varying irradiance conditions. The main plot shows the current stabilizing around 1.1A initially, with stepwise decreases as the irradiance drops. The zoomed-in view captures transient fluctuations during an irradiance change.

III.3.3. Artificial Neural Network (ANN) algorithm

In this simulation, we used the Artificial Neural Network (ANN) algorithm to obtain results for power, voltage, and current. Figure (III.17) represents the general system simulation, showcasing the overall setup and performance of the ANN-based MPPT system. The figure illustrates the integration of PV panels with the ANN-based MPPT controller, which adjusts the duty cycle to optimize power extraction.

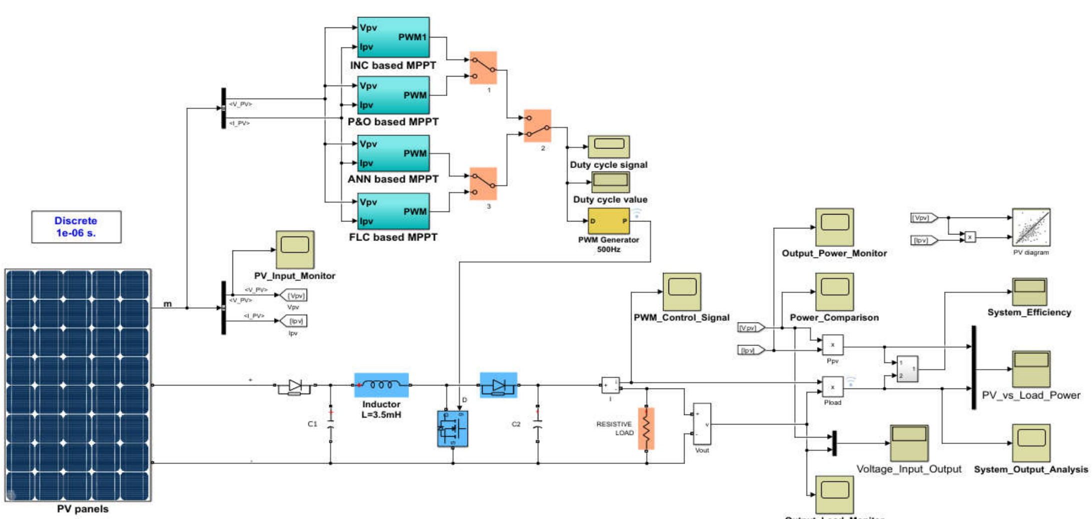

Figure (III.17): Schematic simulation system with ANN

a)- Constant irradiance (1000 W/m²) and constant temperature (25°C)

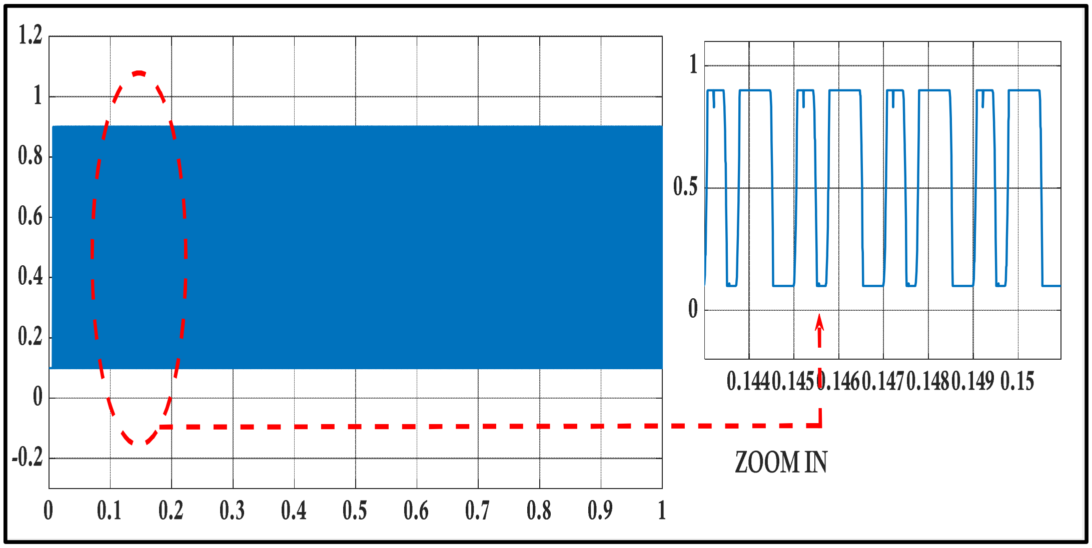

Figure (III.18): Duty Cycle Simulation Result versus time

The Figure (III.18) demonstrates the stability and fine-tuning of the duty cycle by an ANN based MPPT system. The main plot shows a stable duty cycle near 1, while the zoomed-in view reveals periodic adjustments, indicating the ANN's responsiveness to optimize performance.

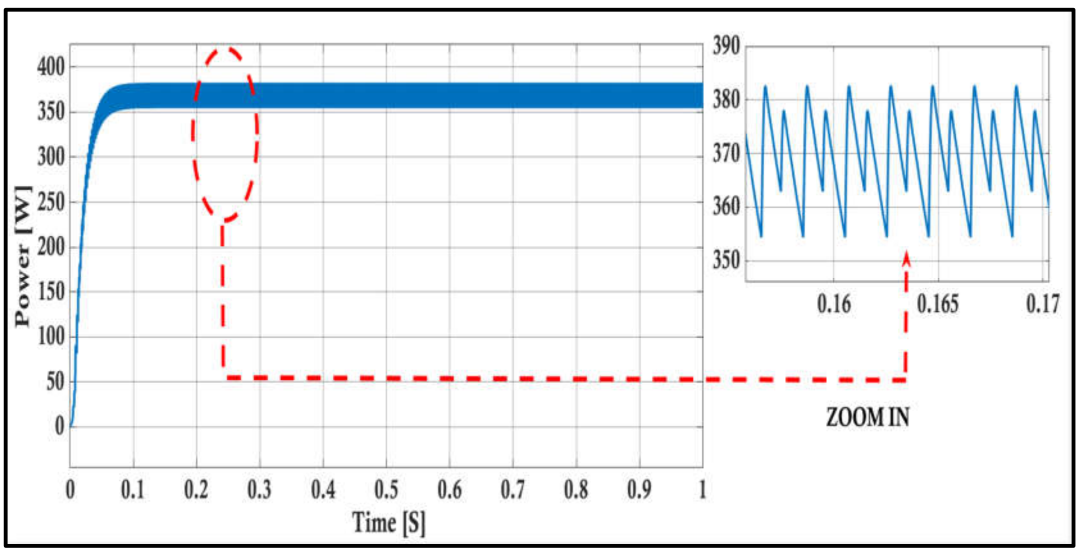

Figure (III.19): Power simulation result versus time for ANN in constant irradiance

The Figure (III.19) demonstrates the power stabilization behavior of an MPPT system managed by an ANN algorithm. The main plot indicates a rapid rise and stabilization of power at approximately 380W, reflecting the system's efficiency. The zoomed-in view highlights periodic fluctuations, illustrating the ANN's ongoing adjustments to maintain optimal power output. This analysis underscores the ANN algorithm's capability to dynamically track the maximum power point with precision.

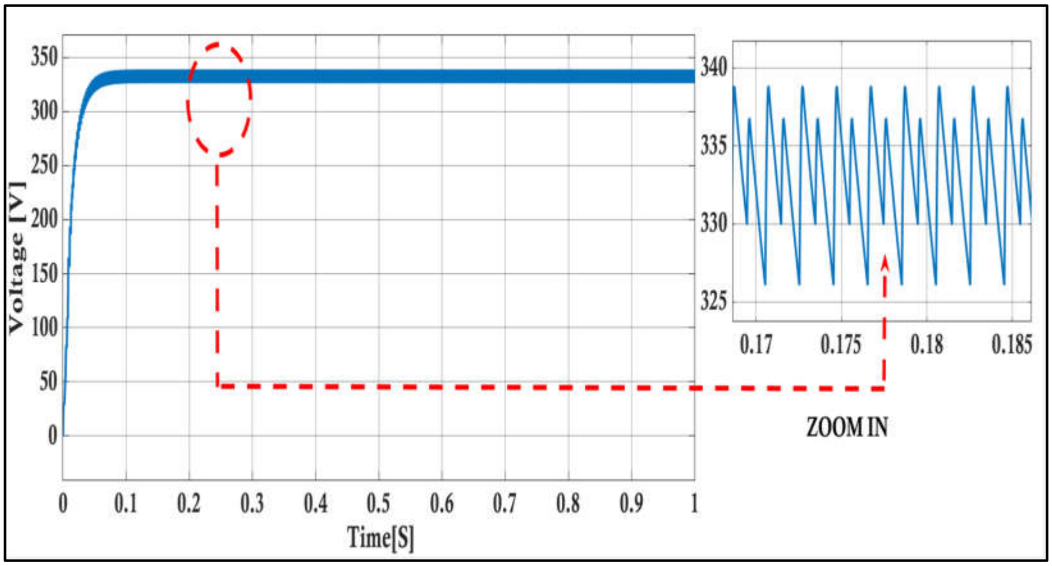

Figure (III.20): Voltage simulation result versus time for ANN in constant irradiance

The Figure (III.20) illustrates the voltage behavior of an ANN-based MPPT system. The main plot shows a quick rise and stabilization around 335V, while the zoomed-in view captures small fluctuations.

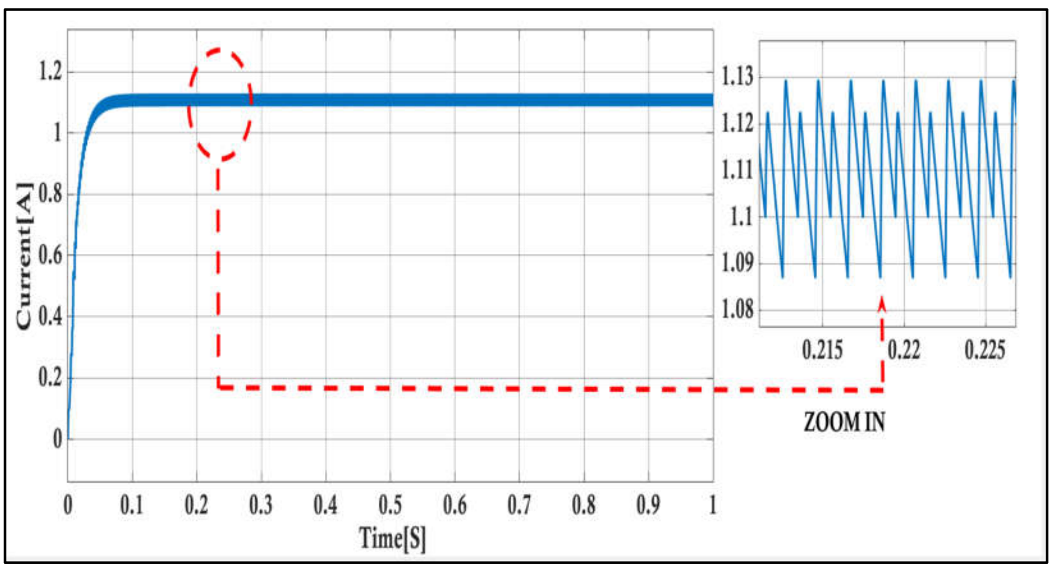

Figure (III.21): Current simulation result versus time for ANN in constant irradiance

The Figure (III.21) shows the current stabilization of an ANN-based MPPT system. The main plot displays a rapid rise in current, stabilizing around 1.1A. The zoomed-in view highlights small fluctuations.

b)- Variable irradiances (1000, 800, 600, 400 W/m²) and constant temperature (25°C)

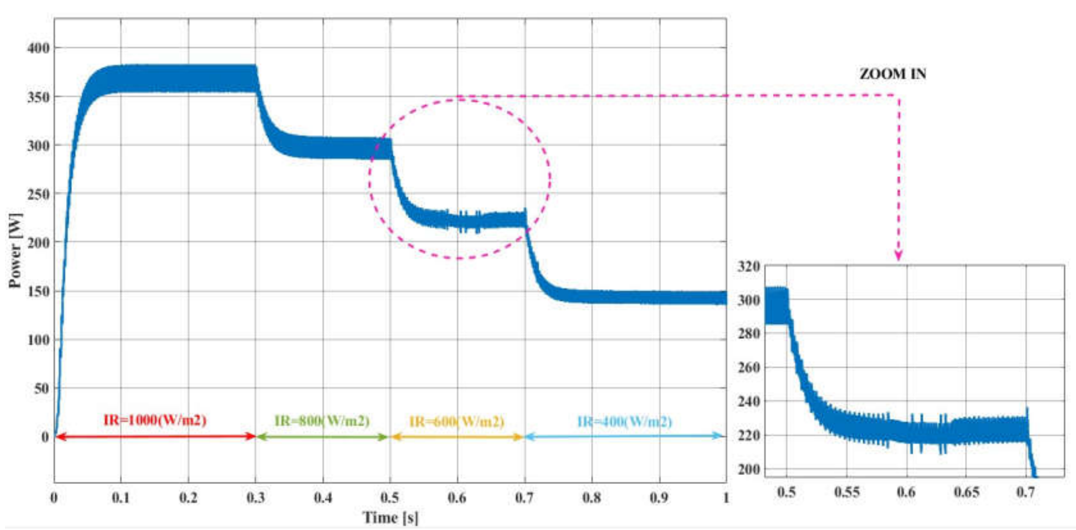

Figure (III.22): Power simulation result versus time for ANN in variable irradiances

The Figure (III.22) demonstrates how the ANN-based MPPT system adjusts its power output under varying irradiance conditions. The main plot shows the power stabilizing at approximately 350W initially, with stepwise decreases as the irradiance drops. The zoomed-in view captures the transient fluctuations during an irradiance change.

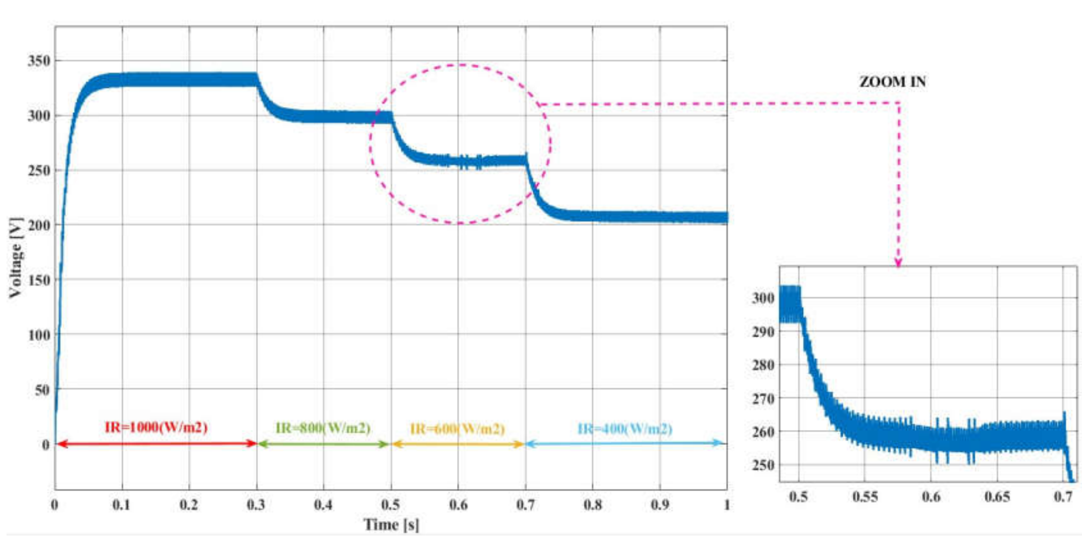

Figure (III.23): Voltage simulation result versus time for ANN in variable irradiances

The Figure (III.23) illustrates the ANN-based MPPT system's voltage response to varying irradiance. The main plot shows the voltage stabilizing around 330V and stepping down with decreasing irradiance. The zoomed-in view highlights transient fluctuations This demonstrates the algorithm's capability to dynamically adjust to real-time changes in solar irradiance, ensuring efficient performance.

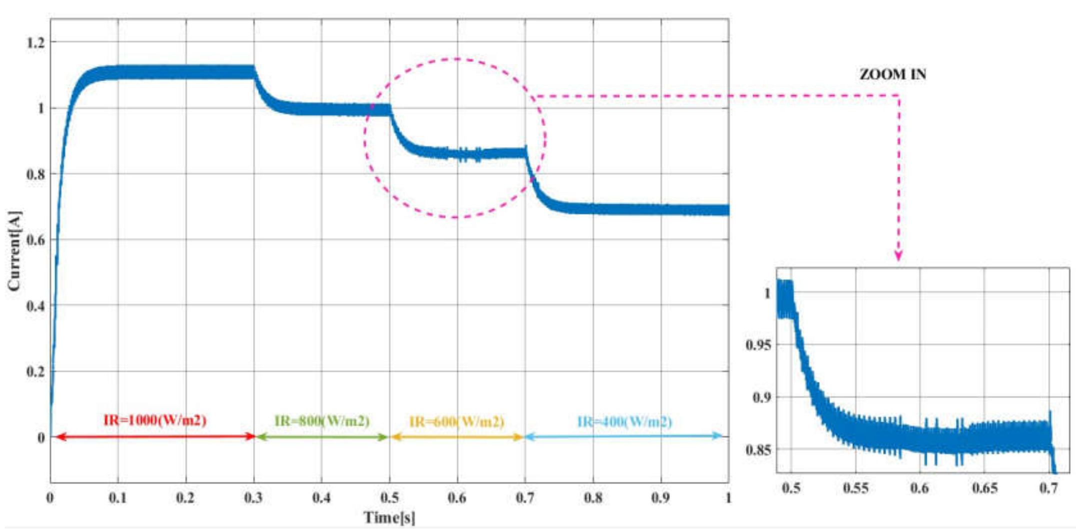

Figure (III.24): Current simulation result versus time for ANN in variable irradiances

The Figure (III.24) demonstrates the current response of an ANN-based MPPT system under varying irradiance conditions. The main plot shows the current stabilizing around 1.1A initially, with stepwise decreases as the irradiance drops. The zoomed-in view captures transient fluctuations during an irradiance change.

III.3.4. Fuzzy Logic Controller (FLC) algorithm

In this simulation, we used the Fuzzy Logic Controller (FLC) algorithm to obtain results for power, voltage, and current. Figure (III.25) represents the general system simulation, showcasing the overall setup and performance of the FLC-based MPPT system. The figure illustrates the integration of PV panels with the FLC-based MPPT controller, which adjusts the duty cycle to optimize power extraction.

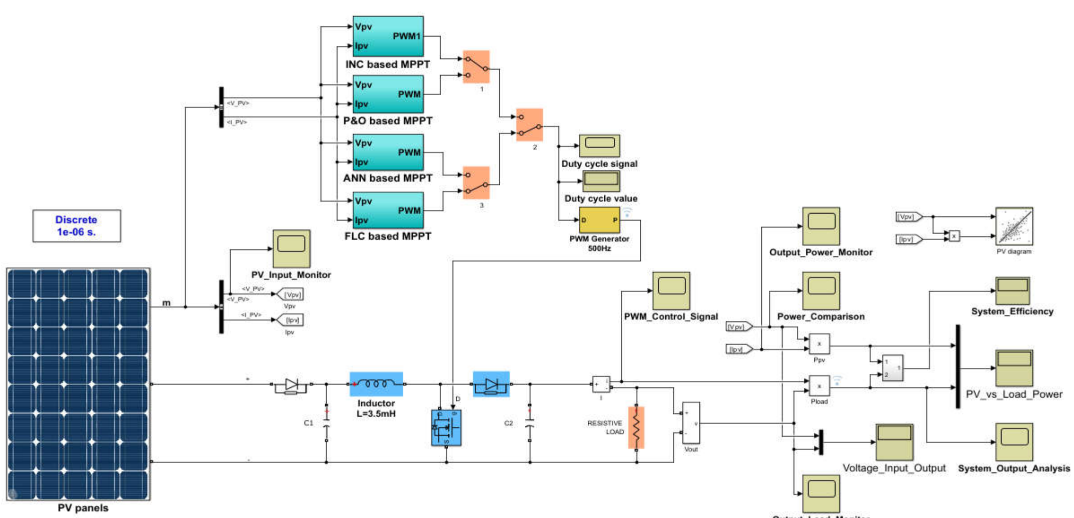

Figure (III.25): Schematic simulation system with FLC

a)- Constant irradiance (1000 W/m²) and constant temperature (25°C)

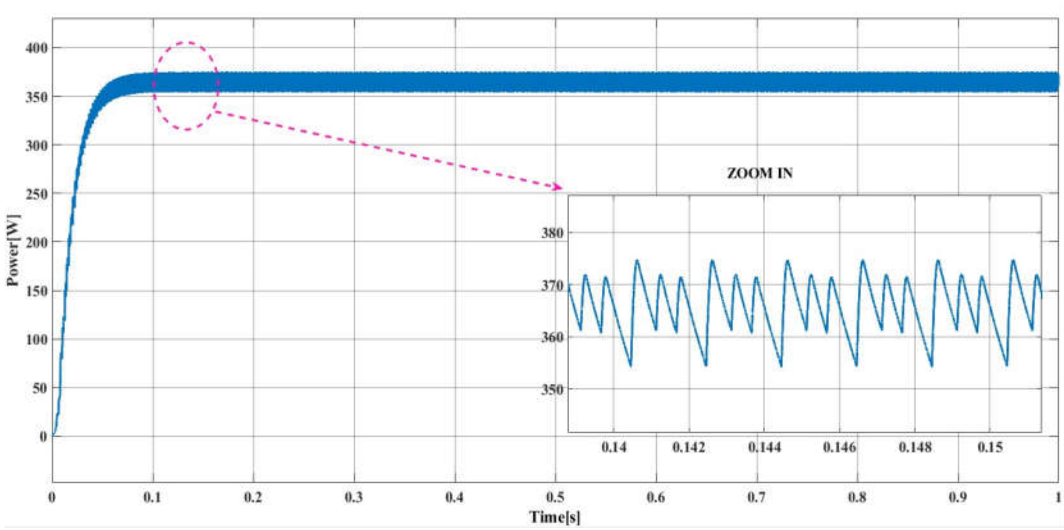

Figure (III.26): Power simulation result versus time for FLC in constant irradiance

The figure (III.26) illustrates the system power output exponentially increasing quickly to around 370 W under constant irradiance, controlled by a Fuzzy Logic Controller (FLC). After this initial rise (transient time), the power stays fairly stable around this value but shows continuous, relatively small-scale, cyclical fluctuations (steady-state). Zooming in stresses these oscillations, suggesting natural dynamics or control reactions within the FLC-controlled system. The FLC performs well in regulating the average power, but there is a steady-state ripple.

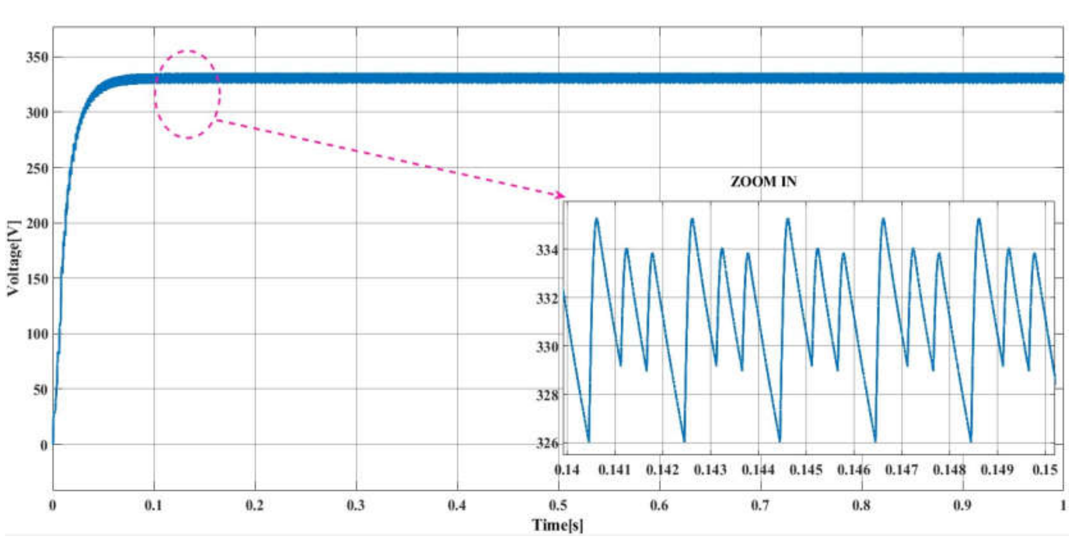

Figure (III.27): Voltage simulation result versus time for FLC in constant irradiance

The figure represents the voltage behavior of an FLC-based MPPT system under constant irradiance conditions. The curve shows a rapid rise in voltage, quickly stabilizing around a specific value (approximately 335V). This indicates the system's ability to adapt efficiently and reach optimal performance under stable environmental conditions. While the zoomed-in views the magnified section reveals minor fluctuations after stabilization, reflecting the system's continuous fine-tuning to maintain maximum power point tracking with high precision despite minor load or condition changes.

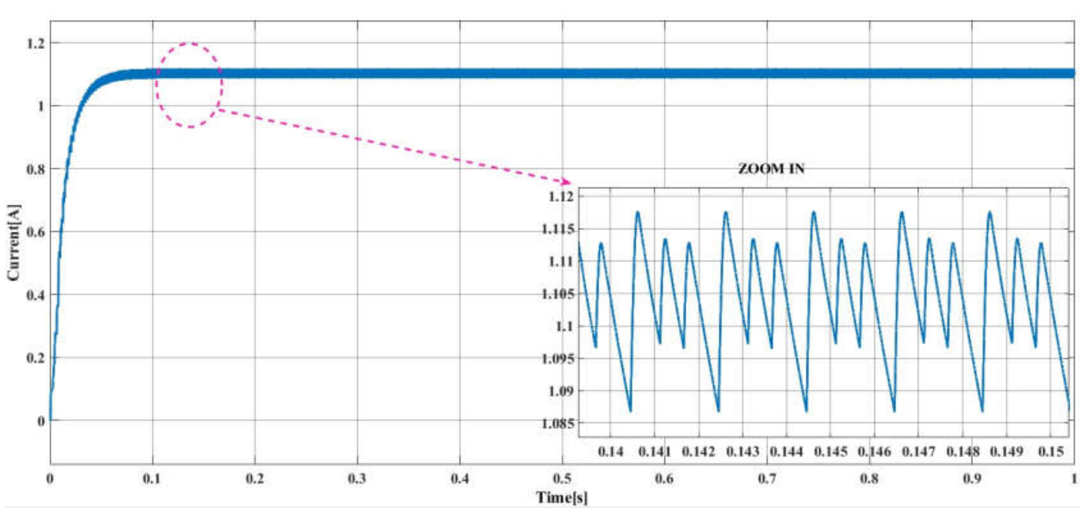

Figure (III.28): Current simulation result versus time for ANN in constant irradiance

The Figure (III.28) illustrates the current stabilization of an FLC-based MPPT system. The main plot shows a rapid rise in current, stabilizing around 1.1A. The zoomed-in view highlights small fluctuations near the stabilization point. This behavior reflects the efficiency of the FLC system under constant irradiance conditions, with minor deviations due to its rule-based nature.

b)- Variable irradiances (1000, 800, 600, 400 W/m^2) and constant temperature (25°C)

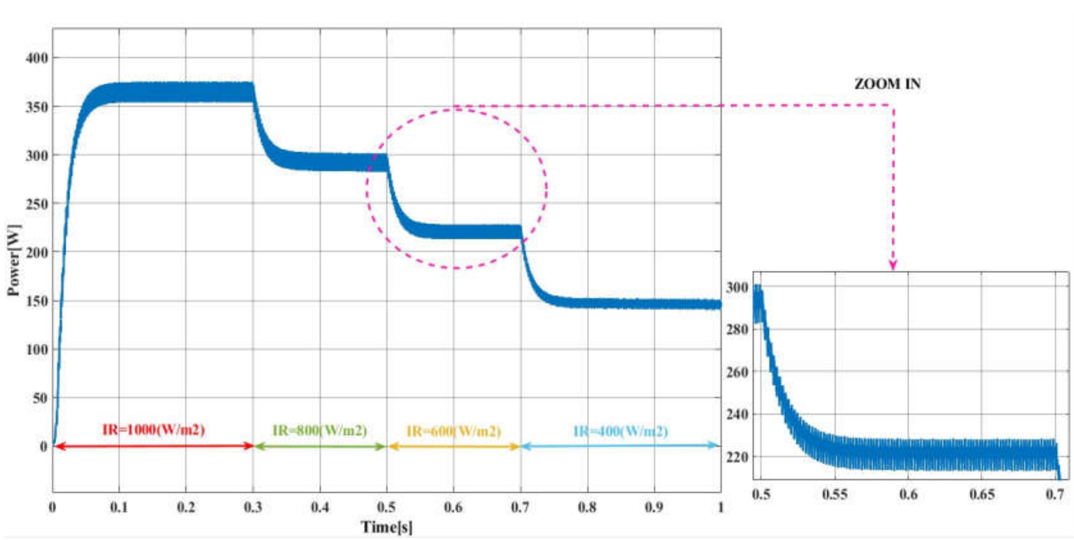

Figure (III.29): Power simulation result versus time for FLC in variable irradiances

The figure illustrates the performance of the Fuzzy Logic Controller (FLC) based MPPT system under fluctuating irradiance conditions. Initially, the power stabilizes at approximately 350W , followed by stepwise decreases as irradiance levels drop over time. The zoomed-in section highlights transient fluctuations during these transitions, with power briefly oscillating between 340W and 350W before stabilizing at a new level. These precise adjustments demonstrate the system's ability to dynamically adapt to rapid changes in irradiance while maintaining efficient energy extraction.

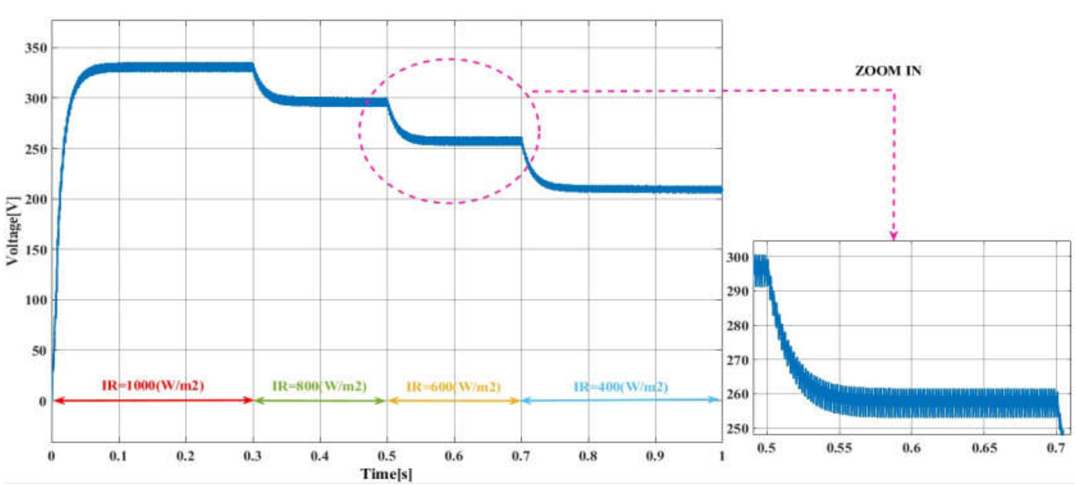

Figure (III.30): Voltage simulation result versus time for FLC in variable irradiances

The Figure (III.30) illustrates the FLC-based MPPT system's voltage response to varying irradiance. The main plot shows the voltage stabilizing around 330V and stepping down to approximately 250-270V with decreasing irradiance. The zoomed-in view reveals minor transient fluctuations during adaptation. Each stabilization period after irradiance changes takes approximately 0.02 to 0.05 seconds. This demonstrates the FLC algorithm's ability to efficiently adapt to dynamic solar irradiance changes while maintaining stable performance.

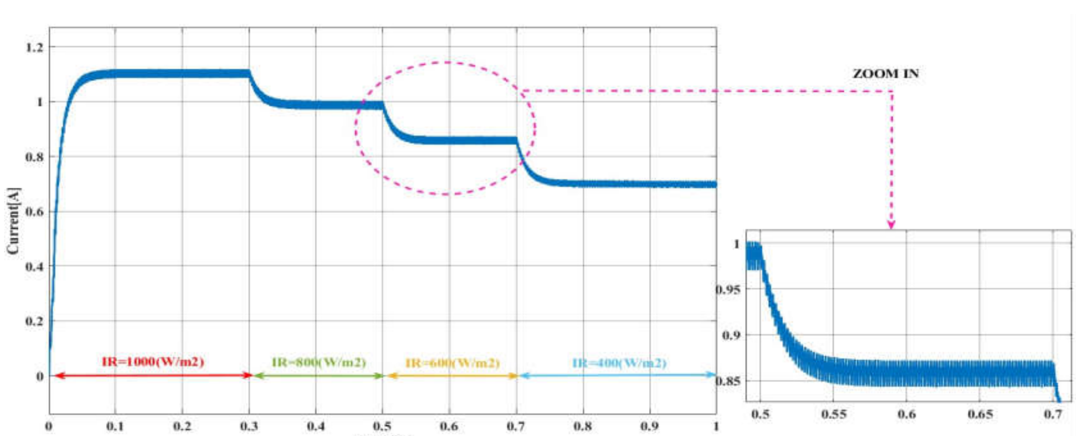

Figure (III.31): Current simulation result versus time for FLC in variable irradiances

The figure (III.31) depicts the current response of an FLC-based MPPT system under fluctuating irradiance levels. Initially, the current stabilizes at approximately 1.1A , showing steady behaviour. As irradiance decreases, the current exhibits stepwise reductions, reaching around 0.8A during lower irradiance periods. The zoomed-in section highlights transient fluctuations, with minor oscillations of about ±0.05A , reflecting the system's dynamic adaptation to rapid changes in irradiance.

III.4. Comparison and Analysis Between P&O, INC, ANN and FLC

III.4.1. Constant Irradiance (1000 W/m^2)

The following figures compare the power, current and voltage in constant irradiance outputs of four MPPT algorithms: Perturb and Observe (P&O), Incremental Conductance (INC), Artificial Neural Network (ANN) and Fuzzy Logic Control (FLC).

a)- Analysis of Voltage Tracking Performance

The provided graph compares the voltage tracking performance of four different control strategies over time. The strategies are:

1. V (P&O) : Perturb and Observe method.
2. V (INC) : Incremental Conductance method.
3. V (ANN) : Artificial Neural Network-based method.
4. V (FLC) : Fuzzy Logic Control-based method.

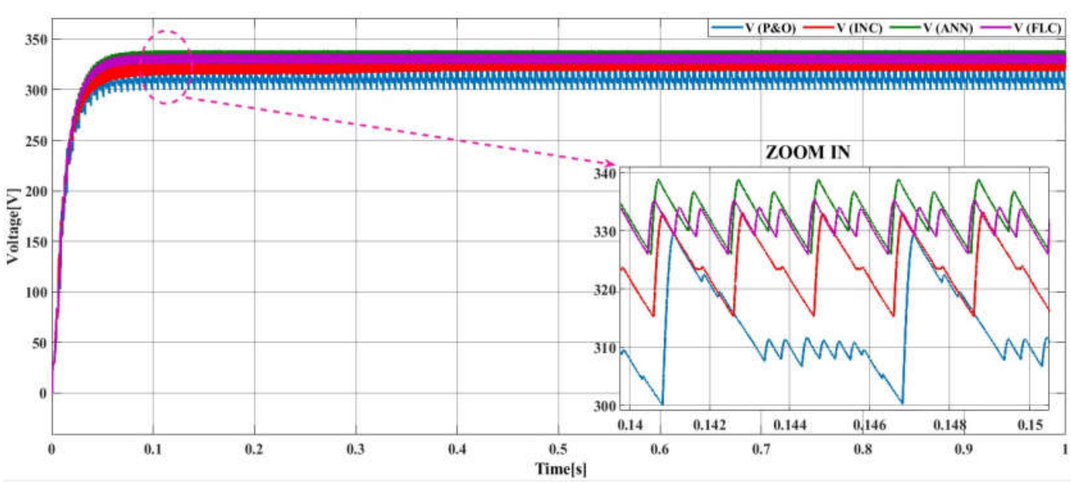

Figure (III.32): Voltage simulation result versus time in constant irradiance of four MPPT algorithms

Main Graph Analysis

- Time Range : The main graph spans from 0 to 1 second.
- Voltage Range : The voltage values range from approximately 0 V to 350 V.
- Initial Transient Behavior :
  - All methods start at 0 V and rapidly increase their voltage output within the first 0.1 seconds.
  - The V (FLC) method (pink dashed line) reaches its peak voltage slightly faster than the others, indicating a quicker response time.
  - The V (P&O) method (blue solid line) shows a smooth and steady increase in voltage.
  - The V (INC) method (red dashed line) and V (ANN) method (green solid line) also show rapid increases but with slight oscillations compared to V (P&O) .
- Steady-State Performance :
  - After approximately 0.1 seconds, all methods stabilize around a voltage level of 330 V .
  - The V (P&O) method maintains a very stable voltage output with minimal fluctuations.
  - The V (INC) and V (ANN) methods exhibit small oscillations around the steady-state value.
  - The V (FLC) method shows a slightly higher steady-state voltage compared to the others, reaching approximately 340 V .

Zoomed-In Section Analysis

- Time Range : The zoomed-in section focuses on the interval from 0.14 to 0.15 seconds.
- Voltage Range : The voltage values in this section range from approximately 300V to 340V.

- Detailed Observations :
  - The V (FLC) method (pink dashed line) consistently achieves the highest voltage output, peaking at 340 V .
  - The V (P&O) method (blue solid line) shows significant fluctuations, dropping as low as 300 V and recovering to around 310 V .
  - The V (INC) method (red dashed line) and V (ANN) method (green solid line) maintain relatively stable outputs around 330 V , with minor oscillations.

Comparison of Methods

Table (III.2): Comparison the voltage between the four methods in constant irradiance

Method	Initial Response	Steady-State Voltage	Fluctuations	Peak Voltage
V (P&O)	Smooth, moderate	~330 V	Minimal	~330 V
V (INC)	Rapid, with oscillations	~330 V	Moderate	~330 V
V (ANN)	Rapid, with oscillations	~330 V	Moderate	~330 V
V (FLC)	Fastest	~340 V	Slight	~340 V

Key Findings

1. Response Time : The V (FLC) method has the fastest initial response, reaching its peak voltage quickest.
2. Steady-State Stability : The V (P&O) method demonstrates the most stable steady-state performance with minimal fluctuations.
3. Peak Voltage Output : The V (FLC) method achieves the highest peak voltage output, reaching 340 V .
4. Oscillations : Both the V (INC) and V (ANN) methods exhibit more noticeable oscillations compared to V (P&O) and V (FLC) .

Conclusion

The V (FLC) method outperforms the others in terms of peak voltage and initial response speed. However, it shows slight fluctuations in the steady state. The V (P&O) method provides the most stable voltage output with minimal fluctuations, making it suitable for applications requiring high reliability. The V (INC) and V (ANN) methods offer good performance but with some oscillations that may affect system stability under certain conditions.

Final Recommendation

For applications prioritizing peak voltage and fast response, the V (FLC) method is recommended. For applications requiring highly stable voltage output, the V (P&O) method is the best choice.

b)- Analysis of Current Tracking Performance

The provided graph compares the current tracking performance of four different control strategies over time. The strategies are:

1. I (P&O) : Perturb and Observe method.
2. I (INC) : Incremental Conductance method.
3. I (ANN) : Artificial Neural Network-based method.
4. I (FLC) : Fuzzy Logic Control-based method.

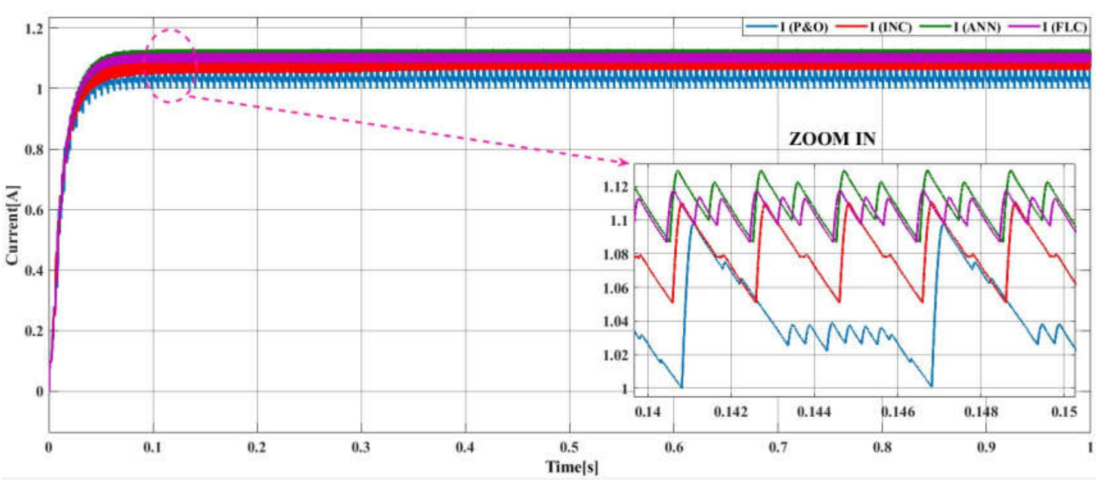

Figure (III.33): Current simulation result versus time in constant irradiance of four MPPT algorithms

Main Graph Analysis

- Time Range : The main graph spans from 0 to 1 second.
- Current Range : The current values range from approximately 0 A to 1.2 A.
- Initial Transient Behavior :
    - All methods start at 0 A and rapidly increase their current output within the first 0.1 seconds.

- The I (FLC) method (pink dashed line) reaches its peak current slightly faster than the others, indicating a quicker response time.
- The I (P&O) method (blue solid line) shows a smooth and steady increase in current.
- The I (INC) method (red dashed line) and I (ANN) method (green solid line) also show rapid increases but with slight oscillations compared to I (P&O) .

- Steady-State Performance :
  - After approximately 0.1 seconds, all methods stabilize around a current level of 1.1A .
  - The I (P&O) method maintains a very stable current output with minimal fluctuations.
  - The I (INC) and I (ANN) methods exhibit small oscillations around the steady-state value.
  - The I (FLC) method shows a slightly higher steady-state current compared to the others, reaching approximately 1.12 A .

Zoomed-In Section Analysis

- Time Range : The zoomed-in section focuses on the interval from 0.14 to 0.15 seconds.
- Current Range : The current values in this section range from approximately 1 A to 1.12A.
- Detailed Observations :
  - The I (FLC) method (pink dashed line) consistently achieves the highest current output, peaking at 1.12 A .
  - The I (P&O) method (blue solid line) shows significant fluctuations, dropping as low as 1 A and recovering to around 1.02 A .
  - The I (INC) method (red dashed line) and I (ANN) method (green solid line) maintain relatively stable outputs around 1.1 A , with minor oscillations.

Comparison of Methods

Table (III.3): Comparison the current between the four methods in constant irradiance

Method	Initial Response	Steady-State Current	Fluctuations	Peak Current
I (P&O)	Smooth, moderate	~1.1 A	Minimal	~1.1 A
I (INC)	Rapid, with oscillations	~1.1 A	Moderate	~1.1 A
I (ANN)	Rapid, with oscillations	~1.1 A	Moderate	~1.1 A
I (FLC)	Fastest	~1.12 A	Slight	~1.12 A

Key Findings

1. Response Time : The I (FLC) method has the fastest initial response, reaching its peak current quickest.
2. Steady-State Stability : The I (P&O) method demonstrates the most stable steady-state performance with minimal fluctuations.
3. Peak Current Output : The I (FLC) method achieves the highest peak current output, reaching 1.12 A .
4. Oscillations : Both the I (INC) and I (ANN) methods exhibit more noticeable oscillations compared to I (P&O) and I (FLC) .

Conclusion

The I (FLC) method outperforms the others in terms of peak current and initial response speed. However, it shows slight fluctuations in the steady state. The I (P&O) method provides the most stable current output with minimal fluctuations, making it suitable for applications requiring high reliability. The I (INC) and I (ANN) methods offer good performance but with some oscillations that may affect system stability under certain conditions.

Final Recommendation

For applications prioritizing peak current and fast response, the I (FLC) method is recommended. For applications requiring highly stable current output, the I (P&O) method is the best choice.

c)- Analysis of Power Tracking Performance

The provided graph compares the power tracking performance of four different control strategies over time. The strategies are:

1. P (P&O) : Perturb and Observe method.
2. P (INC) : Incremental Conductance method.
3. P (ANN) : Artificial Neural Network-based method.
4. P (FLC) : Fuzzy Logic Control-based method.

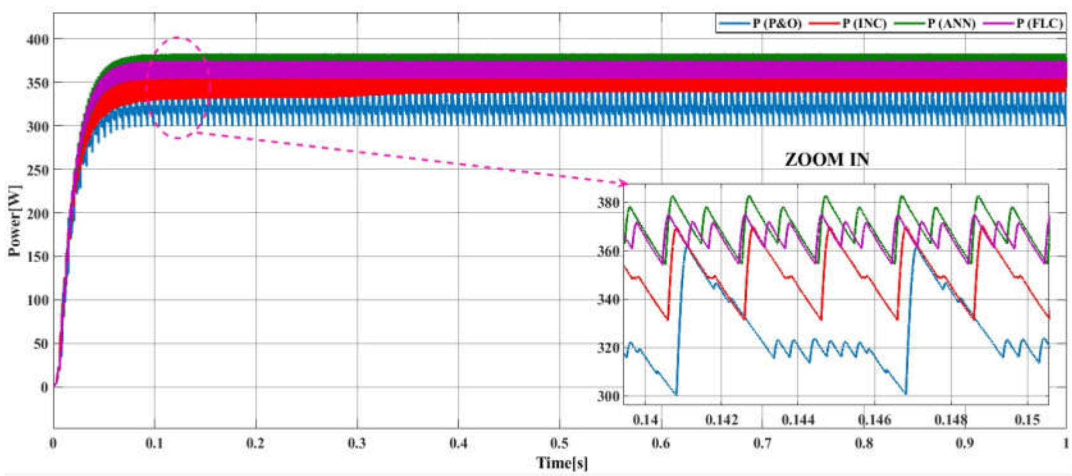

Figure (III.34): Power simulation result versus time in constant irradiance of four MPPT algorithms

Main Graph Analysis

- Time Range : The main graph spans from 0 to 1 second.
- Power Range : The power values range from approximately 0 W to 400 W.
- Initial Transient Behavior :
  - All methods start at 0 W and rapidly increase their power output within the first 0.1 seconds.
  - The P (FLC) method (pink dashed line) reaches its peak power slightly faster than the others, indicating a quicker response time.
  - The P (P&O) method (blue solid line) shows a smooth and steady increase in power.
  - The P (INC) method (red dashed line) and P (ANN) method (green solid line) also show rapid increases but with slight oscillations compared to P (P&O) .

- Steady-State Performance :
  - After approximately 0.1 seconds, all methods stabilize around a power level of 350W .
  - The P (P&O) method maintains a very stable power output with minimal fluctuations.
  - The P (INC) and P (ANN) methods exhibit small oscillations around the steady-state value.
  - The P (FLC) method shows a slightly higher steady-state power level compared to the others, reaching approximately 380 W.

Zoomed-In Section Analysis

- Time Range : The zoomed-in section focuses on the interval from 0.14 to 0.15 seconds.
- Power Range : The power values in this section range from approximately 300 W to 380W.
- Detailed Observations :
  - The P (FLC) method (pink dashed line) consistently achieves the highest power output, peaking at 380 W .
  - The P (P&O) method (blue solid line) shows significant fluctuations, dropping as low as 300 W and recovering to around 320 W .
  - The P (INC) method (red dashed line) and P (ANN) method (green solid line) maintain relatively stable outputs around 360 W , with minor oscillations.

Comparison of Methods

Table (III.4): Comparison the power between the four methods in constant irradiance

Method	Initial Response	Steady-State Power	Fluctuations	Peak Power
P (P&O)	Smooth, moderate	~350 W	Minimal	~350 W
P (INC)	Rapid, with oscillations	~350 W	Moderate	~350 W
P (ANN)	Rapid, with oscillations	~350 W	Moderate	~350 W
P (FLC)	Fastest	~380 W	Slight	~380 W

Key Findings

1. Response Time : The P (FLC) method has the fastest initial response, reaching its peak power quickest.
2. Steady-State Stability : The P (P&O) method demonstrates the most stable steady-state performance with minimal fluctuations.
3. Peak Power Output : The P (FLC) method achieves the highest peak power output, reaching 380 W .
4. Oscillations : Both the P (INC) and P (ANN) methods exhibit more noticeable oscillations compared to P (P&O) and P (FLC).

Conclusion

The P (FLC) method outperforms the others in terms of peak power output and initial response speed. However, it shows slight fluctuations in the steady state. The P (P&O) method provides the most stable power output with minimal fluctuations, making it suitable for applications requiring high reliability. The P (INC) and P (ANN) methods offer good performance but with some oscillations that may affect system stability under certain conditions.

Final Recommendation

For applications prioritizing peak power and fast response, the P (FLC) method is recommended. For applications requiring highly stable power output, the P (P&O) method is the best choice.

III.4.2. Variable Irradiances (1000, 800, 600, 400 W/m^2)

The following figures compare the power, current and voltage in variable irradiances outputs of four MPPT algorithms: Perturb and Observe (P&O), Incremental Conductance (INC), Artificial Neural Network (ANN) and Fuzzy Logic Control (FLC).

a)- Analysis of Voltage Tracking Performance Under Varying Irradiance Conditions

The provided graph compares the voltage tracking performance of four different control strategies under varying irradiance (IR) conditions. The strategies are:

1. V (P&O) : Perturb and Observe method.
2. V (INC) : Incremental Conductance method.

3. V (ANN) : Artificial Neural Network-based method.

4. V (FLC) : Fuzzy Logic Control-based method.

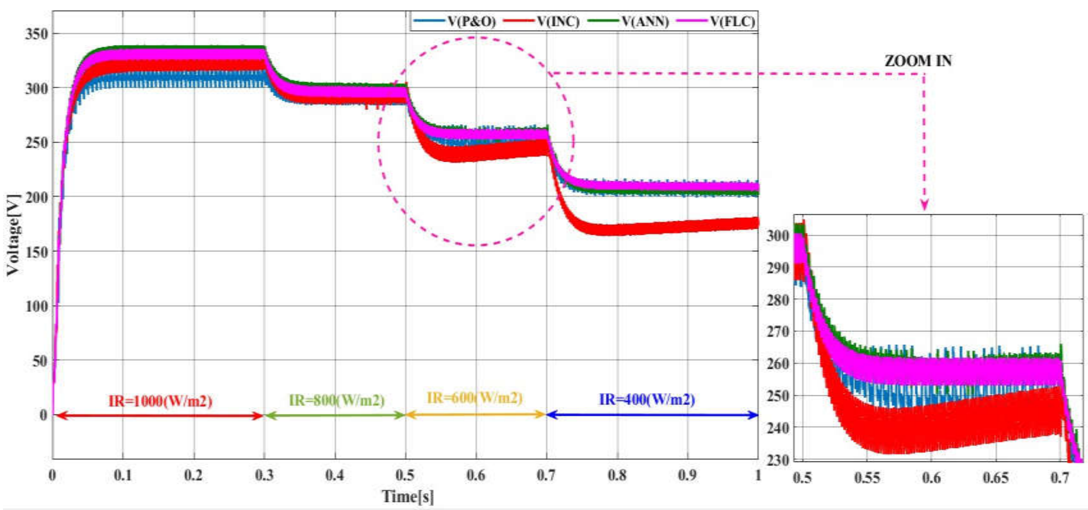

Figure (III.35): Voltage simulation result versus time in variable irradiance of four MPPT algorithms

Main Graph Analysis

- Time Range : The main graph spans from 0 to 1 second.
- Voltage Range : The voltage values range from approximately 0 V to 350 V.
- Irradiance Levels :
    - IR = 1000 W/m² : From 0 to 0.3 seconds.
    - IR = 800 W/m² : From 0.3 to 0.5 seconds.
    - IR = 600 W/m² : From 0.5 to 0.7 seconds.
    - IR = 400 W/m² : From 0.7 to 1 second.

Behavior Under Different Irradiance Levels

1. Initial Transient Behavior (IR = 1000 W/m²) :
    - All methods start at 0 V and rapidly increase their voltage output within the first 0.1 seconds.
    - The V (FLC) method (pink dashed line) reaches its peak voltage slightly faster than the others, indicating a quicker response time.

- The V (P&O) method (blue solid line) shows a smooth and steady increase in voltage.
- The V (INC) method (red dashed line) and V (ANN) method (green solid line) also show rapid increases but with slight oscillations compared to V (P&O) .

2. Steady-State Performance at IR = 1000 W/m² :

- After approximately 0.1 seconds, all methods stabilize around a voltage level of 330 V .
- The V (P&O) method maintains a very stable voltage output with minimal fluctuations.
- The V (INC) and V (ANN) methods exhibit small oscillations around the steady-state value.
- The V (FLC) method shows a slightly higher steady-state voltage compared to the others, reaching approximately 340 V .

3. Response to Decreasing Irradiance :

- As the irradiance decreases from 1000 W/m² to 800 W/m² , all methods show a decrease in voltage.
- The V (FLC) method demonstrates the fastest response to the change in irradiance, maintaining a smoother transition compared to the other methods.
- The V (P&O) method shows a gradual decrease in voltage but with some overshoot and undershoot during the transition.
- The V (INC) and V (ANN) methods exhibit more noticeable oscillations during the transition.

4. Steady-State Performance at Lower Irradiances :

- At IR = 800 W/m² , the steady-state voltage for all methods is around 300V.
- At IR = 600 W/m² , the steady-state voltage drops to approximately 250V.
- At IR = 400 W/m² , the steady-state voltage further decreases to around 200V.

- Throughout these transitions, the V (FLC) method consistently shows the least fluctuation and the fastest adaptation to the new irradiance levels.

Zoomed-In Section Analysis

- Time Range : The zoomed-in section focuses on the interval from 0.5 to 0.7 seconds (transition from IR = 800 W/m² to IR = 600 W/m²).
- Voltage Range : The voltage values in this section range from approximately 200 V to 300V.
- Detailed Observations :
  - The V (FLC) method (pink dashed line) shows the smoothest transition, maintaining a consistent voltage drop without significant overshoot or undershoot.
  - The V (P&O) method (blue solid line) exhibits significant fluctuations, dropping sharply and recovering slowly.
  - The V (INC) method (red dashed line) and V (ANN) method (green solid line) show more pronounced oscillations during the transition.

Comparison of Methods

Table (III.5): Comparison the voltage between the four methods in variable irradiances

Method	Initial Response	Adaptation to Changing Irradiance	Steady-State Voltage	Fluctuations
V (P&O)	Smooth, moderate	Slow adaptation with overshoot/undershoot	Stable	Moderate
V (INC)	Rapid, with oscillations	Moderate adaptation with oscillations	Stable	High
V (ANN)	Rapid, with oscillations	Moderate adaptation with oscillations	Stable	High
V (FLC)	Fastest	Fastest adaptation with minimal oscillations	Stable	Minimal

Key Findings

1. Initial Response : The V (FLC) method has the fastest initial response, reaching its peak voltage quickest.
2. Adaptation to Changing Irradiance : The V (FLC) method demonstrates the fastest and most stable adaptation to decreasing irradiance levels, showing minimal overshoot and undershoot.
3. Steady-State Stability : The V (P&O) method provides the most stable steady-state performance with minimal fluctuations under constant irradiance.
4. Oscillations : Both the V (INC) and V (ANN) methods exhibit more noticeable oscillations compared to V (P&O) and V (FLC) , especially during transitions.

Conclusion

The V(FLC) method outperforms the others in terms of adaptability to changing irradiance conditions, achieving the fastest and smoothest transitions with minimal fluctuations. However, under constant irradiance, the V(P&O) method provides the most stable steady-state performance. The V(INC) and V(ANN) methods offer good performance but with more oscillations during transitions.

Final Recommendation

For applications requiring robust performance under dynamic irradiance conditions, the V(FLC) method is recommended due to its fast adaptation and stability. For applications operating under constant irradiance, the V(P&O) method is the best choice for its steady-state stability.

b)- Analysis of Current Tracking Performance Under Varying Irradiance Conditions

The provided graph compares the current tracking performance of four different control strategies under varying irradiance (IR) conditions. The strategies are:

1. I (P&O) : Perturb and Observe method.
2. I (INC) : Incremental Conductance method.
3. I (ANN) : Artificial Neural Network-based method.
4. I (FLC) : Fuzzy Logic Control-based method.

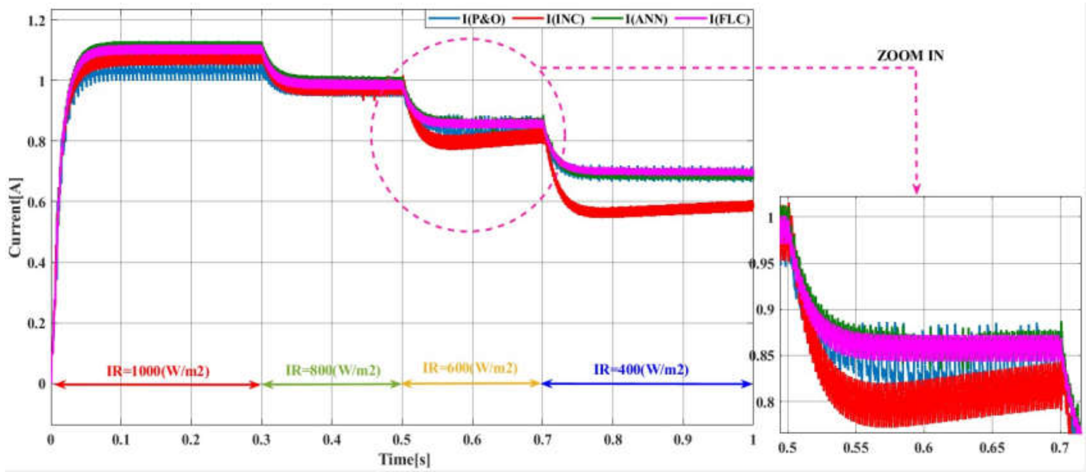

Figure (III.36): Current simulation result versus time in variable irradiance of four MPPT algorithms

Main Graph Analysis

- Time Range : The main graph spans from 0 to 1 second.
- Current Range : The current values range from approximately 0 A to 1.2 A.
- Irradiance Levels :
  - IR = 1000 W/m² : From 0 to 0.3 seconds.
  - IR = 800 W/m² : From 0.3 to 0.5 seconds.
  - IR = 600 W/m² : From 0.5 to 0.7 seconds.
  - IR = 400 W/m² : From 0.7 to 1 second.

Behavior Under Different Irradiance Levels

1. Initial Transient Behavior (IR = 1000 W/m²) :
   - All methods start at 0 A and rapidly increase their current output within the first 0.1 seconds.
   - The I (FLC) method (pink dashed line) reaches its peak current slightly faster than the others, indicating a quicker response time.
   - The I (P&O) method (blue solid line) shows a smooth and steady increase in current.

- The I (INC) method (red dashed line) and I (ANN) method (green solid line) also show rapid increases but with slight oscillations compared to I (P&O) .

2. Steady-State Performance at IR = 1000 W/m² :

- After approximately 0.1 seconds, all methods stabilize around a current level of 1.1A .
- The I (P&O) method maintains a very stable current output with minimal fluctuations.
- The I (INC) and I (ANN) methods exhibit small oscillations around the steady-state value.
- The I (FLC) method shows a slightly higher steady-state current compared to the others, reaching approximately 1.12 A .

3. Response to Decreasing Irradiance :

- As the irradiance decreases from 1000 W/m² to 800 W/m² , all methods show a decrease in current.
- The I (FLC) method demonstrates the fastest response to the change in irradiance, maintaining a smoother transition compared to the other methods.
- The I (P&O) method shows a gradual decrease in current but with some overshoot and undershoot during the transition.
- The I (INC) and I (ANN) methods exhibit more noticeable oscillations during the transition.

4. Steady-State Performance at Lower Irradiances :

- At IR = 800 W/m² , the steady-state current for all methods is around 1 A .
- At IR = 600 W/m² , the steady-state current drops to approximately 0.8 A .
- At IR = 400 W/m² , the steady-state current further decreases to around 0.6 A .
- Throughout these transitions, the I (FLC) method consistently shows the least fluctuation and the fastest adaptation to the new irradiance levels.

Zoomed-In Section Analysis

- Time Range : The zoomed-in section focuses on the interval from 0.5 to 0.7 seconds (transition from IR = 800 W/m² to IR = 600 W/m²).
- Current Range : The current values in this section range from approximately 0.6 A to 1 A.
- Detailed Observations :
    - The I (FLC) method (pink dashed line) shows the smoothest transition, maintaining a consistent current drop without significant overshoot or undershoot.
    - The I (P&O) method (blue solid line) exhibits significant fluctuations, dropping sharply and recovering slowly.
    - The I (INC) method (red dashed line) and I (ANN) method (green solid line) show more pronounced oscillations during the transition.

Comparison of Methods

Table (III.6): Comparison the current between the four methods in variable irradiances

Method	Initial Response	Adaptation to Changing Irradiance	Steady-State Voltage	Fluctuations
I (P&O)	Smooth, moderate	Slow adaptation with overshoot/undershoot	Stable	Moderate
I (INC)	Rapid, with oscillations	Moderate adaptation with oscillations	Stable	High
I (ANN)	Rapid, with oscillations	Moderate adaptation with oscillations	Stable	High
I (FLC)	Fastest	Fastest adaptation with minimal oscillations	Stable	Minimal

Key Findings

1. Initial Response : The I (FLC) method has the fastest initial response, reaching its peak current quickest.

2. Adaptation to Changing Irradiance : The I (FLC) method demonstrates the fastest and most stable adaptation to decreasing irradiance levels, showing minimal overshoot and undershoot.

3. Steady-State Stability : The I (P&O) method provides the most stable steady-state performance with minimal fluctuations under constant irradiance.

4. Oscillations : Both the I (INC) and I (ANN) methods exhibit more noticeable oscillations compared to I (P&O) and I (FLC) , especially during transitions.

Conclusion

The I (FLC) method outperforms the others in terms of adaptability to changing irradiance conditions, achieving the fastest and smoothest transitions with minimal fluctuations. However, under constant irradiance, the I (P&O) method provides the most stable steady-state performance. The I (INC) and I (ANN) methods offer good performance but with more oscillations during transitions.

Final Recommendation

For applications requiring robust performance under dynamic irradiance conditions, the I(FLC) method is recommended due to its fast adaptation and stability. For applications operating under constant irradiance, the I(P&O) method is the best choice for its steady-state stability.

Table (III.7): Comparison the power between the four methods in variable irradiances

Method	**Initial Response**	**Adaptation to Changing Irradiance**	**Steady-State Voltage**	**Fluctuations**
P (P&O)	Smooth, moderate	Slow adaptation with overshoot/undershoot	Stable	Moderate
P (INC)	Rapid, with oscillations	Moderate adaptation with oscillations	Stable	High
P (ANN)	Rapid, with oscillations	Moderate adaptation with oscillations	Stable	High
P (FLC)	Fastest	Fastest adaptation with minimal oscillations	Stable	Minimal

Key Findings

1. Initial Response : The P (FLC) method has the fastest initial response, reaching its peak power quickest.
2. Adaptation to Changing Irradiance : The P (FLC) method demonstrates the fastest and most stable adaptation to decreasing irradiance levels, showing minimal overshoot and undershoot.
3. Steady-State Stability : The P (P&O) method provides the most stable steady-state performance with minimal fluctuations under constant irradiance.
4. Oscillations : Both the P (INC) and P (ANN) methods exhibit more noticeable oscillations compared to P (P&O) and P (FLC) , especially during transitions.

Conclusion

The P (FLC) method outperforms the others in terms of adaptability to changing irradiance conditions, achieving the fastest and smoothest transitions with minimal fluctuations. However, under constant irradiance, the P (P&O) method provides the most stable steady-state performance. The P (INC) and P (ANN) methods offer good performance but with more oscillations during transitions.

Final Recommendation

For applications requiring robust performance under dynamic irradiance conditions, the P(FLC) method is recommended due to its fast adaptation and stability. For applications operating under constant irradiance, the P(P&O) method is the best choice for its steady-state stability.

III.5. Comparison of efficiency between algorithms (P&O, INC, ANN and FLC)

III.5.1 Constant Irradiance (1000 W/m^2)

Table (III.8): Table of efficiency in constant irradiance

Algorithm	Efficiency
Perturb and Observe (P&O)	94.72%
Incremental Conductance (INC)	95.58%
Artificial Neural Network (ANN)	96.63%
Fuzzy Logic Controller (FLC)	93.18%

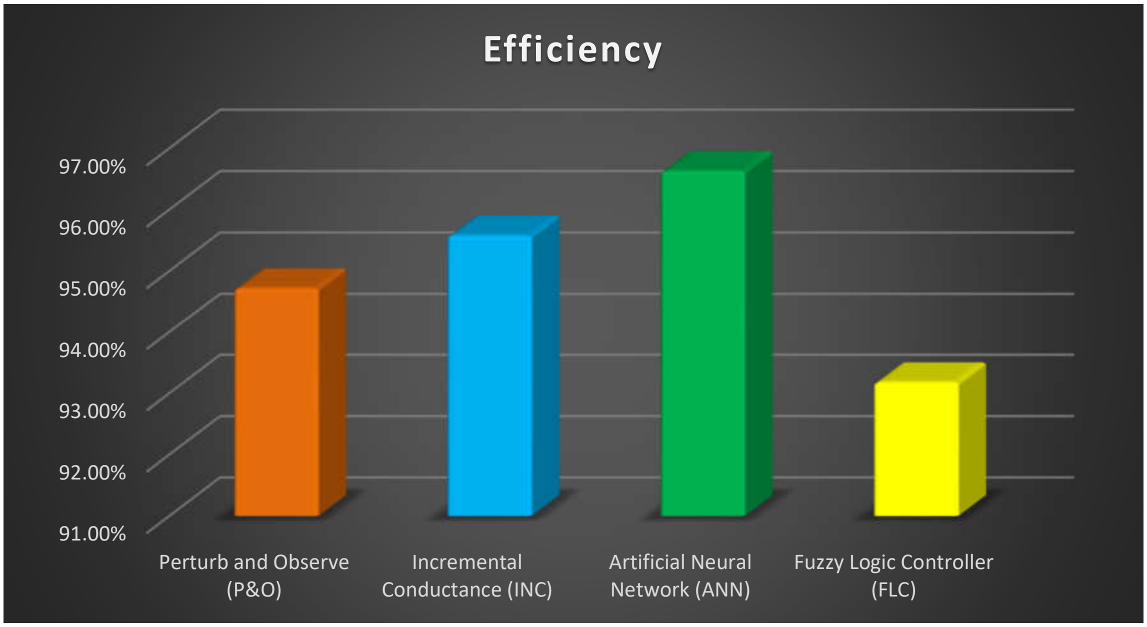

Figure (III.37): Chart of efficiency in constant irradiance

The table (III.8) and curve (III.37) provide efficiency (η) values for four Maximum Power Point Tracking (MPPT) algorithms under constant irradiance (1000W/m^2):

Perturb and Observe (P&O), Incremental Conductance (INC), Artificial Neural Network (ANN) and Fuzzy Logic Controller (FLC)

1. Key Observations

- Highest Efficiency : The Artificial Neural Network (ANN) algorithm achieves the highest efficiency at 96.63% .
- Ranking by Efficiency :ANN > INC > P&O > FLC.
- Lowest Efficiency : The Fuzzy Logic Controller (FLC) algorithm has the lowest efficiency at 93.18% .

These values are calculated using the formula:

$$\eta = \frac{P_{PV}}{P_{load}} \times 100\% \qquad \textbf{(III.1)}$$

where P_{PV} and P_{load} are obtained from the PV_Input_Monitor and Output_Power_Monitor, respectively.

2. Analysis of the Curve

- The curve indicates that ANN outperforms other algorithms in terms of stability and accuracy under constant irradiance conditions.
- P&O and INC show stable performance but with slightly lower efficiencies compared to ANN .
- FLC exhibits larger fluctuations or slower response times, leading to reduced efficiency.

3. Factors Influencing Efficiency

- Response Speed : Algorithms like ANN and INC demonstrate faster and more precise responses to minor changes in environmental conditions.
- Fluctuations : P&O and FLC experience higher oscillations around the maximum power point (MPP), which reduces overall efficiency.
- Tracking Accuracy : ANN uses advanced predictive models to accurately locate the MPP, making it the most efficient.

4. Conclusion

- Best Algorithm : ANN achieves the highest efficiency (96.63%) due to its superior adaptability and precision.
- Alternative Choice : INC is a strong second choice (95.58%) for balancing efficiency and complexity.
- Limitations : P&O (94.72%) and FLC (93.18%) are less efficient and may only be suitable for simpler or low-cost applications.

5. Summary

Based on the provided data:

- Recommended Algorithm : ANN for achieving the highest efficiency and stability.
- Alternative Algorithm : INC if slightly lower efficiency is acceptable.
- Constraints : P&O and FLC are better suited for basic or cost-sensitive applications.

III.5.2 Variable irradiance (1000, 800, 600, 400 W/m^2)

Table (III.9): Table of efficiency in variable irradiance

Algorithm	Efficiency
Perturb and Observe (P&O)	84.84%
Incremental Conductance (INC)	88.04%
Artificial Neural Network (ANN)	95.06%
Fuzzy Logic Controller (FLC)	91.79%

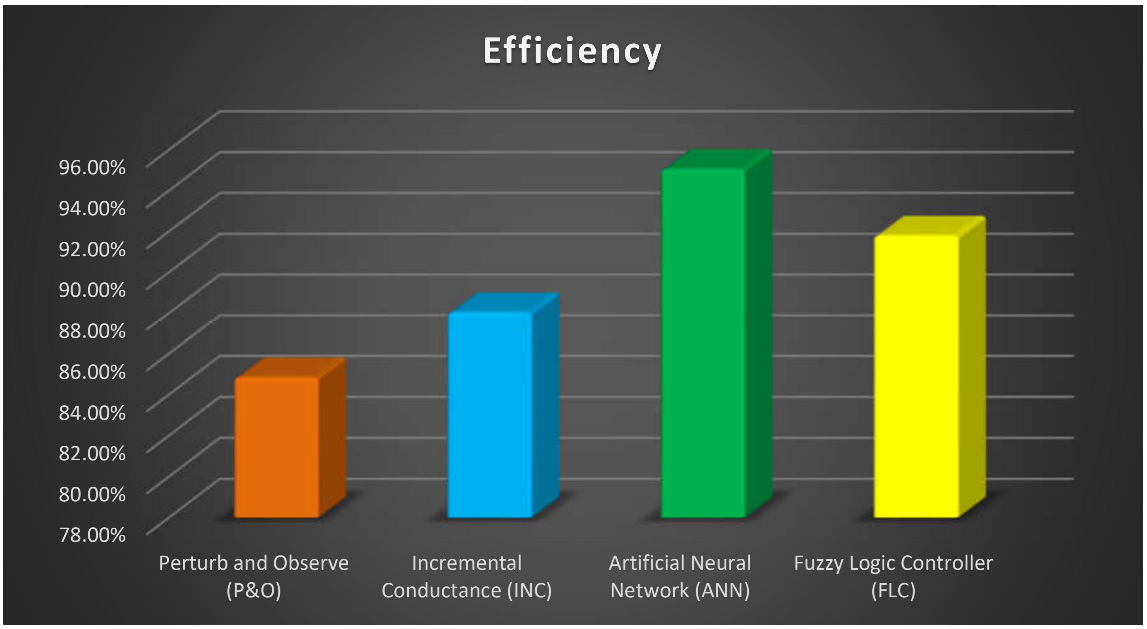

Figure (III.38): Chart of efficiency in variable irradiance

The table (III.9) and curve (III.38) provide efficiency (η) values for four Maximum Power Point Tracking (MPPT) algorithms under variable irradiance (1000, 800, 600, 400 W/m^2): Perturb and Observe (P&O), Incremental Conductance (INC), Artificial Neural Network (ANN) and Fuzzy Logic Controller (FLC).

1. Key observations

1. Highest Efficiency :

    - The Artificial Neural Network (ANN) algorithm achieves the highest efficiency at 95.06%, demonstrating its superior adaptability to rapidly changing irradiance levels.

2. Second Best :

   - The Fuzzy Logic Controller (FLC) follows with an efficiency of 91.79%, showing reasonable performance but slightly lower stability compared to ANN.

3. Moderate Performance :

   - The Incremental Conductance (INC) algorithm achieves 88.04%, indicating moderate adaptability to variable irradiance conditions.

4. Lowest Efficiency :

   - The Perturb and Observe (P&O) algorithm has the lowest efficiency at 84.84%, reflecting its susceptibility to fluctuations and slower response under dynamic irradiance changes.

2. Analysis of the chart (Figure III.33)

- The chart visually confirms the rankings observed in the table:
  - ANN shows a consistently high efficiency curve, even as irradiance levels change.
  - FLC follows closely but exhibits minor fluctuations during transitions between irradiance levels.
  - INC demonstrates a stable but lower efficiency curve compared to ANN and FLC.
  - P&O shows significant drops in efficiency during irradiance transitions, highlighting its limitations in dynamic environments.

3. Factors influencing efficiency

1. Adaptability to Rapid Changes :

   - Algorithms like ANN excel due to their ability to predict and adapt quickly to changes in irradiance.
   - P&O struggles because it relies on perturbation, which is less effective under rapidly changing conditions.

2. Stability :

    - ANN and FLC maintain higher stability, minimizing oscillations around the maximum power point (MPP).
    - P&O and INC exhibit more oscillations, reducing overall efficiency.

3. Complexity vs. Performance :

    - ANN and FLC are computationally more complex but deliver superior performance in dynamic conditions.
    - P&O and INC are simpler but less efficient under variable irradiance.

4. Conclusion

- Best Algorithm : ANN is the most effective under variable irradiance, achieving 95.06% efficiency due to its advanced predictive capabilities.
- Alternative Choice : FLC is a strong second choice (91.79%) for applications requiring good performance without the computational demands of ANN.
- Limitations : P&O (84.84%) and INC (88.04%) are less suitable for dynamic environments, as they struggle with rapid changes in irradiance.

5. Summary

Based on the provided data:

- Recommended Algorithm : ANN for optimal performance in variable irradiance conditions.
- Alternative Algorithm : FLC if computational complexity is a concern.

Constraints : P&O and INC are better suited for static or slowly changing environments.

III.5.3. Comparison of efficiency between constant an variable irradiances

The comparison of efficiency between the four algorithms (P&O, INC, ANN, and FLC) under both constant and variable irradiance conditions:

Constant Irradiance (1000 W/m²):

1. Artificial Neural Network (ANN) : 96.63%

2. Incremental Conductance (INC) : 95.58%
3. Perturb and Observe (P&O) : 94.72%
4. Fuzzy Logic Controller (FLC) : 93.18%

Variable Irradiance (1000, 800, 600, 400 W/m²):

1. Artificial Neural Network (ANN) : 95.06%
2. Incremental Conductance (INC) : 88.04%
3. Fuzzy Logic Controller (FLC) : 91.79%
4. Perturb and Observe (P&O) : 84.84%

Comparison and Analysis:

1. Artificial Neural Network (ANN) :
   - Constant Irradiance : Highest efficiency at 96.63%.
   - Variable Irradiance : Still the highest efficiency at 95.06%.
   - Reason : ANN can adapt to changing conditions and learn from data, making it robust under both constant and variable conditions.
2. Incremental Conductance (INC) :
   - Constant Irradiance : Second highest at 95.58%.
   - Variable Irradiance : Efficiency drops significantly to 88.04%.
   - Reason : INC is more sensitive to rapid changes in irradiance, which affects its performance under variable conditions.
3. Fuzzy Logic Controller (FLC) :
   - Constant Irradiance : Lowest efficiency at 93.18%.
   - Variable Irradiance : Efficiency increases slightly relatively to P&O but remains lower than ANN and INC.
   - Reason : FLC's rule-based system might handle variability better than P&O but still not as effectively as ANN.

4. Perturb and Observe (P&O) :

    - Constant Irradiance : Third highest at 94.72%.
    - Variable Irradiance : Significant drop to 84.84%, the lowest among all.
    - Reason : P&O struggles with fluctuating conditions because it continuously perturbs and observes, leading to oscillations and reduced efficiency when irradiance varies.

Cause of Differences Between Tables and Charts:

- Constant vs. Variable Irradiance :
    - The efficiency values are generally higher under constant irradiance compared to variable irradiance.
    - This is expected because constant conditions provide a stable environment where algorithms can operate optimally.
    - Under variable irradiance, the environmental changes challenge the adaptive capabilities of each algorithm, causing efficiency to drop.
- Algorithm Sensitivity :
    - Algorithms like P&O and INC show significant drops in efficiency under variable conditions due to their reliance on steady-state assumptions.
    - ANN shows minimal decrease in efficiency due to its ability to learn and adapt to varying inputs.
    - FLC lies in between, showing moderate adaptability but not as pronounced as ANN.

In conclusion, the Artificial Neural Network (ANN) demonstrates superior performance across both constant and variable irradiance conditions, while Perturb and Observe (P&O) exhibits the most significant decline in efficiency under variable irradiance. The differences in efficiency values between constant and variable conditions highlight the strengths and weaknesses of each algorithm's adaptability to environmental changes.

III.6. Conclusion

The performance of four Maximum Power Point Tracking algorithms, Artificial Neural Network (ANN), Fuzzy Logic Controller (FLC), Incremental Conductance (INC), and Perturb and Observe (P&O), is compared under constant and variable irradiation conditions in this research. The result indicates that ANN has highest efficiency always, 96.63% under constant irradiation and 95.06% under variable irradiation, due to its improved adaptability and predictability feature. INC is a tolerable second best, with the best performance (95.58% steady-state, 88.04% transient) but mean computational complexity. FLC and P&O are below optimal, particularly under dynamic conditions, and P&O experiences considerable reductions owing to oscillations and lower response times. FLC is superior to P&O under changing illumination but is less stable and efficient than ANN and INC. Thus, ANN suits maximum efficiency for varying environments, whereas P&O and INC suit easier or cost-cutting systems. The above finding comes to serve as a pointer towards the need for selecting an algorithm for environment stability and system need.

General Conclusion

Conclusion

In this graduation thesis, we studied various Maximum Power Point Tracking (MPPT) techniques for photovoltaic systems. Focus was given to their performance under constant and variable irradiance conditions. We have taken some of the primary algorithms such as Perturb and Observe (P&O), Incremental Conductance (INC), Artificial Neural Network (ANN), and Fuzzy Logic Controller (FLC). Each algorithm has its pros and cons, and we were able to conduct a comparative study in detail on efficiency and flexibility.

We learned from our study that the P&O algorithm is simple but is highly oscillatory near the maximum power point. The INC algorithm offers better accuracy but is unstable under dynamic conditions. But ANN was more efficient, with up to 96.63% under steady irradiance, though it demands a high amount of computational power. Though FLC provides good performance with moderate complexity but not as efficient as ANN. These results highlight the compromises between simplicity, efficiency, and computational demand.

We compared these algorithms in depth using MATLAB-Simulink simulations. The result showed that ANN is superior to others regarding efficiency with 95.06% under variable irradiance due to its advanced predictive capability. INC was a close second at 88.04%. P&O and FLC had efficiencies of 84.84% and 91.79%, respectively. The above values confirm that ANN is the most suitable algorithm for varying environments, while FLC can be applied to situations where computational complexity is not an issue.

Based on the analysis, ANN was selected as the most effective algorithm due to its high efficiency and stability. However, FLC can also be a good choice for applications that require a trade-off between performance and computational complexity. Algorithms like P&O and INC are only fitting for low-cost or low-complexity applications where a high rate of irradiance variation is not a primary concern.

Future research could focus on refining these algorithms or combining them to leverage their collective strengths. For instance, hybridizing ANN with P&O could reduce oscillations while maintaining high efficiency. Additionally, exploring new techniques such as ANFIS (Adaptive Neuro-Fuzzy Inference System) might lead to even better performance. Further studies should also consider practical implementations by testing these algorithms in real-world conditions.

Experimental validations in the future through physical models will be required to compare real-world performances with MATLAB-Simulink-based simulations. Such experiments will not only validate theoretical assumptions but also provide clearer indications toward improved PV system designs. This forms a crucial step toward developing improved and more efficient systems to resist dynamic weather conditions.

References

[1] Sera, D., Márquez, A. M., Kerekes, T., Blaabjerg, F., & Ortega, M. G, “On the perturb-and-observe and incremental conductance MPPT methods for PV systems: Revisited”, IEEE Journal of Photovoltaics, 9(1), 181–191, 2019.

[2] Al-Greer, M., Szabo, C., & Conlon, M., “Comparative Study of MPPT Algorithms Under Real Outdoor Conditions Using Low-Cost Hardware Platform”, Energies, 14(2), 395, 2021.

[3] Eltamaly, A. M., & Farh, H. M, “Maximum power point tracking using adaptive neuro-fuzzy inference system for photovoltaic power systems: Review and experimental comparison”, Renewable and Sustainable Energy Reviews, 152, 111642, 2021.

[4] Ram, J. P., Rajasekar, N., & Kumar, Y, “Recent advancements in MPPT techniques for PV applications—A review”, Renewable and Sustainable Energy Reviews, 133, 110290, 2020.

[5] Singh, R., & Hussain, I, “Performance evaluation of MPPT algorithms under varying irradiance conditions”, Journal of Renewable and Sustainable Energy, 14(3), 033502, 2022.

[6] Elgendy, M. A., Zahawi, B., & Atkinson, D. J, “Assessment of the incremental conductance maximum power point tracking algorithm”, IET Renewable Power Generation, 14(11), 1958–1966, 2020.

[7] Intergovernmental Panel on Climate Change (IPCC), “Global Warming of 1.5°C”, Special Report, 2018.

[8] National Renewable Energy Laboratory (NREL), “Best Research-Cell Efficiency Chart,” 2022.

[9] International Renewable Energy Agency (IRENA), “Renewable Capacity Statistics 2023”. Abu Dhabi, UAE, 2023.

[10] International Energy Agency (IEA), “Renewables 2023: Analysis and forecast to 2030”. Paris, France, 2023.

[11] J. Cao, L. Zheng, J. Peng, W. Wang, M. K. Leung, Z. Zheng, M. Hu, Q. Wang, J. Cai, G. Pei, and J. Ji, “Advances in coupled use of renewable energy sources for performance enhancement of vapour compression heat pump: A systematic review of applications to buildings,”Applied Energy, vol. 332, p. 120571, 2023.

[12] T. Hassan, H. Song, Y. Khan, and D. Kirikkaleli, “Energy efficiency a source of low carbon energy sources? Evidence from 16 high-income OECD economies,” Energy, vol. 243, p. 123063, 2022.

[13] A. K. Thakur, R. Singh, A. Gehlot, A. K. Kaviti, R. Aseer, S. K. Suraparaju, S. K. Natarajan, and V. S. Sikarwar, “Advancements in solar technologies for sustainable development of agricultural sector in India: a comprehensive review on challenges and opportunities,” Environmental Science and Pollution Research, vol. 29, no. 29, pp. 43607– 43634, 2022

[14] M. Tutak and J. Brodny, "Renewable energy consumption in economic sectors in the EU-27. The impact on economics, environment and conventional energy sources. A 20-year perspective," Journal of Cleaner Production, vol. 345, p. 131076, 2022.

[15] R. Cergibozan, "Renewable energy sources as a solution for energy security risk: Empirical evidence from OECD countries," Renewable Energy, vol. 183, pp. 617–626, 2022.

[16] S. Bouyghrissi, M. Murshed, A. Jindal, A. Berjaoui, H. Mahmood, and M. Khanniba, "The importance of facilitating renewable energy transition for abating CO2 emissions in Morocco," Environmental Science and Pollution Research, vol. 29, no. 14, pp. 20752–20767, 2022.

[17] J. M. Guerrero, J. C. Vasquez, and M. Mathe, "Integration of Renewable Energy Sources with Power Electronics for Smart Grid Applications," *IEEE Transactions on Industrial Electronics* , vol. 60, no. 4, pp. 1284-1295, April 2013

[18] Environmental Pollution Volume 326, 1 June 2023, 121474

[19] A.-H. I. Mourad, H. Shareef, N. Ameen, A. H. Alhammadi, M. Iratni, and A. S. Alkaabi, A State-of-the-art Review: Solar trackers, IEEE, Advances in Science and Engineering Technology International Conferences, 2022.

[20] B. Aboagye, "Investigation into the impacts of design, installation, operation and maintenance issues on performance and degradation of installed solar photovoltaic (PV) systems," Energy for Sustainable Development, vol. 66, pp. 165–176, 2022.

[21] A. Chellakhi, S. E. Beid, and Y. Abouelmahjoub, "An improved adaptable step-size P&O MPPT approach for standalone photovoltaic systems with battery station," Simulation Modelling Practice and Theory, vol. 121, p. 102655, 2022.

[22] J. F. Peters, "Best practices for life cycle assessment of batteries," Nature Sustainability, vol. 1-3, 2023.

[23] G. Raina, S. Sinha, G. Saini, S. Sharma, and N. Prashant Malik, "Assessment of photovoltaic power generation using fin augmented passive cooling technique for different climates," Sustainable Energy Technologies and Assessments, vol. 52, p. 102095, 2022.

[24] M. Shafique and X. Luo, "Environmental life cycle assessment of battery electric vehicles from the current and future energy mix perspective," Journal of Environmental Management, vol. 303, p. 114050, 2022.

[25] A. A. Stonier, G. Peter, and S. Iderus, "Relay Switch Matrix based Optimized reconfigurable Solar PV Battery Charger," IEEE 19th India Council International Conference, 2022.

[26] Fahrenbruch, Alan, RB. photovoltaic solar energy conversion. California: Elsevier;2012

[27] Tyagi VV, Rahim NAA, Rahim NA, Selvaraj JAL. Progress in solar PV technology: research and achievement. Renew Sustain Energy Rev 2013;20:443–61.

[28] V. Shah, G. Kumawat, and S. Payami, “Solar powered electric drivetrain with integrated multifunctional dual power on-board charger incorporating N-phase SRM,” IEEE International Conference on Power Electronics, Drives and Energy Systems, 2023.

[29] International Energy Agency (IEA). (2023). “Renewables 2023: Analysis and forecast to 2030”. Retrieved from https://www.iea.org/reports/renewables-2023

[30] International Renewable Energy Agency (IRENA). (2024). “Renewable Capacity Statistics 2024”. Abu Dhabi: IRENA. Retrieved from: https://www.irena.org/publications/2024/March/Renewable-Capacity-Statistics-2024

[31] Zhang, D., et al. (2023). “China’s Renewable Energy Expansion and Global Leadership in Solar PV Deployment”. Nature Energy, 8(11), 1123–1130. https://doi.org/10.1038/s41560-023-01345-z

[32] BloombergNEF. (2023). “New Energy Outlook 2023”. Retrieved from https://about.bnef.com/new-energy-outlook/

[33] International Renewable Energy Agency (IRENA). (2023). “Renewable Capacity Statistics 2023”. Abu Dhabi: IRENA. Retrieved from https://www.irena.org/publications/2023/March/Renewable-Capacity-Statistics-2023

[34] International Renewable Energy Agency (IRENA), 2024.

[35] E. Hossain, S. Petrovic, Renewable Energy Crash Course (2021)

[36] XIAOJING SUN, Solar technology got cheaper and better in the 2010s. Now what? (2021).https://www.greentechmedia.com/articles/read/solar-pv-has-become-cheaperand-better-in-the-2010s-now-what

[37] NREL, Best Research Cell Efficiencies (2019). https://www.nrel.gov/pv/assets/pdfs/bestresearch-cell-efficiencies-rev210726.pdf

[38] Center for Sustainable Systems, University of Michigan, Photovoltaic Energy Factsheet(2020). https://css.umich.edu/sites/default/files/Photovoltaic%20Energy_CSS07-08_e2020.pdf Pub. No. CSS07-08

[39] A. Han, Efficiency of solar PV, then, now and future (2015). https://sites.lafayette.edu/egrs352-sp14-pv/technology/history-of-pv-technology/

[40] B. G. Streetman and S. Banerjee, “Solid State Electronic Devices”, 8th ed. Pearson, 2020.

[41] J. Nelson, “The Physics of Solar Cells”. Imperial College Press, 2020.

[42] S. O. Kasap, “Principles of Electronic Materials and Devices”, 5th ed. McGraw-Hill Education, 2021.

[43] P. A. Tipler and G. Mosca, “Physics for Scientists and Engineers”, 9th ed. W. H. Freeman, 2019.

[44] N. W. Ashcroft and N. D. Mermin, “Solid State Physics”. Cengage Learning, 2022.

[45] R. A. Serway and J. W. Jewett, “Physics for Scientists and Engineers with Modern Physics”, 10th ed. Cengage Learning, 2020.

[46] E. Hughes, J. Hiley, K. Brown, and I. M. Smith, “Hughes Electrical and Electronic Technology”, 12th ed. Pearson, 2021.

[47] Photovoltaic Systems Fundamentals and Applications Photovoltaic Systems: Fundamentals and Applications | SpringerLink

[48] M. Woodhouse, B. Smith, A. Ramdas, R. Margolis, Crystalline silicon photovoltaic module manufacturing costs and sustainable pricing: 1h 2018

[49] M.K Fuentes, A simplified thermal model for flat-plate photovoltaic arrays. Technical report, Sandia National Labs., Albuquerque, NM (USA), 1987

[50] M. A. G. de Brito, L. C. Canha, R. T. Coelho, and J. A. Cobben, "PV Systems: Fault Detection and Diagnosis," “Renewable and Sustainable Energy Reviews”, vol. 117, p. 109490, Jan. 2020.

[51] D. C. Jordan and S. R. Kurtz, "Photovoltaic Degradation Rates—An Analytical Review," “Progress in Photovoltaics: Research and Applications”, vol. 21, no. 1, pp. 12–29, Jan. 2013.

[52] F. Al-Ashry, M. A. G. de Brito, L. P. Kunzel, and J. A. Cobben, "Review of Failures in Photovoltaic Modules," “IEEE Access”, vol. 9, pp. 44526–44539, Mar. 2021

[53] N. O. Jensen et al., "Failure modes of photovoltaic modules under damp heat conditions," “Proc. 35th European PV Solar Energy Conference”, 2018, pp. 1135–1141.

[54] A. Chaki et al., "Mechanical Failure Analysis of Glass in PV Modules Using Digital Image Correlation," “Solar Energy Materials and Solar Cells”, vol. 194, pp. 215–223, Jun. 2019.

[55] IRENA, "Renewable Energy Explained: Photovoltaic Solar Energy," International Renewable Energy Agency, Technical Report, 2021.

[56] K. Zhou et al., "Degradation of EVA Encapsulant in PV Modules Under Accelerated Aging Conditions," “IEEE Journal of Photovoltaics”, vol. 10, no. 6, pp. 1650–1658, Nov. 2020.

[57] T. Sample et al., "Micro-crack detection and analysis in crystalline silicon PV modules," “Proc. 28th European PV Solar Energy Conference”, pp. 2834–2839, Sep. 2013.

[58] Y. Zhang et al., "Impact of Microcracks on the Performance of Photovoltaic Modules," “IEEE Transactions on Device and Materials Reliability”, vol. 19, no. 2, pp. 247–254, Jun. 2019.

[59] A. G. Aberle et al., "Reliability of Bypass Diodes in PV Modules – A Review," “Proc. 31st European PV Solar Energy Conference”, pp. 1353–1358, Sep. 2015.

[60] M. Köntges et al., "The Risk of Hot Spot Induced Damage in Photovoltaic Modules," “Progress in Photovoltaics: Research and Applications”, vol. 22, no. 1, pp. 1–11, Jan. 2014.

[61] A. K. Maurya, A. K. Rai, and H. Ahuja, “Comparative analysis of different MPPT algorithms for Roof-top solar PV system,” in IEE International Conference on Automation, Computing and Renewable Systems 2022.

[62] A. M. Humada, M. Hojabri, S. Mekhilef, and H. M. Hamdan, "Solar cell temperature estimation using the five-parameter model," *Renewable Energy*, vol. 179, pp. 1657–1666, Nov. 2021.

[63] M. A. G. de Brito, C. B. Renner, L. Q. Ribeiro, and W. N. Macêdo, "PV Module Modeling for Simulation Studies Based on Manufacturer Datasheet Parameters," *IEEE Latin America Transactions*, vol. 19, no. 6, pp. 1023–1031, Jun. 2021.

[64] S. K. Amini, M. E. Baghdadi, and H. A. Shabestani, "Accurate determination of maximum power point using analytical methods applied to different models of solar cells," *Energy Reports*, vol. 7, pp. 582–591, Nov. 2021.

[65] A. Belkaid, I. Colak, and O. Isik, "Photovoltaic maximum power point tracking under partial shading conditions: A survey," *International Journal of Energy Research*, vol. 44, no. 10, pp. 7905–7940, Aug. 2020.

[66] M. A. G. de Brito, C. B. Renner, L. Q. Ribeiro, and W. N. Macêdo, "PV Module Modeling for Simulation Studies Based on Manufacturer Datasheet Parameters," *IEEE Latin America Transactions*, vol. 19, no. 6, pp. 1023–1031, Jun. 2021.

[67] S. K. Amini, M. E. Baghdadi, and H. A. Shabestani, "Accurate determination of maximum power point using analytical methods applied to different models of solar cells," *Energy Reports*, vol. 7, pp. 582–591, Nov. 2021.

[68] A. M. Humada, M. Hojabri, S. Mekhilef, and H. M. Hamdan, "Solar cell temperature estimation using the five-parameter model," *Renewable Energy*, vol. 179, pp. 1657–1666, Nov. 2021.

[69] J. Singh, P. Agarwal, and R. Kumar, "Modeling and simulation of photovoltaic module based on one-diode and two-diode models using MATLAB/Simulink," *International Journal of Renewable Energy Research*, vol. 10, no. 1, pp. 272–282, Mar. 2020.

[70] M. A. G. Villalva, J. R. Gazoli, and E. R. Filho, "Comprehensive Approach to Modeling and Simulation of Photovoltaic Arrays," *IEEE Transactions on Energy Conversion*, vol. 24, no. 1, pp. 115–124, Mar. 2009.

[71] A. Belkaid, I. Colak, and O. Isik, "Photovoltaic maximum power point tracking under partial shading conditions: A survey," *International Journal of Energy Research*, vol. 44, no. 10, pp. 7905–7940, Aug. 2020.

[72] F. Khan, S. Baek, and J. Heo, "Diode parameters extraction of solar cells under different environmental conditions," *Solar Energy Materials and Solar Cells*, vol. 203, p. 110129, Dec. 2019.

[73] N. Pandiarajan, R. Muthu, F. S. A. Chidambaram, M. Lakshminarasamma, and M. Ramasamy, "Mathematical modeling of photovoltaic system with effect of temperature and irradiation," *International Journal of Photoenergy*, vol. 2019, Article ID 398457, Jan. 2019.

[74] T. Ma, H. Yang, and L. Wang, "Development of a model for technical and economic optimization of photovoltaic systems," *Energy Conversion and Management*, vol. 85, pp. 504–519, Sep. 2014.

[75] A. N. Celik and N. Acikgoz, "Modeling and experimental verification of the operating current of mono-crystalline photovoltaic modules using four- and five-parameter models," *Applied Energy*, vol. 84, no. 1, pp. 1–15, Jan. 2007.

[76] D. Sera, R. Teodorescu, P. Rodriguez, S. B. Kjaer, J. Pou, and B. W. Johnson, "On the Perturbation-Related Oscillations in Wide Load Range Maximum Power Point Trackers," *Proc. IEEE 38th Annual Power Electronics Specialists Conference (PESC)*, Orlando, FL, USA, 2007, pp. 1310–1315.

[77] A. M. Humada, M. Hojabri, S. Mekhilef, and H. M. Hamdan, "Solar cell temperature estimation using the five-parameter model," *Renewable Energy*, vol. 179, pp. 1657–1666, Nov. 2021.

[78] F. Khan, S. Baek, and J. Heo, "Diode parameters extraction of solar cells under different environmental conditions," *Solar Energy Materials and Solar Cells*, vol. 203, p. 110129, Dec. 2019.

[79] N. Pandiarajan, R. Muthu, F. S. A. Chidambaram, M. Lakshminarasamma, and M. Ramasamy, "Mathematical modeling of photovoltaic system with effect of temperature and irradiation," *International Journal of Photoenergy*, vol. 2019, Article ID 398457, Jan. 2019.

[80] A. Belkaid, I. Colak, and O. Isik, "Photovoltaic maximum power point tracking under partial shading conditions: A survey," *International Journal of Energy Research*, vol. 44, no. 10, pp. 7905–7940, Aug. 2020.

[81] S. K. Amini, M. E. Baghdadi, and H. A. Shabestani, "Accurate determination of maximum power point using analytical methods applied to different models of solar cells," *Energy Reports*, vol. 7, pp. 582–591, Nov. 2021.

[82] M. A. G. de Brito, C. B. Renner, L. Q. Ribeiro, and W. N. Macêdo, "PV Module Modeling for Simulation Studies Based on Manufacturer Datasheet Parameters," *IEEE Latin America Transactions*, vol. 19, no. 6, pp. 1023–1031, Jun. 2021.

[83] J. Singh, P. Agarwal, and R. Kumar, "Modeling and simulation of photovoltaic module based on one-diode and two-diode models using MATLAB/Simulink," *International Journal of Renewable Energy Research*, vol. 10, no. 1, pp. 272–282, Mar. 2020.

[84] Bloomberg NEF (BNEF), "New Energy Outlook 2020," London, UK, 2020.

[85] European Commission Joint Research Centre (JRC), "The Role of Innovation in the Energy System – Focus on Photovoltaics," EUR 30069 EN, Publications Office of the EU, Luxembourg, 2020, ISBN 978-92-76-14526-9

[86] Springer Nature Switzerland AG 2020 A. M. Eltamaly and A. Y. Abdelaziz (eds.), Modern Maximum Power Point Tracking Techniques for Photovoltaic Energy Systems, Green Energy and Technology, https://doi.org/10.1007/978-3-030-05578-3_1

[87] Masoum, M.A.S., Dehbonei, H., Fuchs, E.F., et al.: 'Theoretical and experimental analyses of photovoltaic systems with voltage and current-based maximum power point tracking', IEEE Trans. Energy Conv., 2002, 17, (4), pp. 514–522

[88] Ahmad, R., Murtaza, A.F., Sher, and H.A.: 'Power tracking techniques for efficient operation of photovoltaic array in solar applications – a review', Renew. Sustain. Energy Rev., 2019, 101, pp. 82–102

[89] de Brito, M.A.G., Galotto, L., Sampaio, L.P., et al.: 'Evaluation of the main MPPT techniques for photovoltaic applications', IEEE Trans. Ind. Electron., 2013, 60, (3), pp. 1156–1167

[90] Seyedmahmoudian, M., Horan, B., Soon, T. K., et al.: 'State of the art artificial intelligence-based MPPT techniques for mitigating partial shading effects on PV systems – a review', Renew. Sustain. Energy Rev., 2016, 64, pp. 435–455

[91] Islam, H., Mekhilef, S., Shah, N.B.M., et al.: 'Performance evaluation of maximum power point tracking approaches and photovoltaic systems', Energies, 2018, 11, (2), p. 365

[92] Esram, T., Chapman, P.L.: 'Comparison of photovoltaic array maximum power point tracking techniques', IEEE Trans. Energy Convers., 2007, 22, (2), pp. 439–449

[93] Pandey, A., Dasgupta, N., Mukerjee, A.K.: 'A simple single-sensor MPPT solution', IEEE Trans. Power Electron., 2007, 22, (6), pp. 698–700

[94] Lasheen, M., Abdel Rahman, A.K., Abdel-Salam, M., et al.: 'Adaptive reference voltage-based MPPT technique for PV applications', IET Renew. Power Gener., 2017, 11, (5), pp. 715–722

[95] Kota, V.R., Bhukya, M.N.: 'A novel linear tangents based P & O scheme for MPPT of a PV system', Renew. Sustain. Energy Rev., 2017, 71, pp. 257–267

[96] Sher, H.A., Murtaza, A.F., Noman, A., et al.: 'A new sensorless hybrid MPPT algorithm based on fractional short-circuit current measurement and P&O mppt', IEEE Trans. Sustain. Energy, 2015, 6, (4), pp. 1426–1434

[97] Subudhi, B., Pradhan, R., et al.: 'A Comparative Study on Maximum Power Point Tracking Techniques for Photovoltaic Power Systems', in IEEE Trans. Sustainable Energy, 2013, 4, (1), pp. 89–98

[98] Frezzetti, A., Manfredi, S., Suardi, A.: 'Adaptive FOCV-based control scheme to improve the MPP tracking performance: an experimental validation', IFAC Proc. Vol., 2014, 47, (3), pp. 4967–4971

[99] Wu Z, Yu D (2018) Application of improved bat algorithm for solar PV maximum power point tracking under partially shaded condition. Appl Soft Comput 62:101–109

[100] Ishaque K, Salam Z, Lauss G (2014) The performance of perturb and observe and incremental conductance maximum power point tracking method under dynamic weather conditions. Appl Energy 119:228–236

[101] Karami, N., Moubayed, N., Outbib, R.: 'General review and classification of different MPPT techniques', Renew. Sustain. Energy Rev., 2017, 68, (1), pp. 1–18

[102] Hua, C., Lin, J.: 'An on-line MPPT algorithm for rapidly changing illuminations of solar arrays', Renew. Energy, 2003, 28, (7), pp. 1129–1142

[103] Faraji, R., Rouholamini, A., Naji, H.R., et al.: 'FPGA-based real time incremental conductance maximum power point tracking controller for PV systems', IET Power Electron., 2014, 7, (5), pp. 1294–1304

[104] Huynh, D.C., Dunnigan, M.W.: 'Development and comparison of an improved incremental conductance algorithm for tracking the mpp of a solar PV panel', IEEE Trans. Sustain. Energy, 2016, 7, (4), pp. 1421–1429

[105] Sera, D., Mathe, L., Kerekes, T., et al.: 'On the perturb-and-observe and incremental conductance MPPT methods for PV systems', IEEE J. Photovolt., 2013, 3, (3), pp. 1070–1078

[106] Sivakumar, P., Abdul Kader, A., Kaliavaradhan, Y., et al.: 'Analysis and enhancement of PV efficiency with incremental conductance MPPT technique under non-linear loading conditions', Renew. Energy, 2015, 81, pp. 543–550

[107] Boonmee, C., Kumsuwan, Y.: 'Modified maximum power point tracking based-on ripple correlation control application for single phase vsi gridconnected pv systems'. 10th IEEE Int. Conf. ECTI-CON, Krabi, 2013, pp. 1–6

[108] Farh HM, Eltamaly AM, Othman MF (2018) Hybrid PSO-FLC for dynamic global peak extraction of the partially shaded photovoltaic system. PloS one 13(11):e0206171

[109] Azzouzi M (2012) Comparaison between MPPT P&O and MPPT fuzzy controls in optimizing the photovoltaic generator. Int J Adv Comput Sci Appl 3(12):57–62

[110] Chekired F, Mellit A, Kalogirou S, Larbes C (2014) Intelligent maximum power point trackers for photovoltaic applications using FPGA chip: a comparative study. Sol Energy 101:83–99

[111] Rezk H, Eltamaly AM (2015) A comprehensive comparison of different MPPT techniques for photovoltaic systems. Solar energy 112:1–11

[112] Nabipour M, Razaz M, Seifossadat SG, Mortazavi S (2017) A new MPPT scheme based on a novel fuzzy approach. Renew Sustain Energy Rev 74:1147–1169

[113] Boukenoui R, Salhi H, Bradai R, Mellit A (2016) A new intelligent MPPT method for standalone photovoltaic systems operating under fast transient variations of shading patterns. Sol Energy 124:124–142

[114] Kamarzaman NA, Tan CW (2014) A comprehensive review of maximum power point tracking algorithms for photovoltaic systems. Renew Sustain Energy Rev 37:585–598

[115] Mancilla-David F, Riganti-Fulginei F, Laudani A, Salvini A (2014) A neural network-based low-cost solar irradiance sensor. IEEE Trans Instrum Meas 63(3):583–591

[116] Punitha K, Devaraj D, Sakthivel S (2013) Artificial neural network basedmodified incremental conductance algorithmformaximum power point tracking in photovoltaic system under partial shading conditions. Energy 62:330–340

[117] Jiang LL, Nayanasiri D, Maskell DL, Vilathgamuwa D (2015) A hybrid maximum power point tracking for partially shaded photovoltaic systems in the tropics. Renew Energy 76:53–65

[118] Hiyama, T., Kouzuma, S., Imakubo, T.: 'Identification of optimal operating point of PV modules using neural network for real time maximum power tracking control', IEEE Trans. Energy Convers., 1995, 10, (2), pp. 360–367

[119] Younis, M.A.A.Y., Khatib, T., Ahmed, M., et al.: 'An improved maximum power point tracking controller for PV systems using artificial neural network', Prz. Elektrotech. (Electr. Rev.), 2012, 3, pp. 116–121

[120] Rai, A.K., Kaushika, N.D., Singh, B., et al.: 'Simulation model of ANN based maximum power point tracking controller for solar PV system', Solar Energy Mater. Solar Cells, 2011, 95, pp. 773–778

[121] Zhang, L., Bai, Y., Al-Amoudi, A.: 'GA-RBF neural network based maximum power point tracking for grid-connected photovoltaic systems'. Int. Conf. on Power Electronics, Machines and Drives, (Con Pub. No. 487), Sante Fe, NM, USA, 4–7 June 2002, pp. 18–23

[122] Eberhart R, Kennedy J (1995) A new optimizer using particle swarm theory. In: Proceedings of the sixth international symposium on micro machine and human science: New York, NY, pp 39–43

[123] Seo J, Im CH, Heo C, Kim J, Jung H, Lee C (2006) Multimodal function optimization based on particle swarm optimization. IEEE Trans Magn 42:1095–1098

[124] Rezk H, Fathy A, Abdelaziz AY (2017) A comparison of different global MPPT techniques based on meta-heuristic algorithms for photovoltaic system subjected to partial shading conditions. Renew Sustain Energy Rev 74:377–386

[125] Seyedmahmoudiana M, Horan B, Soon T, Rahmani R, Oo A, Mekhilef S, Stojcevski A (2016) State of the art artificial intelligence-based MPPT techniques for mitigating partial shading effects on PV systems—a review. Renew Sustain Energy Rev 64:435–455

[126] Lian L, Nayanasiri D, Maskell D, Vilathgamuwa D (2013) A simple and efficient hybrid maximum power point tracking method for PV systems under partially shaded condition. In: Proceedings of the annual conference on IEEE industrial electronics society, pp 14–19, 2013

[127] Souza N, Lopes L, Liu X (2005) An intelligentmaximum power point tracker using peak current control. In: Proceedings of the IEEE power electronics specialists conference, pp 172–177

[128] Punitha K, Devaraj D, Sakthivel S (2013) Artificial neural network based modified incremental conductance algorithm for maximum power point tracking in photovoltaic system under partial shading conditions. Energy 62:330–340

[129] Daraban S, Petreus D, Morel C (2014) A novel MPPT (maximum power point tracking) algorithm based on a modified genetic algorithm specialized on tracking the global maximum power point in photovoltaic systems affected by partial shading. Energy 74:374–388

[130] Shaiek Y, Smida M, Sakly A, Mimouni M (2013) Comparison between conventional methods and GA approach for maximum power point tracking of shaded solar PV generators. Sol Energy 90:107–122

[131] Unlu M, Camur S, Arifoglu B (2013) A new maximum power point tracking method for PV systems under partially shaded conditions. In: Proceedings of the international conference on power engineering, energy and electrical drives, pp 13–17

[132] Lian K, Jhang J, Tian I (2014) A maximum power point tracking method based on perturband-observe combined with particle swarm optimization. IEEE J Photovoltaics 4:626–633

[133] A. Mohapatra, B. Nayak, P. Das, and K. B. Mohanty, "A review on MPPT techniques of PV system under partial shading condition," Renewable and Sustainable Energy Reviews, vol. 80, pp. 854–867, Dec. 2017.

[134] N. Priyadarshi, S. Padmanaban, P. Kiran Maroti and A. Sharma, "An Extensive Practical Investigation of FPSO-Based MPPT for Grid Integrated PV System Under Variable Operating Conditions With AntiIslanding Protection," IEEE Syst. J., vol. 13, no. 2, pp. 1861-1871, June 2019, doi: 10.1109/JSYST.2018.2817584.

[135] L. K. Letting, J. L. Munda and Y. Hamam, Optimization of a fuzzy logic controller for PV grid inverter control using S-function based PSO," Solar Energy, vol. 86, no. 6, pp. 1689-1700, Jun. 2012.

[136] N. Priyadarshi, F. Azam, A. K. Sharma and M. Vardia, An Adaptive Neuro-Fuzzy Inference System-Based Intelligent Grid-Connected Photovoltaic Power Generation," in Advances in Computational Intelligence, pp. 3-14, Springer, Singapore, 2019.

[137] F. Belhachat and C. Larbes, "Global maximum power point tracking based on ANFIS approach for PV array configurations under partial shading conditions," Renew. and Sustain. Energy Rev., vol. 77, pp. 875- 889, Sept. 2017.

[138] M. A. Abido, M. S. Khalid and M. Y. Worku, An efficient ANFIS-based PI controller for maximum power point tracking of PV systems," Ara. J. for Sci. and Eng., vol. 40, no. 9, pp. 2641-2651, Sept. 2015.

[139] Rashid, M. H. (2021). Power Electronics Handbook . Academic Press. ISBN: 978-0128214343

[140] Mohan, N., Undeland, T. M., & Robbins, W. P. (2020). Power Electronics: Converters, Applications, and Design . John Wiley & Sons. ISBN: 978-0471226932

[141] Hart, D. W. (2018). Power Electronics . McGraw-Hill Education. ISBN: 978-0073380674

[142] Singh, B., Bhattacharya, S., & Jain, P. (2019). A review on DC-DC converters. IEEE Access , 7, 10769–10788. https://doi.org/10.1109/ACCESS.2019.2891685

[143] Prabhala, V. A. N., Baddipadiga, B. P., Fajri, P., & Ferdowsi, M. (2018). A DC–DC converter with continuous input current and high voltage conversion ratio. IEEE Transactions on Industrial Electronics , 65(3), 2269–2277. https://doi.org/10.1109/TIE.2017.2739680

[144] Al-Saffar, M. A., Ismail, E. H., & Sabzali, A. J. (2020). A new family of non-isolated DC–DC SEPIC–Cuk based bidirectional converters for distributed energy systems. Renewable Energy , 150, 1102–1114. https://doi.org/10.1016/j.renene.2019.12.046

[145] Erickson, R. W., & Maksimović, D. (2020). Fundamentals of Power Electronics . Springer. ISBN: 978-3030439493

[146] Liu, Y.-F., & Sen, P. K. (2019). Modeling and control of power electronic converters for microgrid applications. IEEE Transactions on Smart Grid , 10(1), 722–734. https://doi.org/10.1109/TSG.2017.2763265

[147] Kazimierczuk, M. K. (2019). Pulse-Width Modulated DC–DC Power Converters (2nd ed.). Wiley. ISBN: 978-1119048100

[148] Al-Hosani, K., Malakar, T., & Ahmed, K. H. (2018). Steady-state and dynamic analysis of Ćuk converter with parasitic elements. IET Power Electronics , 11(1), 172–181. https://doi.org/10.1049/iet-pel.2017.0284

[149] Babaei, E., & Laali, S. (2020). Analysis and design of a new non-isolated multiple-input DC–DC converter. IET Renewable Power Generation , 14(3), 452–460. https://doi.org/10.1049/iet-rpg.2019.0735

[150] Zhang, X., Wang, Y., & Li, K. (2021). A novel duty-cycle-controlled buck-boost converter with high efficiency and wide input/output voltage range. IEEE Transactions on Industrial Electronics , 68(8), 7202–7212. https://doi.org/10.1109/TIE.2020.3018032

[151] Xiao, H., & Dinavahi, V. (2019). Real-time simulation and hardware implementation of advanced control strategies for DC–DC converters. IEEE Transactions on Industrial Informatics , 15(6), 3611–3621. https://doi.org/10.1109/TII.2018.2876441

[152] Chen, C.-L., & Huang, Y.-J. (2020). Comparative study of non-isolated DC–DC converters for photovoltaic applications. Renewable Energy , 145, 1028–1040. https://doi.org/10.1016/j.renene.2019.06.054